THE UNIVERSITY OF MANITOBA

STATICAL BEHAVIOR OF CROPPED-WEB JOINTS IN TUBULAR TRUSSES

BY

NIPON THIENSIRIPIPAT

A THESIS

SUBMITTED TO THE FACULTY OF GRADUATE STUDIES

IN PARTIAL FULFIIMENT OF THE REQUIREMENTS FOR THE DEGREE

DOCTOR OF PHILOSOPHY

DEPARTMENT OF CIVIL ENGINEERING

WINNIPEG, MANITOBA

OCTOBER 1978

STATICAL BEHAVIOR
OF CROPPED-WEB JOINTS
IN TUBULAR TRUSSES

BY

NIPON THIENSIRIPIPAT

A dissertation submitted to the Faculty of Graduate Studies of the University of Manitoba in partial fulfillment of the requirements of the degree of

DOCTOR OF PHILOSOPHY

ABSTRACT

An experimental and theoretical investigation of the statical behavior of cropped-web joints is reported. The joints have square hollow sections as chords and circular hollow sections with longitudinally-oriented cropped ends as web members. Such joints have the advantage of low fabrication costs compared to sawn- or profiled-web joints. Tests of 34 isolated joints with a Pratt- or N-truss configuration are reported. Equations obtained using multiple regression analysis to relate the strengths and stiffnesses of the joints to various parameters are presented. The strengths of the joints are found to be usually acceptable and comparable to those of similar sawn-web joints with small gaps between the web members. The stiffnesses of the joints are also found to be acceptable, provided that the chord walls are not too flexible. The stiffnesses and stress distributions of the joints are satisfactorily estimated using simplified models of the joints and a linear finite element analysis program. Computer programs for plotting the joint models and generating the data required for the analyses are described. Design recommendations and recommendations for further study are provided.

ACKNOWLEDGEMENT

The author wishes to express his deep gratitude to Dr. R. B. Pinkney, his advisor, and Dr. G. A. Morris, Head of the Civil Engineering Department, for their kind advice, assistance, and encouragement during his study. He also thanks them and Mr. J. A. Cran, Dr. K. S. Mount, and Dr. J. Shewchuk, for reviewing the thesis and offering helpful suggestions. He appreciates the assistance and cooperation of Mr. E. Lemke, Chief Technician of the Civil Engineering Laboratory, and his staff.

Thanks are also due to the Comite International pour le Developpement et l'Etude de la Construction Tubulaire (CIDECT) for providing some financial assistance for the project, and to the Steel Company of Canada, Limited, (Stelco) for providing testing materials and many research papers.

The author gratefully acknowledges the financial assistance for his Ph.D. program provided by the University of Manitoba Graduate Fellowship and the Assistantship of the Civil Engineering Department. He also thanks the Canadian International Development Agency (CIDA) for awarding him a Colombo Plan Scholarship for his M.Sc. study. His leave of absence from Khon Kaen University, Thailand, granted by his Government is also very much appreciated.

He thanks many of his professors, especially Professor J. I. Glanville, and friends, particularly Mrs. E. Piamsalee, for their help and kindness. He is greatly indebted to his wife for her support, understanding, encouragement, and assistance in numerous ways.

TABLE OF CONTENTS

Page

ABSTRACT iv

ACKNOWLEDGEMENT v

LIST OF TABLES viii

LIST OF FIGURES ix

LIST OF SYMBOLS xiii

Chapter

1. INTRODUCTION 1

1.1. Tubular Trusses and Their Joints 1

1.2. Tubular Truss Joint Research 4

1.3. Objectives and Scope of Investigation 14

2. TEST PROGRAM 16

2.1. Joint Parameters 16

2.2. Specimen Designation 16

2.3. Specimen Design 19

2.4. Materials 19

2.5. Fabrication 21

2.6. Deformation Measurements 21

2.7. Strain Measurements 26

2.8. Loading Arrangement 29

2.9. Data Acquisition 29

3. TEST RESULTS AND DISCUSSION 32

3.1. Local Deflections of Chord Faces 32

Chapter Page

3.2. Buckling of Compression Web Members 40

3.3. Strains of Chord Faces 43

3.4. Strains in Compression Web Members 50

3.5. Strains in Tension Web Members 57

3.6. Failure Modes 64

3.7. Joint Strength 71

3.8. Joint Stiffness 82

4. THEORETICAL ANALYSIS 93

4.1. The Finite Element Method 93

4.2. The Computer Program Used 94

4.3. Finite Element Models of Joints 95

4.4. Data Generation Program 99

5. THEORETICAL RESULTS AND DISCUSSION 102

5.1. Deformations of Chord Faces 102

5.2. Deflections of Compression Webs 113

5.3. Stresses and Strains on Chord Faces 115

5.4. Stresses in Web Members 123

6. CONCLUSIONS AND RECOMMENDATIONS 127

6.1. Conclusions 127

6.2. Design Recommendations 129

6.3. Recommendations for Further Studies 130

REFERENCES 131

APPENDIX A 134

LIST OF TABLES

Table		Page
2.1.	Specimen Properties	17
3.1.	Test Results	65
3.2.	Joint Stiffnesses and Truss Deflections	85
5.1.	Ratios of Peak Theoretical and Experimental Deformations - of Chord Faces, δ_t/δ_e, using 135-element Models	110

LIST OF FIGURES

Figure		Page
1.1.	Tubular Truss Joints	3
1.2.	Joint Properties	6
2.1.	Pratt- or N-truss and Test Specimen	20
2.2.	Cropping Machine	20
2.3.	Welding Jig	22
2.4.	Welding Specification	22
2.5.	Transducer Locations on Chord Wall	23
2.6.	Transducer Assembly	24
2.7.	Transducer Locations on Compression Web	25
2.8a.	Strain Gauge Locations	27
2.8b.	Strain Gauge Locations on Specimen 5B75	28
2.9a.	Loading Frame	30
2.9b.	Loading Assembly	31
3.1.	Load-deformation Curves of Loaded Chord Face of Specimen 3A50	33
3.2.	Deformation of Loaded Chord Face of Specimen 3A50	34
3.3.	Deformation of Loaded Chord Face of Specimen 5B00	37
3.4.	Maximum Deformations of Loaded Chord Faces of Specimens 5A00, 5A50, and 5A75	38
3.5.	Deformations of Loaded Chord Faces of Specimens 3C75, 4C75, and 5C75	39
3.6.	Maximum Deformations of Loaded Chord Faces of Specimens 3B50, 4B50, and 5B50	41
3.7.	Load-deflection Curves of Compression Web Member of Specimen 3A50	42

Figure Page

3.8. Longitudinal Strains on Chord Faces of Specimen 5B75 . . . 44

3.9. Transverse Strains on Chord Faces of Specimen 5B75 45

3.10. Loads vs. Transverse Strains near the Weld on Loaded Chord Face of Specimen 5B75 46

3.11. Transverse Strains on Loaded Chord Faces of Specimens 3B75, 4B75, and 5B75 48

3.12. Transverse Strains on Loaded Chord Faces of Specimens 5B00, 5B50, and 5B75 49

3.13. Strains on Loaded Chord Face of Specimen 1B75 51

3.14. Longitudinal Strains on Compression Web Member of Specimen 5B75 54

3.15. Longitudinal Strains on Compression Web Member of Specimen 5B50 55

3.16. Longitudinal Strains on Compression Web Member of Specimen 5C75 56

3.17. Longitudinal Strains on Compression Web Member of Specimen 1B75 58

3.18. Longitudinal Strains on Compression Web Member of Specimen 4B75 59

3.19. Longitudinal Strains on Tension Web Member of Specimen 5A75 60

3.20. Strains on Specimen 5A75 61

3.21. Strains on Specimen 4B75 62

3.22. Strains on Specimen 5C75 63

3.23. Failure Mode A - Large Deformation of Loaded Chord Face 66

3.24. Failure Mode B - Buckling of Compression Web Member 67

3.25. Failure Mode C - Tearing of Tension Web Member 68

3.26. Strength of Cropped-Web Joints 73

Figure Page

3.27. Comparative strengths of Cropped- and Sawn-Web Joints . . . 78

3.28. Joint Efficiency 79

3.29. Ratio of Joint Strength to Compression-Web Strength 81

3.30. Joint Stiffness 83

3.31. Joint Stiffness along Compression Web Axis 86

3.32. Joint Stiffness along Tension Web Axis 88

3.33. Increase in Truss Deflection due to Joint Deformation . . . 91

4.1. Finite-Element Model of Cropped-Web Joints 96

4.2a. Compression Web Profiles 97

4.2b. Tension Web Profiles 98

4.3. Numbers of Elements and Length Factors 100

5.1. Finite-Element Models for Specimen 5B00 103

5.2. Deformations of Loaded Chord Faces of Specimen 5B00 105

5.3. Finite-Element Models for Specimens 5A00, 5A50, and 5A50- 106

5.4. Deformation of Loaded Chord Faces of Specimens 5A00, 5A50, and 5A50- 108

5.5. Finite-Element Models for Specimen 1A50 111

5.6. Deformations of Loaded Chord Face of Specimen 1A50 112

5.7. Deflections of Compression Web of Specimen 5B00 114

5.8. Bending Moments per Unit Length and Membrane Stresses . . . 116

5.9. Finite-Element Models for Specimen 5B75 118

5.10a. M_{xx} for Loaded Chord Face of Specimen 5B75 (283 Nodes) . . . 119

5.10b. M_{yy} for Loaded Chord Face of Specimen 5B75 (283 Nodes) . . . 120

5.11. Bending Moments at Section A of Specimen 5B75 122

Figure Page

5.12. Strains on Chord Faces of Specimen 5B75 124

5.13. Maximum and Minimum Stresses in Webs of Specimen 5B75 (352 Nodes) 125

LIST OF SYMBOLS

Symbol	
A	Cross-sectional area; or failure by excessive deformation of loaded chord face
A_0, A_1, A_2	Cross-sectional areas of chord, compression web, and tension web, respectively
B	Failure by buckling of compression web member
b_0	Outside width of chord
CHS	Circular hollow sections
C_r	Factored compressive resistance of a compression web
d	Average outside diameter of compression and tension webs
d_0, d_1, d_2	Outside diameters of chord, compression web, and tension web, respectively
d'	Equivalent width of a compression or tension web
E	Modulus of elasticity (29000 ksi or 200000 N/mm^2)
e	Eccentricity of joint, equal to distance between the point of intersection of the web axes and the chord axis
F.S.	Factor of safety
g	Gap between the compression and tension webs measured along the chord face
HSS	Hollow structural section(s)
h_0	Outside depth of a rectangular chord
in.	Inches (1 in. = 25.4 mm)
J_r	Factored joint resistance
J_u	Joint strength, equal to the ultimate web-force component normal to the chord
J_w	Maximum allowable load normal to the chord of a cropped-web joint

K	Effective length factor
k, kips	Kilo-pounds (1000 pounds = 4.45 kN)
$(KL/r)_1$	Slenderness ratio of a compression web member
kN	Kilo-Newtons
ksi	Kips per square inch (1 ksi = 6.89 N/mm^2)
k_1, k_2	Stiffness of a cropped-web joint along the compression and tension web axis, respectively
L	Member length
LCCT9	Linear curvature compatible triangles with 9 nodes
LVDT	Linear voltage displacement transducer(s)
L_0, L_1, L_2	Lengths of a chord, compression web, and tension web, respectively
M_{xx}, M_{yy}	Bending moments per unit length of a plate element, in a local coordinate system, in the xz and yz plane, respectively
m	Meters
mm	Millimeters
N/mm^2	Newtons per square millimeter
N_1, N_2	Linear forces along compression and tension web axes, respectively, at the loaded chord face
N1 to N14	Numbers of elements to be generated in each of 14 element fields
N_{1b}	Buckling strength of a compression web member
N_{1u}, N_{2u}	Ultimate loads in compression and tension webs, respectively
N_{1w}, N_{2w}	Maximum allowable loads for compression and tension webs, respectively
o_g	Gap, equal to g/d_2
o_v	Overlap, equal to q/d_2

p	Cropped length of a tension web
q	Overlap length of a tension web
RHS	Rectangular hollow sections
r	Radius of gyration
SAPIV	A structural analysis program for static and dynamic response of linear system
T_r	Factored tensile resistance of a tension web member
t	Average thickness of compression and tension webs
t_0, t_1, t_2	Thicknesses of chord, compression web, and tension web, respectively
t'	Equivalent thickness of a compression or tension web
YYL, YYR	Numbers of times of $(b_0-t_0)/2$ to be used for lengths adjacent to compression and tension webs, respectively
Δ	Overall deflection at mid-span of a truss
Δ_j, Δ_m	Mid-span deflection of a tubular truss due to joint and member deformation, respectively
δ_e, δ_t	Peak values of experimental and theoretical deflections, respectively, of loaded chord faces
δ_1, δ_2	Linear displacement along the compression and tension web, respectively, at the loaded chord face
ε_{xb}, ε_{yb}	Surface bending strains in the x and y direction, respectively
ε_{xm}, ε_{ym}	Membrane strains along x and y axes, respectively
ε_{xx}, ε_{yy}	Total surface strains along x and y axes, respectively
λ	Non-dimensional slenderness ratio in column formula
ν	Poisson's ratio (0.3)
σ_e	Yield stress (at 0.2% offset) of chords
σ_u	Ultimate stress

σ_{xb}, σ_{yb}	Surface bending stresses in the x and y-directions, respectively
σ_{1a}	Maximum allowable stress for a compression web
σ_{1e}, σ_{2e}	Yield stresses (at 0.2% offset) of compression and tension webs, respectively
ϕ	Performance factor
'	Foot; Feet
"	Inch(es)

Chapter 1

INTRODUCTION

Trusses fabricated of tubular sections, herein referred to as tubular trusses, possess many attractive features, and have become increasingly popular. Below is a summary of the advantages of these trusses, as well as problems and solutions involving the fabrication of their joints. In addition, the behavior of joints previously investigated is reviewed. Finally, the objectives and scope of the present investigation are stated.

1.1. Tubular Trusses and Their Joints

In recent years, tubular trusses have become more economical and have been used increasingly. Difficulties in the fabrication of some tubular truss joints have been largely overcome. The design and fabrication of these joints have become more efficient, as a result of research and experience.

Tubular trusses have many advantages. They are commonly 20% lighter than other trusses, because tubes have exceptional buckling resistance (Stelco 1973). The trusses have minimum exposed surface areas, which minimizes wind or wave loadings, as well as the costs of fire and corrosion protection, painting and maintenance. Furthermore, they look neat and pleasing, and thus need not be hidden.

According to Beckett, tubular trusses were used by Robert Stephenson in the construction of a railway bridge at Conway, U.K., in

1849. Such early tubular trusses were fabricated from plates and rivets, and were expensive. The fabrication cost was still high even in the mid-1930's when electric-arc welding became more accepted. This is because only circular tubes were rolled and their joints required profiling and were difficult to fabricate.(Beckett 1970)

Several methods for overcoming the difficulty in fabricating tubular truss joints have been used. They include the use of semi-automatic profiling machines, gusset plates, cropping, or rectangular tubes. Some of the resulting joints are illustrated in Fig. 1.1.

Semi-automatic profiling machines can efficiently profile the ends of circular tubes if the inside diameter of the web tube, the outside diameter of the chord tube, and the angle between the tube axes are given (Robinson 1969). However, such machines are used for small tubes and not widely available in Canada (Cran et al. 1971).

Gusset plates have been used to eliminate the profiling, but they tend to cause stress concentration, and are expensive (Cran et al. 1971).

Cropping (flattening and cutting of a circular tube using two V-shaped steel blades) has also been used to eliminate the profiling (Jamm 1951; Anderson 1961; Sammet 1963; Bouwkamp 1964; Hlavacek 1973; Morris et al. 1974). The process is fast, simple, and efficient. It requires no extra material and simplifies welding of the joints.

The profiling can also be eliminated by the use of rectangular hollow sections, rolled in U.K. and Canada since 1958 and 1962, respectively. The flat surfaces of these tubes allow circular or rectangular

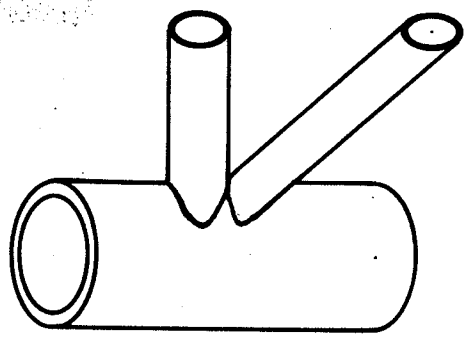

a. Profiled - web Joint

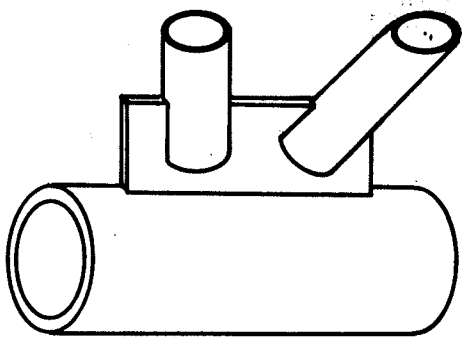

b. Joint with Gusset Plate

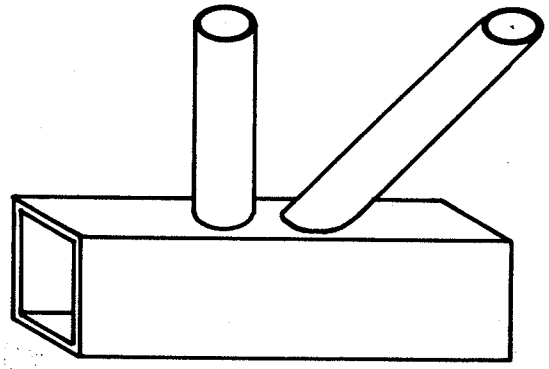

c. Sawn - web Joint

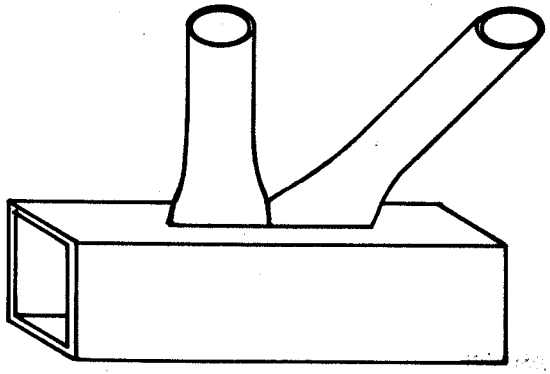

d. Cropped - web Joint

Fig. 1.1. Tubular Truss Joints

tubes to be welded to them without profiling, provided that the web tubes do not overlap. If the web tubes overlap, they may be profiled, used with gusset plates, cropped, or other tube sizes selected.

Among the different methods for eliminating profiling, cropping is relatively economical. However, the cropped-web joints have been used mainly in small trusses, because their behavior has not been throughly investigated. If these joints are found to be structurally acceptable and efficient, they may be more widely used and significantly increase the economy of tubular trusses.

1.2. Tubular Truss Joint Research

Since the chord member of a tubular truss joint has no central web element to provide a direct support for the web members, the joint may be very flexible and weak, particularly when the chord thickness/width and web-width/chord-width are small. The behavior of some types of these joints has been extensively investigated, as described below.

In the following, joint efficiency is defined as the ratio of the test failure load to the yield load in the tension web member (Cran et al. 1971), although Bouwkamp (1967) has defined it in terms of the ultimate load of the tension web rather than the yield load. The joint load factor is defined as the ratio of the ultimate load to the working load of the tension web member. In addition, a joint is said to have a negative eccentricity if the web member axes intersect before meeting the chord axis; if they intersect beyond the chord axis, the eccentricity is positive; when the web and chord axes are concurrent, there is

zero eccentricity. The eccentricities, as well as overlap and gap are illustrated in Fig. 1.2. The overlap is defined as $o_v = q/d_2$, although other investigators may use $o_v = q/p$ (see Fig. 1.2). Similarly, the gap is defined as $o_g = g/d_2$.

Joints between Circular Tubes

Jamm (1951) found that a direct connection of the tube walls was preferable to an indirect connection via gusset plates or wedges. In addition, joints with an overlap between the web members were stronger than joints with a gap between the webs.

Jamm et al. stated that, in order to achieve 100% joint efficiency, the amount of overlap of the web tubes measured perpendicular to the chord tube must be at least 15% of the diameter of the chord tube. The overlap can cause some moment, but this is acceptable as long as the point of intersection of the web tube axes lies within the middle half of the chord tube diameter. If the diameters of the web tubes are relatively large, the tube ends should be flattened to 20 or 25% of the chord tube diameter, in order to preserve the flexibility of the chord tube. (Jamm et al. 1952)

Tests of tubular joints conducted by Tubemakers of Australia Limited (1960) showed that profiled joints had approximately the same collapse loads as joints whose web member ends were sheared. The profiled compression webs, however, showed no preferred direction of buckling, while sheared-end compression webs usually buckled out of the plane of the truss. Yielding in the compression web occurred at half

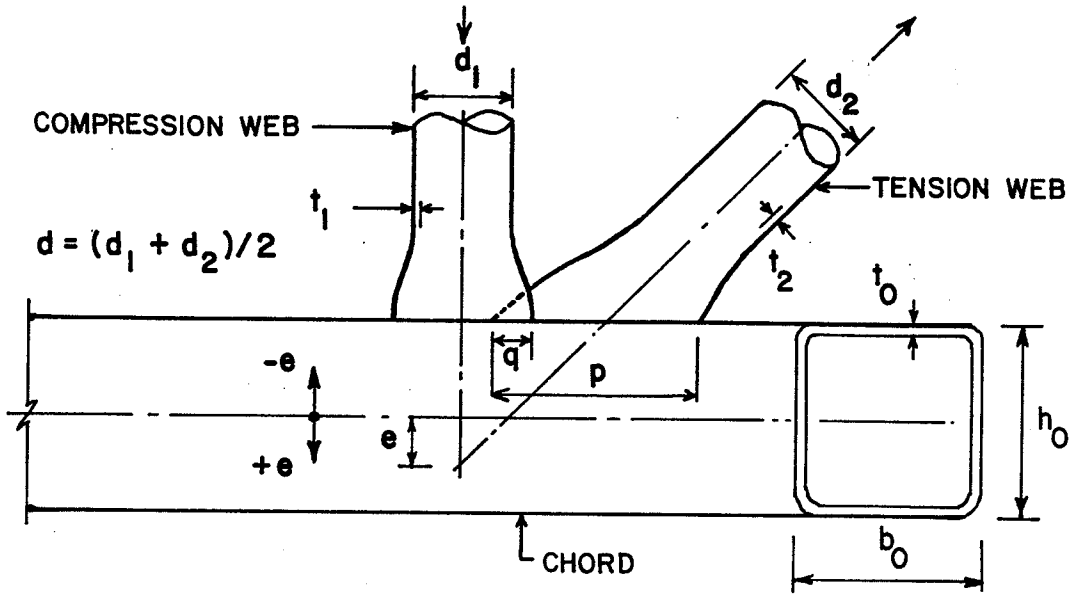

a. Eccentricity (e) and Overlap ($o_v = q/d_2$)

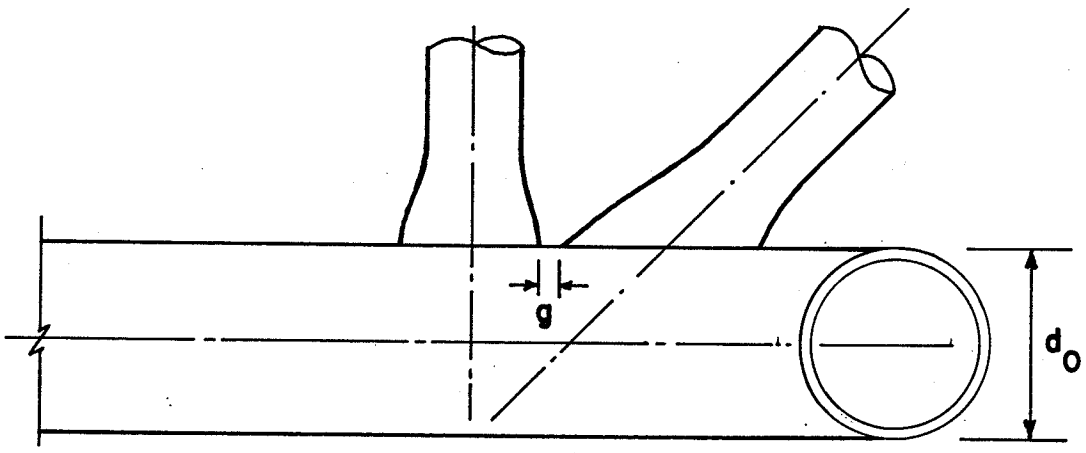

b. Gap ($o_g = g/d_2$)

Fig. I.2. Joint Properties

the failure load for a joint with a negative eccentricity.

Anderson (1961) found that profiled joints and cropped joints had comparable ultimate loads, although the former had much lower maximum stresses and better stress distribution than the latter. For the former, the maximum stresses occurred adjacent to the flanks of the web members, but for the latter, it occurred in the crotches. The chord stresses were reduced by increases in the overlap between the web members, and in the negative eccentricity. He recommended that cropped joints with large overlaps between the web members could be used as safe and economical substitutes for profiled joints, provided the loads were static.

Sammet (1963) found that tubular truss joints could fail through tearing or excessive deformation of the tubular chord, without damage to the weld. And the rigidity and load at fracture were changed by an alteration of the configuration of the joint.

Bouwkamp (1964) found that interwelded joints with profiled members were more efficient than joints with gusset plates and joints with cropped ends. The stress distributions of the former were more uniform and their chord stresses near the weld in the truss plane were less than half the corresponding stresses in the cropped joints. The elastic and ultimate load capacity of a tubular joint was increased considerably by overlapping the profiled web members, as this resulted in a direct load transfer between these members and subsequently prevented the development of high bending stresses in the chord tube wall. Like Anderson, he concluded that cropped joints could be used

successfully provided that the load was static and moderate, and the cropped tube diameters were small.

Bouwkamp (1968) also tested 21 Pratt-type truss joints of circular tubes under static loads. He concluded that negative eccentricity joints (often with overlaps of webs) had a strength superior to that of zero or positive eccentricity joints. Furthermore, joint strength was increased by increasing the chord wall thickness or the web member diameters. The increase in web diameters increased the length of weld between the web and the chord members, which resulted in an improved load transfer and a higher strength. He also found that a compressive force added to the chord did not influence the failure load.

Tests of profiled K joints with ratio of diameters of web to chord of 0.4, conducted at the Otto Graff Institute of the Stuttgart College of Technology (1967), showed that statically loaded joints failed by deformation of chord members at a compression web load of 50% to 67% of the ultimate load.

Hlavacek (1973) tested K-joints and found that the average efficiency of flattened web joints was about 80% and was smaller than that of profiled joints. In addition, compression webs with longitudinally flattened ends were about 20% weaker than the same webs with profiled ends. He suggested that the flattened ends should be shorter than 20 to 30 mm (0.8 to 1.2 in.). He found that joint strength increased with overlap. Overlap obtained by cutting either the compression web or the tension web produced better results than that obtained by cutting both webs equally. Negative eccentricity and gusset

plates which did not cut through the tubes increased the joint strength.

Joints having Rectangular Chords

Eastwood et al.(1967a) statically tested 60 N-type tubular truss joints having round webs and rectangular chords. Their results suggested that web members should have a modest overlap of about one third of the web diameter, as this would substantially decrease the local deflection of the chord face. In addition, secondary moments caused by eccentricity did not affect the ultimate strength of the truss.

Mee (1969) tested 61 statically loaded N-joints between rectangular hollow sections and found that the transfer of load between the branches improved with increasing overlap. A joint with a gap could yield prematurely due to excessive deformation of the chord face, but had a large reserve of strength. The joint strength increased with an increase in the ratio of branch width to chord width, since more load was transmitted through the side walls of the chord. The strength also increased with an increase in the chord thickness but only when the load between the branches was transmitted through the chord wall. The stiffness of the joint increased with an increase in overlap. The overall behavior of joints with rectangular sections was similar to that of similar joints with circular webs having diameters equal to the widths of the rectangular webs. If the webs did not overlap, the former joints had smaller deflections and strength. A change in chord preload was found to have little effect on the joint behavior.

Eastwood and Wood (1970) found that when the web members of test joints overlapped, the joint behavior was in general extremely satisfac-

tory with consistently high load factors obtained, and failure almost always occurred in the web members, not in the joints. When there was a weld gap, the load factor was generally smaller than when the web members overlapped, and failure occurred almost invariably by considerable deformation of the chord face rather than by buckling of the web members.

Based on test results on joints with rectangular chords and circular or rectangular webs, Eastwood and Wood (1970) concluded that when the webs overlapped by more than 50% of their mean diameter, the normal load transmitted into the chord was unlikely to be a limiting factor for the usual range of load conditions, and deflections in the chord face would be small. The greater the degree of overlap, the smaller the deflections in the chord face and the greater the resistance to fatigue would be. In addition, a joint with a small weld gap would have less chord-wall distortion, but would be more prone to fatigue failure, than one with a wide weld gap. Eastwood and Wood provided an empirical formula for calculating the strength of a joint having a weld gap, later presented in Cran et al. (1971).

Dasgupta (1970) tested full-scale tubular N-trusses having rectangular chord members and circular branches with small gaps at the joints. He found that the failure loads of the joints were about 25% to 30% lower than those of the isolated joint tests conducted by Eastwood et al.(1967a). He attributed the differences to the secondary moments in the trusses. He also found that failures occurred variously by strut

buckling, by tensile failure at the toe of the tension web, or by premature failure of welds. Furthermore, the deflections of the truss were increased due to the flexibility of the gap joints. And the secondary moments due to positive eccentricity caused unfavorable stresses at the crotch of the joint, but those due to negative eccentricity relieved the stresses.

Davie and Giddings (1971) tested 31 N-truss gap joints between rectangular chords and rectangular or circular branches to complement tests done by Eastwood et al. (1967a, 1970) and Dasgupta (1970). They provided some curves for predicting the joint strength.

Morris et al.(1974) tested 18 Pratt truss joints having flattened-end webs and round or square chords. They found that joints having square chords were about one third as stiff as similar joints with round chords. The former joints had yield loads about 25%, and ultimate loads about 10%, lower than the latter. The ultimate loads were not significantly lower than those of joints having unflattened-end webs. The orientation of the flattened ends did not substantially affect yield load, ultimate load, or joint stiffness. The joint eccentricity and overlap greatly affected the joint stiffness but not the yield load or ultimate load. Local deformation of chord walls slightly increased overall truss deflection. The specimens failed by buckling of the compression web member or rupture of the tension web member, partially induced by local chord-wall deformation.

Gibson and Pastor (1974) provided comprehensive summaries of research on welded joints of hollow structural sections.

Wardenier (1977) presented some formulas for calculating the strength of different joints having hollow structural sections.

Theoretical Analyses of Joints

Eastwood et al.(1967b) used a beam-on-elastic-foundation analogy and thin plate theory to analyze local deformations and stresses in tubular N-joints with rectangular chord members and circular branch members. Theoretical contours of load distributions, local deflections, and stresses for different values of joint eccentricity were obtained and compared.

Eastwood et al.(1968) employed the elastic theory of thin plates and a finite difference approximation to estimate the local deflections and bending moments in N-truss gap joints between rectangular hollow chords and rectangular or circular hollow web members. The boundary conditions at the corners were put in the form of a moment-rotation relationship, assuming the chord tube-section to be a closed rigid frame. For relatively stiff chord walls, the joint loads were assumed to be uniformly distributed; this resulted in a very conservative estimate, as the assumption did not allow the transfer of loads from the central parts to the stiffer parts nearer the side walls of the chord. For relatively flexible chord walls, the deflections under each web member were assumed to be uniform or to follow a predicted pattern; the results for the uniform deflection assumption were not always realistic, as the parts nearer the side walls and the parts between the branch members tended to undergo small relative deflections.

Mee (1969) also studied the elastic behavior of gap joints between rectangular hollow members; the top face of the chord was treated as a thin plate.

Dasgupta (1970) used the finite element method to study the local deflection characteristics and the flexibilities of tubular truss joints having rectangular chords. The type of element used in the analysis was a four-noded isoparametric quadrilateral flat plate, including the effect of bending and membrane stresses. A data generation program was written to idealize any joint with a rectangular hollow chord and rectangular and/or circular hollow webs, and to generate all of the data required for the analysis. The analytical results compared well with experimental results.

Mouty (1977) used yield-line theory to predict the ultimate loads of tubular joints. Most predicted loads were less than or equal to the experimental failure loads.

In summary, the experimental and theoretical results showed that the strength of a tubular truss joint is increased by:

(1) an increase in the ratio of the thickness-to-diameter, t_0/d_0, of the chord member, as this increases the stiffness of the chord wall;

(2) an increase in the ratio of web-diameter to chord-diameter, d/d_0, as this improves the stress distributions on the loaded chord face;

(3) an increase in the ratio of overlap to web diameter, q/d_2, as this permits more web-member force to be transmitted directly between web members instead of through bending of the chord wall;

(4) an increase in the negative eccentricity, as this decreases the

lever arm along the chord wall between the web-member axes and thus reduces the bending in the wall;

(5) an increase in the yield strength of the members, and

(6) using profiled ends rather than cropped ends, flattened ends or gusset plates, as this distributes the forces more uniformly on the chord wall.

1.3. Objectives and Scope of Investigation

In this study, tubular truss joints having cropped-end circular web members and rectangular chords, as illustrated in Fig. 1.1d, were investigated. The joints have the advantage of a relatively low fabrication cost, because cropping reduces cutting time, eliminates profiling even when the webs overlap, and simplifies welding of the joints by requiring only straight fillet welds. Moreover, the rectangular chords provide good stability and large bearing surface areas, and facilitate connection to other structural members.

The cropped ends may cause some adverse effects. They may increase the effective lengths of the web members, thus decreasing the ultimate loads. The long, narrow edges of the cropped ends may produce unfavorable stress distributions on the chord faces. In addition, the cropped ends may distort locally when loaded.

However, early investigations of cropped web joints mainly with circular chords (Jamm 1951; Anderson 1961; Sammet 1963; Bouwkamp 1964;

Hlavacek 1973; Frovich 1973; Morris et al.1974; Thiensiripipat and Morris 1975) have indicated that the adverse effects due to the cropped ends are not significant and the joints are acceptable in many cases. Since the cropped web joints with rectangular chords are economical and practical and have not been extensively investigated, the present investigation was carried out.

The objectives of the investigation were to study the statical behavior of the joints and to develop design criteria for them. In the investigation, both experimental and theoretical methods were used. The former was done by testing isolated joints. The latter involved using a finite element program to analyze a simplified model of the joints.

The scope of the investigation was limited as follows. In the experimental investigation, 34 test specimens were considered, each had a Pratt- or N-truss configuration. The two web members of each specimen were identical and had cropped ends welded at angles of 45° and 90°, respectively, to the face of a square chord. The chord was not preloaded since the effect of the larger forces usually existing in the chord did not significantly affect the failure load (Bouwkamp 1968; Eastwood et al. 1970). Three quantities were used as variables: the ratio of chord thickness-to-width (t_0/b_0), the ratio of average web-diameter to chord-width (d/b_0), and the percentage overlap (o_v). The theoretical study was limited to elastic analysis only.

Chapter 2

TEST PROGRAM

2.1. Joint Parameters

The experimental program involved the testing of 34 joints having square chords and longitudinally cropped-end webs, as illustrated in Fig. 1.1d. The effects of three parameters were investigated. These were the chord thickness/width ratio (t_0/b_0), the average web-diameter/chord-width ratio (d/b_0), and the percentage overlap ($o_v = q/d_2$) illustrated in Fig. 1.2. The values of these parameters were varied, while those of other parameters were held constant as far as practicable.

The parameter values are given in Table 2.1. It shows that there are five different groups of t_0/b_0 values (0.031, 0.040, 0.044, 0.062, and 0.076, approximately), three different groups of d/b_0 values (0.4, 0.5, and 0.7, approximately), and three different overlap values (0%, 50%, and 75%).

2.2 Specimen Designation

The specimens were designated as follows. The first five specimens were previously tested (Thiensiripipat and Morris 1975) and were simply designated by a digit from 1 to 5. The remaining 29, tested in the current investigation, had a three-part designation. The first character, a digit from 1 to 5, represented one of the five values of t_0/b_0 used. The next character, A, B, or C, represented one of the

Table 2.1. Specimen Properties

Specimen	Chord			Webs				Lap
	b_0, h_0	t_0	t_0/b_0	d d_1,d_2	t t_1,t_2	t/d	d/b_0	o_v
	in.	in.	%	in.	in.	%	%	%
1	4.00	0.175	4.38	1.90	0.110	5.79	47.5	50
2	4.00	0.175	4.38	1.90	0.110	5.79	47.5	0
3	4.00	0.170	4.25	2.38	0.125	5.25	59.5	0
4	6.00	0.182	3.03	1.90	0.110	5.79	31.7	0
5	6.00	0.182	3.03	2.38	0.125	5.25	39.7	0
1A50	6.00	0.192	3.20	2.38	0.180	7.56	39.7	50
1A75	6.00	0.192	3.20	2.38	0.180	7.56	39.7	75
2A50	6.00	0.242	4.03	2.38	0.180	7.56	39.7	50
2A75	6.00	0.242	4.03	2.38	0.180	7.56	39.7	75
3A50	4.00	0.175	4.38	1.67	0.125	7.48	41.8	50
3A75	4.00	0.175	4.38	1.67	0.125	7.48	41.8	75
4A50	4.00	0.250	6.25	1.67	0.125	7.48	41.8	50
4A75	4.00	0.250	6.25	1.67	0.125	7.48	41.8	75
5A00	4.00	0.300	7.50	1.67	0.125	7.48	41.8	0
5A50	4.00	0.300	7.50	1.67	0.125	7.48	41.8	50
5A75	4.00	0.300	7.50	1.67	0.125	7.48	41.8	75
1B50	6.00	0.188	3.13	2.89	0.240	8.30	48.2	50
1B75	6.00	0.188	3.13	2.89	0.240	8.30	48.2	75
3B50	4.00	0.180	4.50	1.91	0.120	6.28	47.8	50
3B75	4.00	0.180	4.50	1.91	0.120	6.28	47.8	75
4B50	4.00	0.250	6.25	1.90	0.120	6.32	47.5	50
4B75	4.00	0.250	6.25	1.90	0.120	6.32	47.5	75
5B00	4.00	0.310	7.75	1.90	0.120	6.32	47.5	0
5B50	4.00	0.300	7.50	1.90	0.120	6.32	47.5	50
5B75	4.00	0.290	7.25	1.90	0.120	6.32	47.5	75
1C50	6.00	0.182	3.03	4.54	0.297	6.54	75.7	50
1C75	6.00	0.182	3.03	4.54	0.297	6.54	75.7	75
3C50	4.00	0.177	4.42	2.89	0.240	8.30	72.2	50
3C75	4.00	0.177	4.42	2.89	0.250	8.65	72.2	75
4C50	4.00	0.240	6.00	2.88	0.240	8.33	72.0	50
4C75	4.00	0.240	6.00	2.88	0.246	8.54	72.0	75
5C00	4.00	0.290	7.25	2.89	0.243	8.41	72.2	0
5C50	4.00	0.314	7.85	2.89	0.236	8.17	72.2	50
5C75	4.00	0.313	7.82	2.89	0.240	8.30	72.2	75

Table 2.1 (Continued). Specimen Properties

Specimen	Chord		Webs		e/h_0	$(KL/r)_1$	Specified Weld Size
	σ_e ksi	σ_u ksi	σ_e ksi	σ_u ksi		K = 1	in.
1	51.5	84.7	56.1	78.1	0.125	114	1/4
2	51.5	84.7	56.1	78.1	0.375	114	1/4
3	51.5	84.7	48.3	72.8	0.580	90.3	1/4
4	51.7	72.8	56.1	78.1	0.077	114	1/4
5	51.7	72.8	48.3	74.2	0.213	90.3	1/4
1A50	54.7	80.4	48.3	74.2	0.015	92.3	3/8
1A75	54.7	80.4	48.3	74.2	-0.090	92.3	3/8
2A50	53.5	66.9	48.3	72.8	-0.053	92.3	3/8
2A75	53.5	66.9	48.3	72.8	-0.075	92.3	3/8
3A50	51.5	84.7	63.3	80.6	0.048	131	3/16
3A75	51.5	84.7	63.3	80.6	-0.068	131	3/16
4A50	51.2	75.2	63.3	80.6	0.125	131	3/16
4A75	51.2	75.2	63.3	80.6	-0.058	131	3/16
5A00	52.6	79.9	63.3	82.2	0.272	131	3/16
5A50	52.6	79.9	63.3	82.2	0.080	131	3/16
5A75	52.6	79.9	63.3	82.2	-0.068	131	3/16
1B50	51.7	72.8	54.7	79.7	0.088	76.5	3/8
1B75	51.7	72.8	54.7	79.7	-0.075	76.5	3/8
3B50	47.1	72.3	56.1	78.1	0.120	114	3/16
3B75	47.1	72.3	56.1	78.1	0.000	114	3/16
4B50	51.2	75.2	56.1	78.1	0.130	114	3/16
4B75	51.2	75.2	56.1	78.1	0.010	114	3/16
5B00	54.7	80.4	56.1	78.1	0.360	114	3/16
5B50	54.7	80.4	56.1	78.1	0.115	114	3/16
5B75	54.7	80.4	56.1	78.1	0.065	114	3/16
1C50	51.7	72.8	54.7	82.2	0.040	48.0	3/8
1C75	51.7	72.8	54.7	82.2	-0.108	48.0	3/8
3C50	51.5	84.7	54.7	82.2	0.305	76.8	3/8
3C75	51.5	84.7	54.7	82.2	0.168	76.8	3/8
4C50	52.0	76.8	54.7	82.2	0.335	76.8	3/8
4C75	52.0	76.8	54.7	82.2	0.140	76.8	3/8
5C00	52.6	79.9	54.7	82.2	0.632	76.6	3/8
5C50	52.6	79.9	54.7	82.2	0.290	76.4	3/8
5C75	52.6	79.9	54.7	82.2	0.290	76.4	3/8

three values of d/b_0 used. The final two characters, 00, 50, or 75, indicated the percentage overlap of the web members.

2.3. Specimen Design

To facilitate comparisons with other investigations, and to produce a relatively severe loading of the chord face, a Pratt- or N-joint geometry, as illustrated on Fig. 2.1, was used. Each test specimen consisted of a chord and two web members, each extending from the test joints half way to the adjacent joints.

For simplicity, the sizes of the two webs of each specimen were kept the same. Relatively large chord sizes were chosen such that the capacity of the loading jack used (200 kips or 890 kN) was not exceeeed.

2.4. Materials

The rectangular hollow sections (RHS) 6 x 6 in. (152 x 152 mm), used for the chords, were cold-formed and stress relieved, while RHS 4 x 4 in. (102 x 102 mm) and the circular hollow sections (CHS) were hot-formed. All of these sections conformed to C.S.A. Specification G40.21 Class H Grade 50W. Tension tests indicated that the yield stresses σ_e, at 0.2% offset, of the RHS ranged from 47.1 to 54.7 ksi (325 to 377 N/mm^2) and those of the CHS ranged from 48.3 to 63.3 ksi (333 to 436 N/mm^2), as given in Table 2.1. The ultimate stresses σ_u are also given.

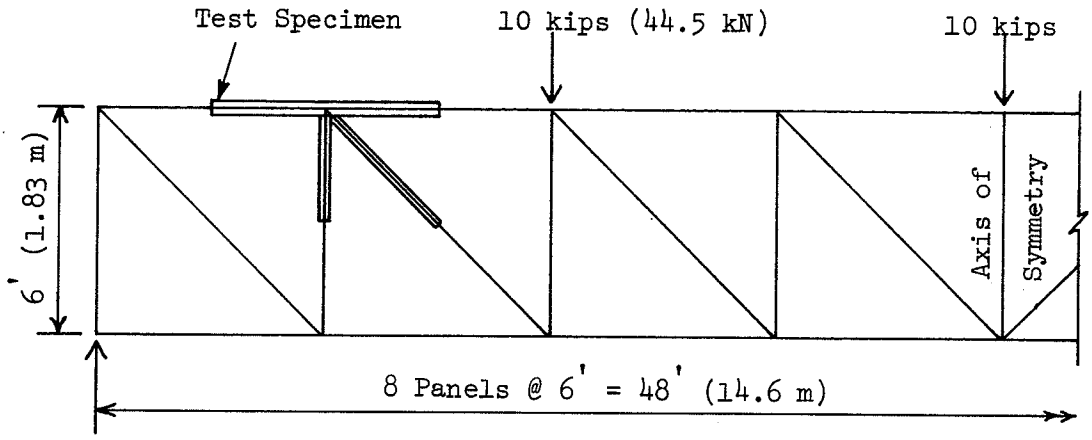

Fig. 2.1. Pratt- or N-truss and Test Specimen

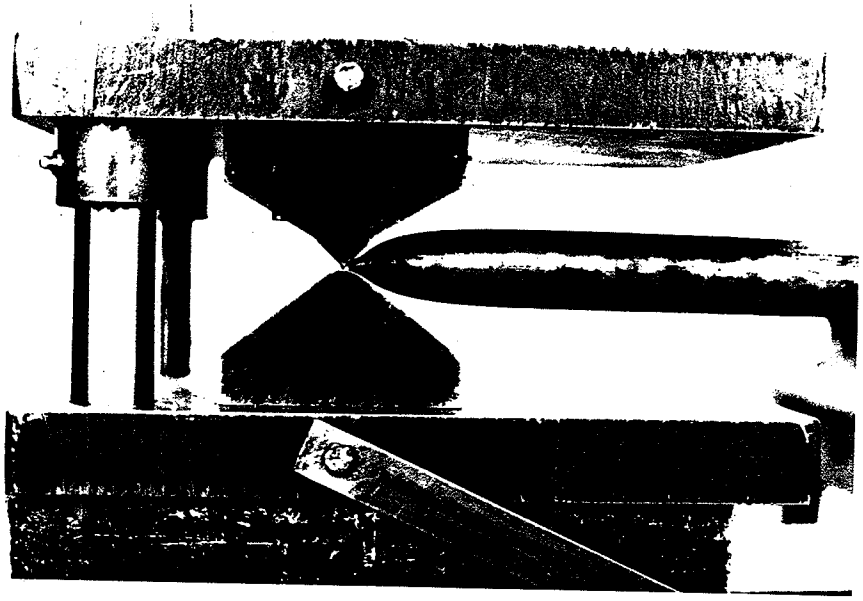

Fig. 2.2. Cropping Machine

2.5. Fabrication

The web tubes were cropped in a cropping machine, as illustrated in Fig. 2.2. The cropped tubes and a chord tube were assembled for tack welding in a jig as shown in Fig. 2.3. The final welding was done by a certified welder of the Dominion Bridge Company, Winnipeg.

The welds were designed to be stronger than the members. An example of the welding specification of the specimens is illustrated in Fig. 2.4. The weld sizes of the specimens are given in Table 2.1.

2.6. Deformation Measurements

The deformation along the center line of the loaded face of the chord was measured at six locations, as illustrated in Fig. 2.5. The locations were chosen based on previous tests (Thiensiripipat and Morris 1975), which showed large deformations near the extreme edges of the webs. The choice of transducer locations was also restricted by available space; thus two patterns were used.

The measurements were taken using six linear voltage displacement transducers (LVDT's), manufactured by Hewlett Packard. The transducers were of Series 7DCDT, had a stroke of $\pm$0.250 in. (6.35mm) and an accuracy of 0.001 in. (0.025mm). They were mounted on the unloaded face of the chord, as shown in Fig. 2.6. The steel core of the transducer was connected to a twisted stainless steel wire of 0.015 in. (0.381mm) diameter. The wire was cemented to a 3/16 in.

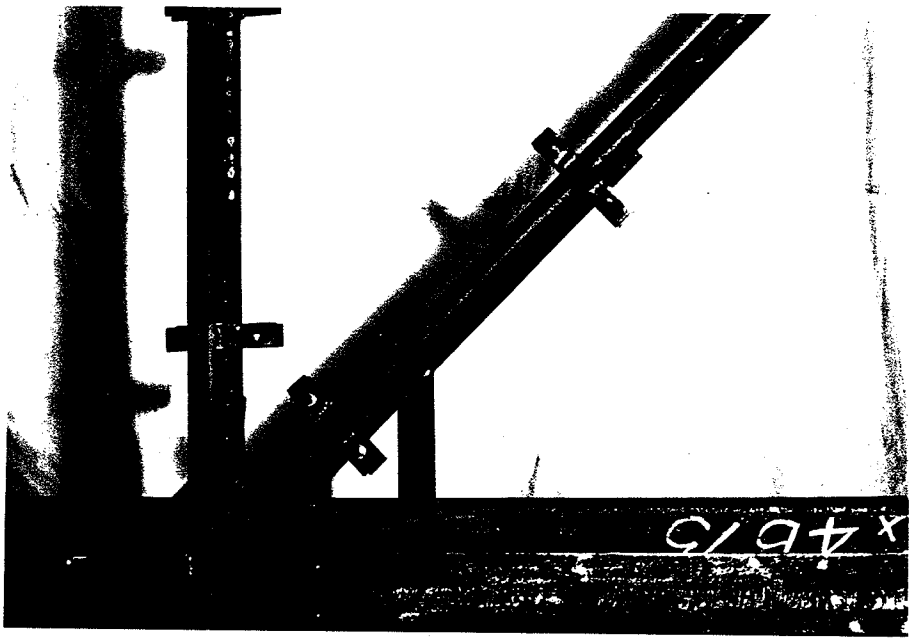

Fig. 2.3. Welding Jig

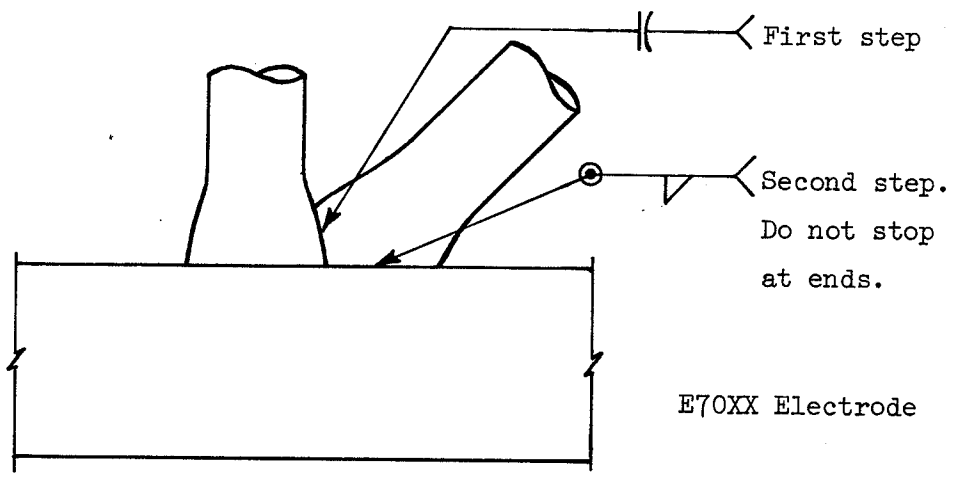

Fig. 2.4. Welding Specification

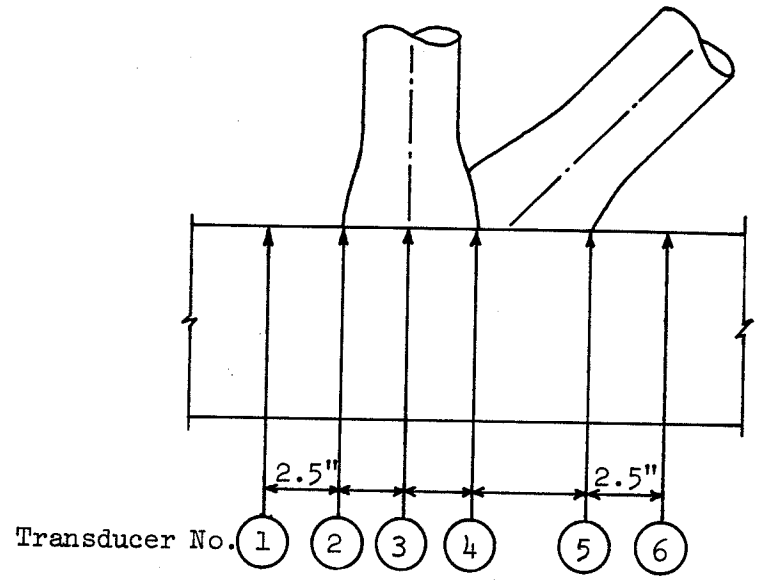

(a)

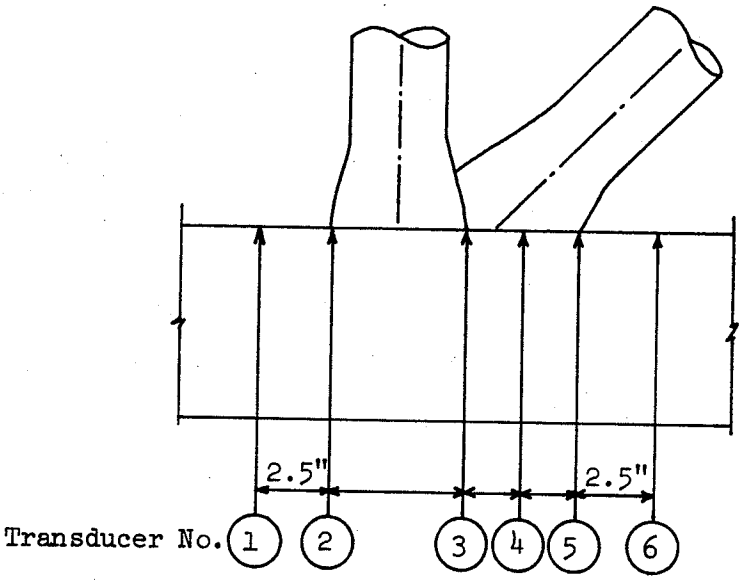

(b)

Fig. 2.5. Transducer Locations on Chord Wall

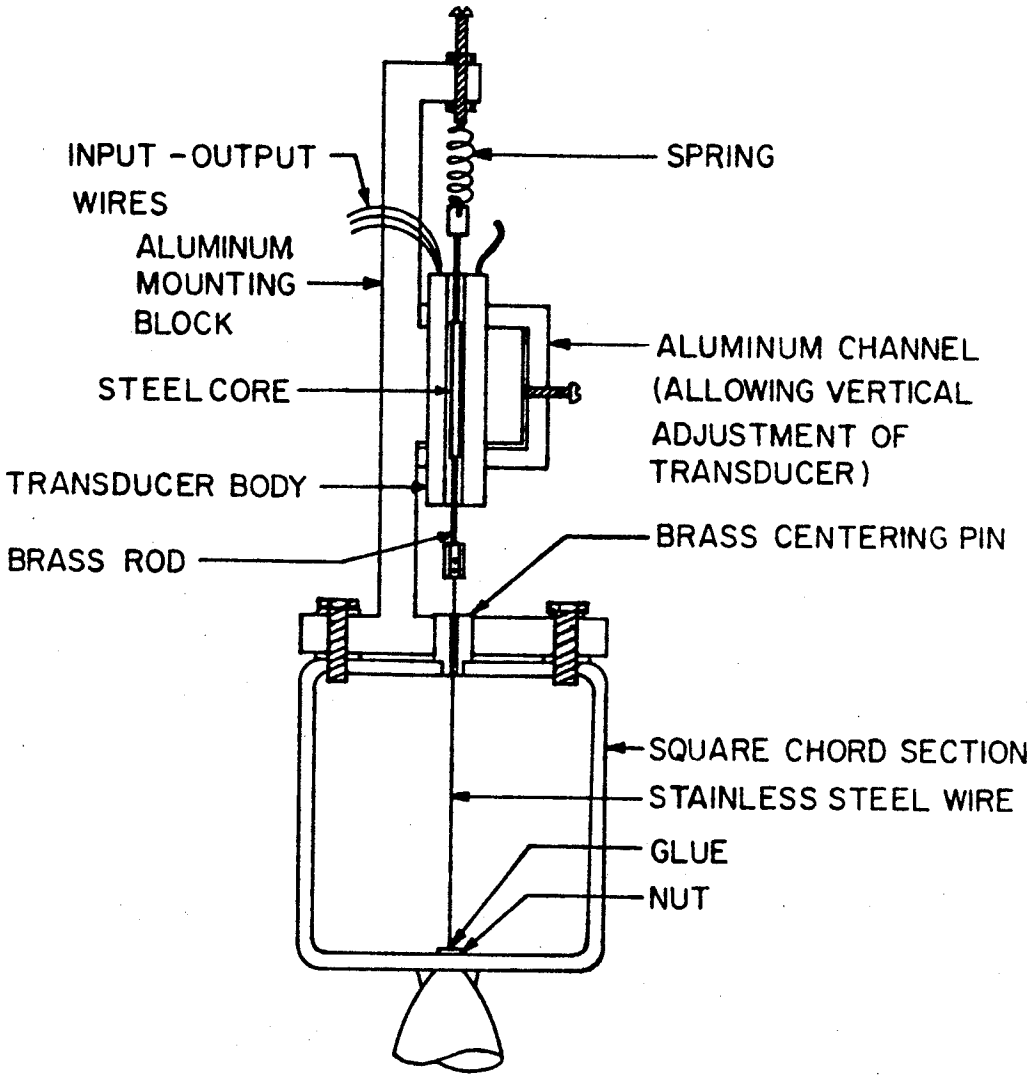

Fig. 2.6a. Transducer Assembly

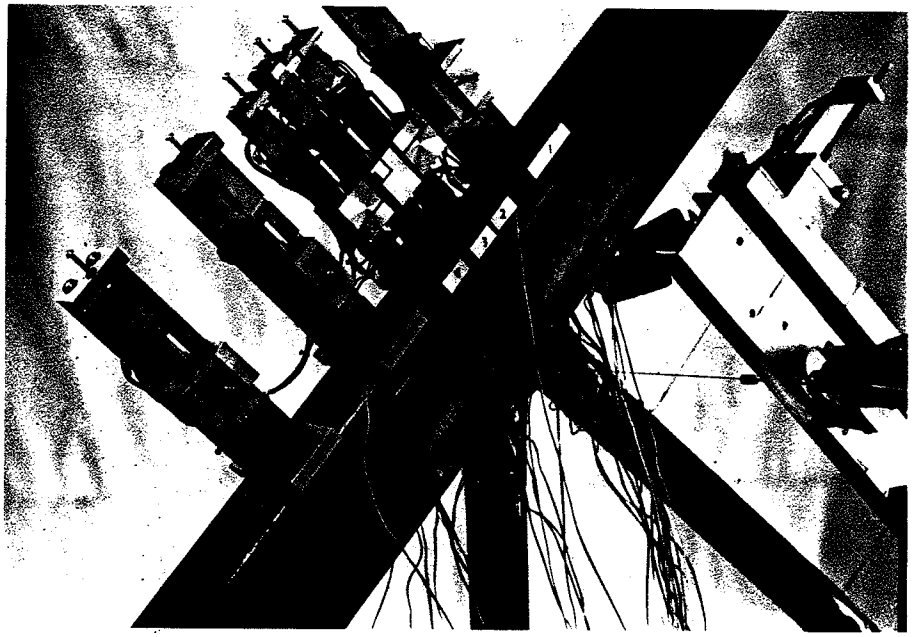

Fig. 2.6b. Transducer Assembly

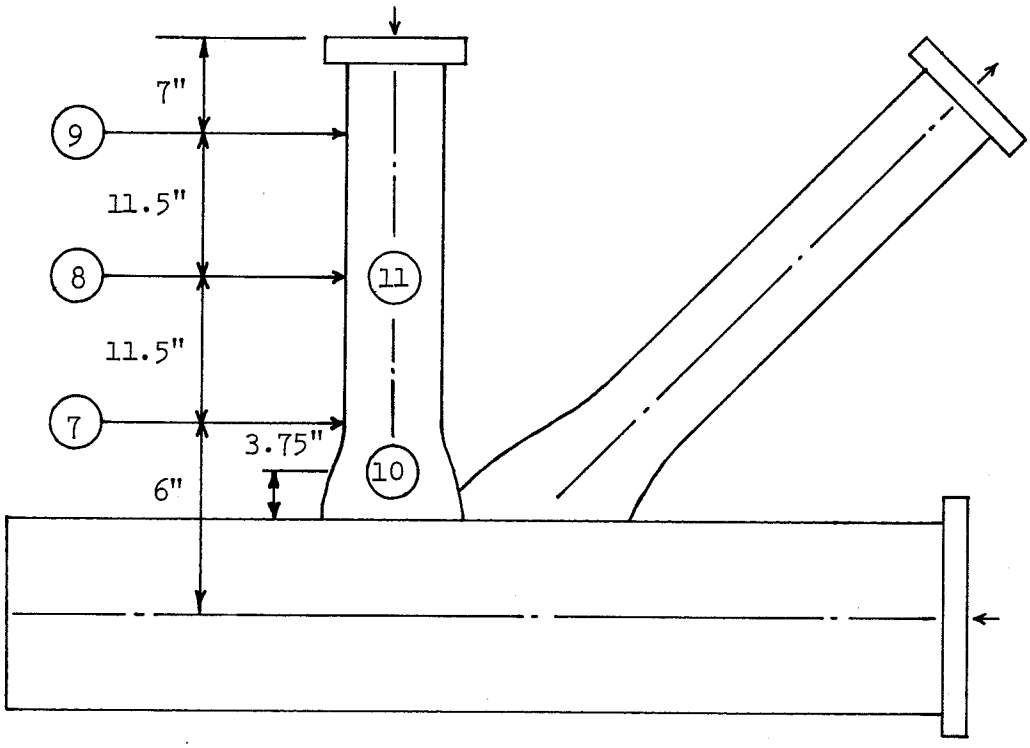

Fig. 2.7. Transducer Locations on Compression Web

(4.76mm) nut by KYOWA EP-18 strain gauge cement. After the interior of the loaded face of the chord was brushed and cleaned with acetone solution, the nut was passed through a 0.25 in. (6.35mm) hole in the chord wall by means of a small tube, and cemented to the chord face using a drop of CC-15A KYOWA strain gauge cement.

The lateral displacement of each compression web member was measured by using five transducers, three of which were located in the plane of the specimen to measure in-plane bending, and two in the perpendicular plane to measure out-of-plane bending. The locations and numbering of the transducers are shown in Fig. 2.7.

2.7. Strain Measurements

The strains at several points on the specimens were measured to determine strain and stress distribution and to check yielding of the materials. The locations of electrical resistance strain gauges are shown in Fig. 2.8. Gauges 1 to 4 were installed at the mid-length of most compression webs to detect bending and to check member force. Gauges 5 to 26 were installed on eight specimens (5A75, 1B75, 3B75, 4B75, 5B00, 5B50, 5B75, and 5C75). Only specimen 5B75 had a total of 42 gauges.

The strain gauges used were precision strain gauges manufactured by Micro-Measurements (M-M) and were of EA-06-250BG-120 type. They were 0.25 in. (6.35mm) long and had a strain limit of 5%.

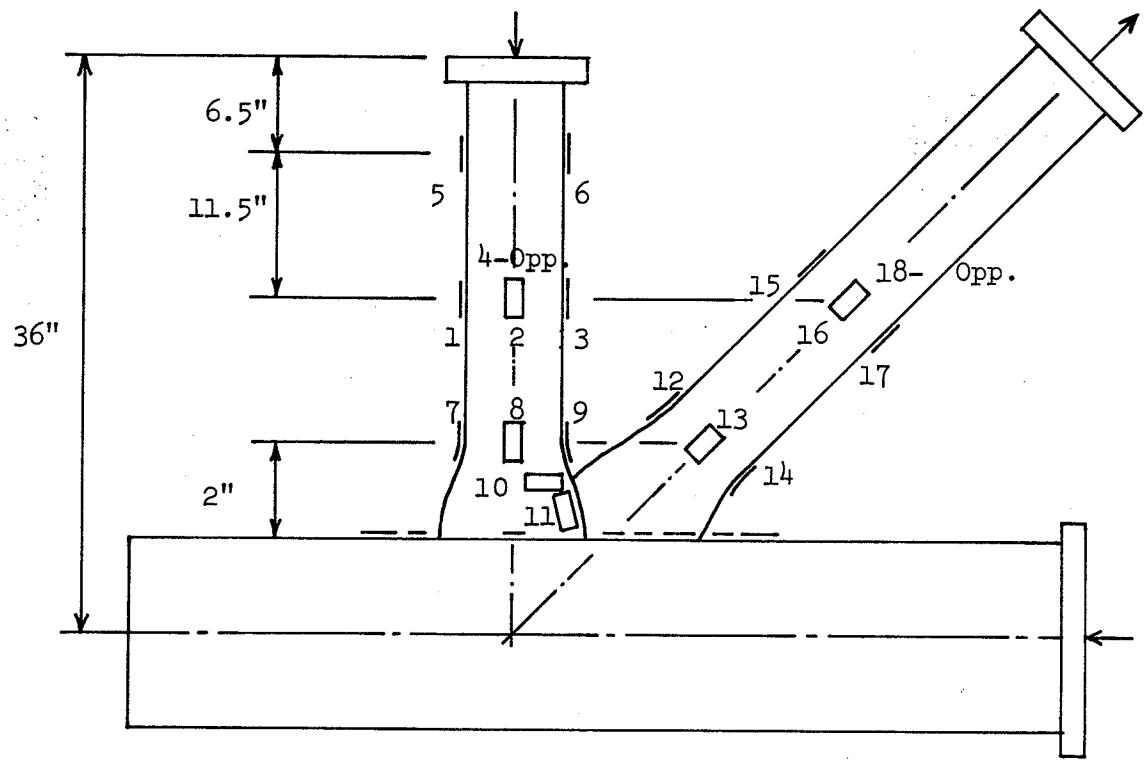

Side Elevation

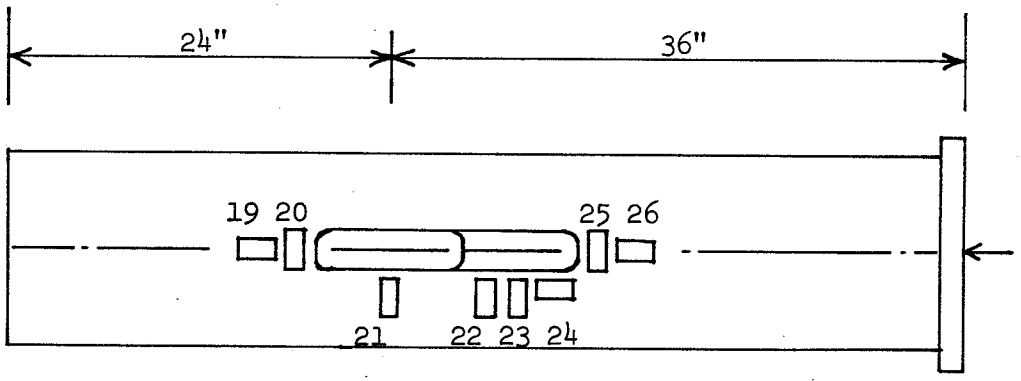

Plan

Fig. 2.8a. Strain Gauge Locations

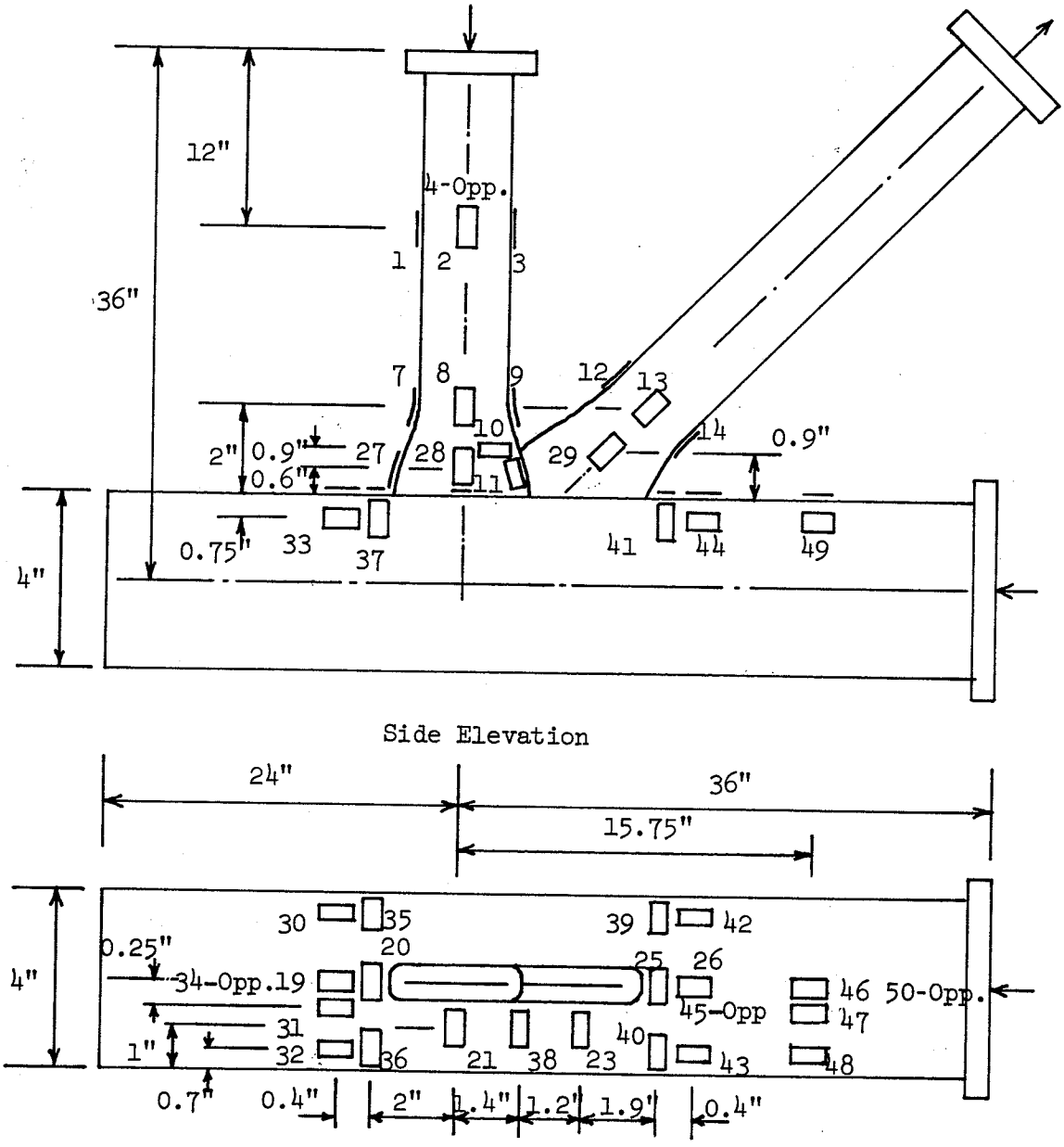

Fig. 2.8b. Strain Gauge Locations on Specimen 5B75

2.8. Loading Arrangement

The specimens were loaded in a loading frame, as illustrated in Fig. 2.9. Load was applied to the tension web, through a shaft calibrated as a load cell, by a 200-kip (890-kN) jack. The compression web and the chord were pin-supported to simulate points of inflection assumed to occur at the mid-lengths of the members. Eastwood et al.(1970) used this assumption in their tests and suggested that the conditions approximated those existing in a relatively stiff truss. They found that differences in support conditions (pins or rollers) did not significantly affect joint performance.

2.9. Data Acquisition

At a loading increment of about 1 kip (4.45 kN), or smaller when yielding occurred, the loads and the corresponding displacements and strains of the specimens were recorded in terms of voltages on a magnetic tape by using a Hewlett-Packard data acquisition system (model 9830A). The data were subsequently reduced and plotted by using the programmable calculator and printer of the system.

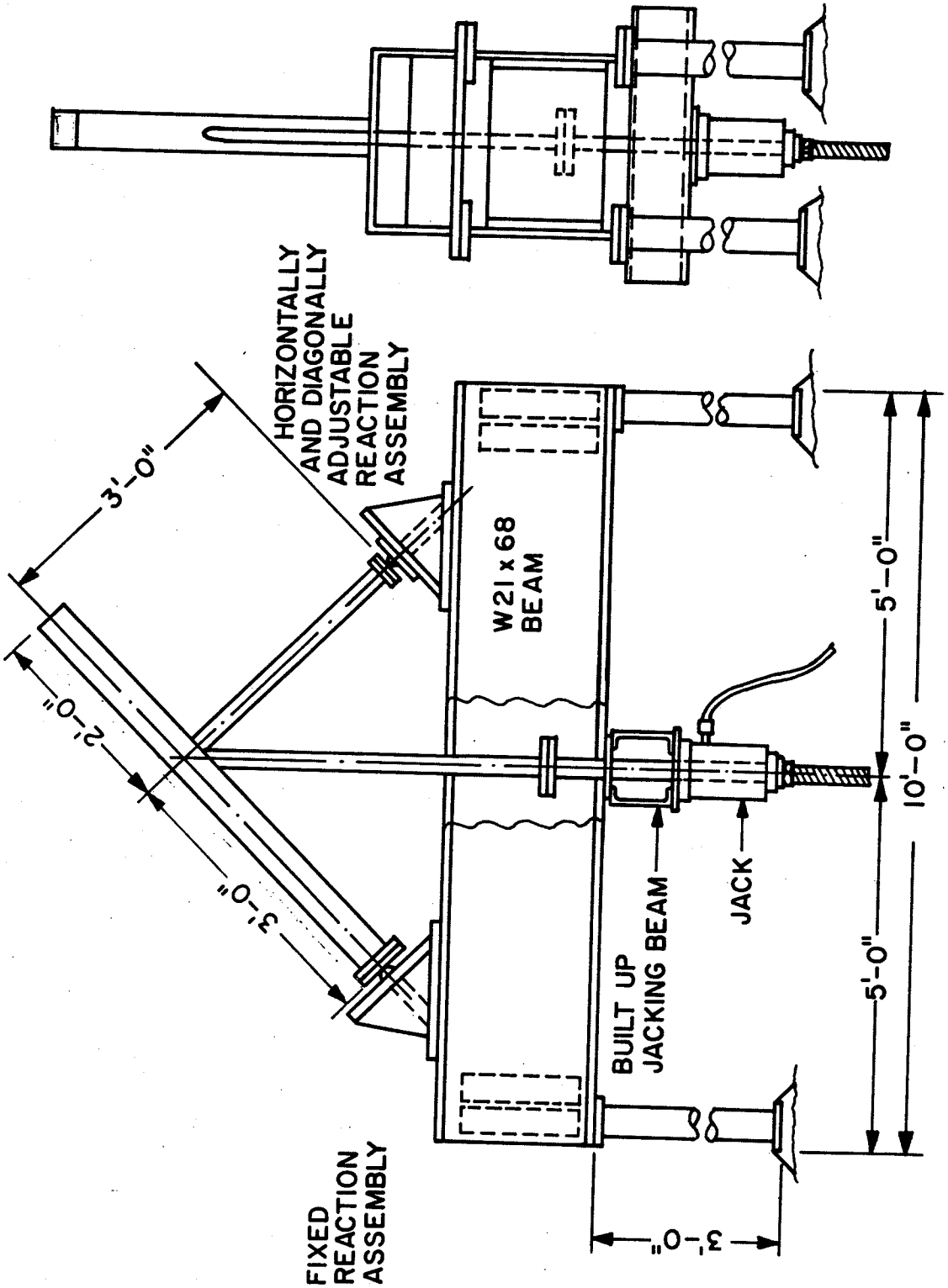

Fig. 2.9a. Loading Frame

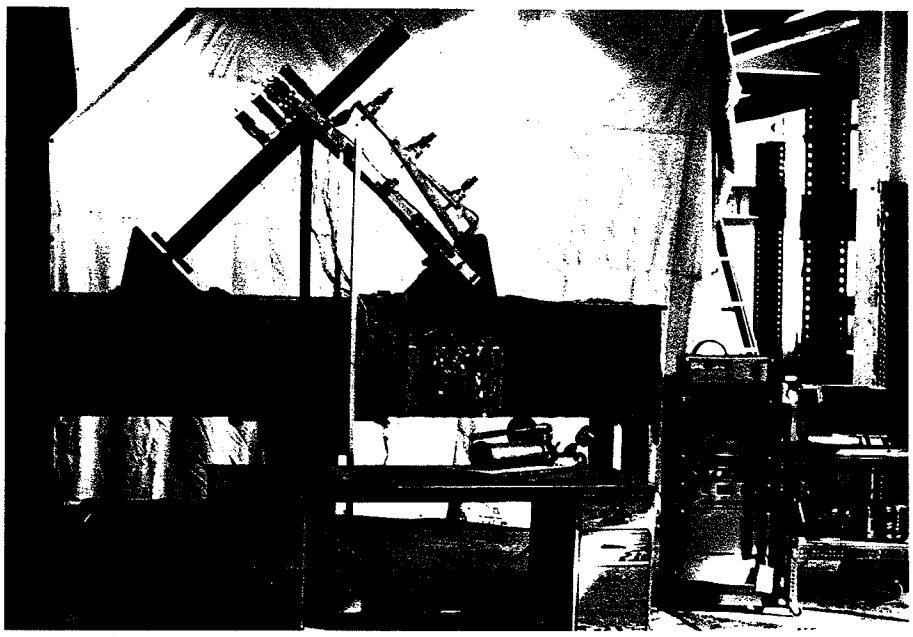

Fig. 2.9b. Loading Assembly

Chapter 3

TEST RESULTS AND DISCUSSION

Test results on cropped-web joints, presented and discussed in this chapter, include the load-deformation behavior, modes of failure, strength, and stiffness of the joints.

3.1. Local Deflections of Chord Faces

The behavior of a cropped-web joint is conveniently shown by load-deformation curves, as illustrated for specimen 3A50 in Fig. 3.1. The load shown is the measured load in the tension web, while the deformation is the local deflection of the loaded chord face. The curves were used to plot the deformed shapes of the chord face at different loads, as illustrated in Fig. 3.2.

Fig. 3.1 shows that the deformation increased linearly as the load was increased up to about 10 kips (44.5 kN), or an axial stress in the tension web of 16.5 ksi (114 N/mm^2). Then the deformation increased nonlinearly, gradually at first but very rapidly as the load approached the maximum (ultimate) load of 32.4 kips (144 kN), or 53.4 ksi, (368N/mm^2). After this load, the deformation increased further but with a drop in load so that equilibrium was maintained.

Figures 3.1 and 3.2 show that the deformations of the chord face under the web members were nonuniform, being relatively large near the extremities of the web members (transducers 2 and 5) and small near the lap (transducer 4). The chord wall and the web member ends appeared to

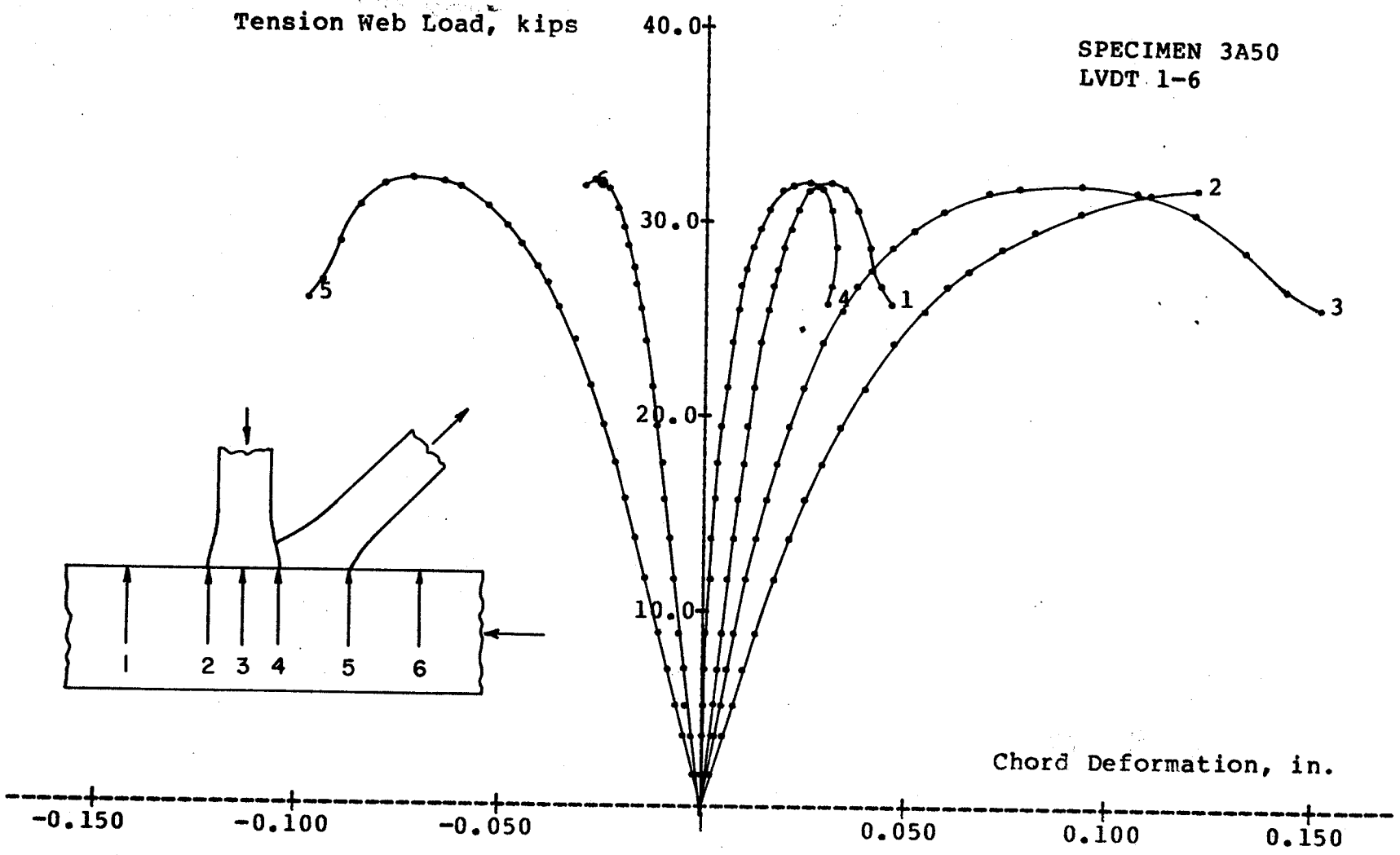

Fig. 3.1. Load-deformation Curves of Loaded Chord Face of Specimen 3A50

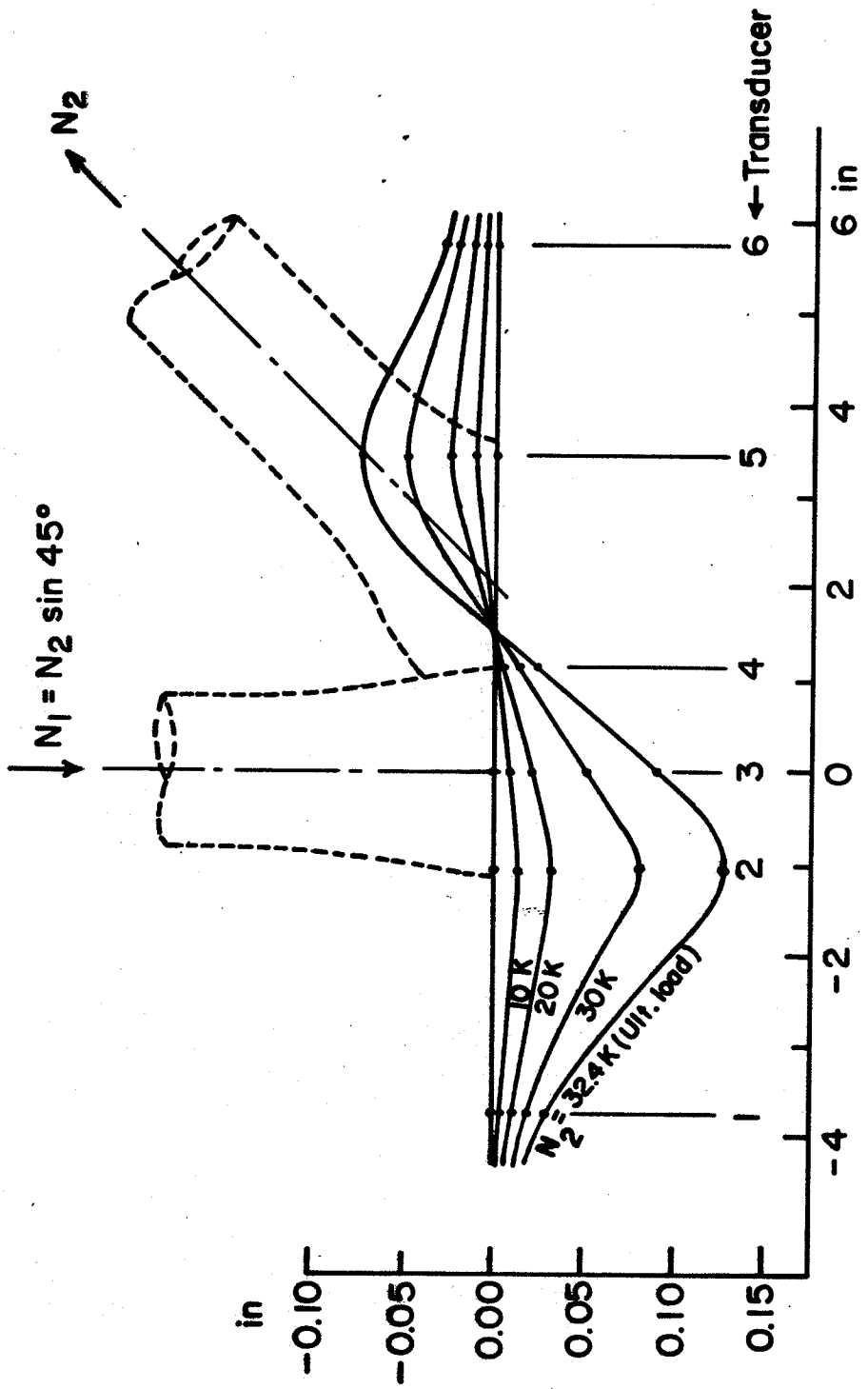

Fig. 3.2. Deformation of Loaded Chord Face of Specimen 3A50.

rotate as a unit about a pivotal point, because they were relatively flexible. The chord-wall rotation was caused by the force couple of the web members which usually had a moment arm between their axes along the chord face, as illustrated in Fig. 3.2.

The chord-wall rotation induced bending in the compression web member, which caused further bending in the chord face. These bending actions aggravated each other until the chord face failed by excessive deformation or the compression web failed by buckling. The bending of the compression web, usually away from the tension web, could induce a fracture failure in the tension web near the lap. A yielding failure in the tension web could also occur.

At the ultimate load of 32.4 kips in the tension web, the maximum local deflection in the chord wall of specimen 3A50 was about 0.125 in. (3.18 mm), which is 71% of the chord-wall thickness, or 3.1% of the chord width. Deformation of this order is considered large.

According to the CSA Standard S16-1969, the maximum allowable load in the tension web of specimen 3A50 was $0.6\sigma_{2e}A_2$ = 0.6 (63.3 ksi) (0.607 in^2) = 23.1 kips (103 kN). Assuming an effective length of six feet, the maximum allowable load of the compression web was $\sigma_{1a}A_1 = (\pi^2 E/1.92\ (KL/r)_1^2)A_1$ = (149000 ksi/131.4^2) (0.607 in^2) = 5.24 kips (23.3 kN). This corresponded to a load of (5.24 kips)/sin 45° = 7.41 kips (33.0 kN) in the tension web. As this load is smaller than the maximum allowable load in the tension web, it governed the design of the web members. At this load, the maximum local deflection of the chord wall was only 0.01 in. (0.254 mm), 5.7% of the chord-wall thickness or 0.25% of the chord

width. The local deflections along the web axes were even smaller and thus acceptable.

The deformed shapes of the chord face of specimen 3A50 were typical of those of other specimens having 50% or 75% laps. The deformed shapes of a zero-lap joint were also quite similar, although the web member ends appeared to rotate less as a unit, as illustrated using specimen 5B00 in Fig. 3.3.

When the ultimate load of 43.3 kips (193 kN) or 64.5 ksi (444 N/mm^2) was reached in the tension web of specimen 5B00, the maximum deformation in the chord was only about 0.037 in. (0.940 mm), 12% of the chord-wall thickness or 0.9% of the chord width. This illustrates that the local deflection of a zero-lap joint can be acceptably small when t_0/b_0 of the chord is considerably large. In this case, t_0/b_0 was equal to 0.0775.

The local deflections of the chord faces were decreased by an increase in overlap, as more load was directly transferred between the webs instead of through the chord face. This is illustrated in Fig. 3.4, which shows the maximum deformations of specimens 5A00, 5A50, and 5A75. The specimens were similar except that their overlaps were zero, 50%, and 75%, respectively.

The local deformations of the loaded chord faces were also decreased by an increase in t_0/b_0. This is illustrated in Fig. 3.5, which shows the deformations of specimens 3C75, 4C75, and 5C75, at a load of 60 kips (267 kN) in the tension web. The specimens were similar

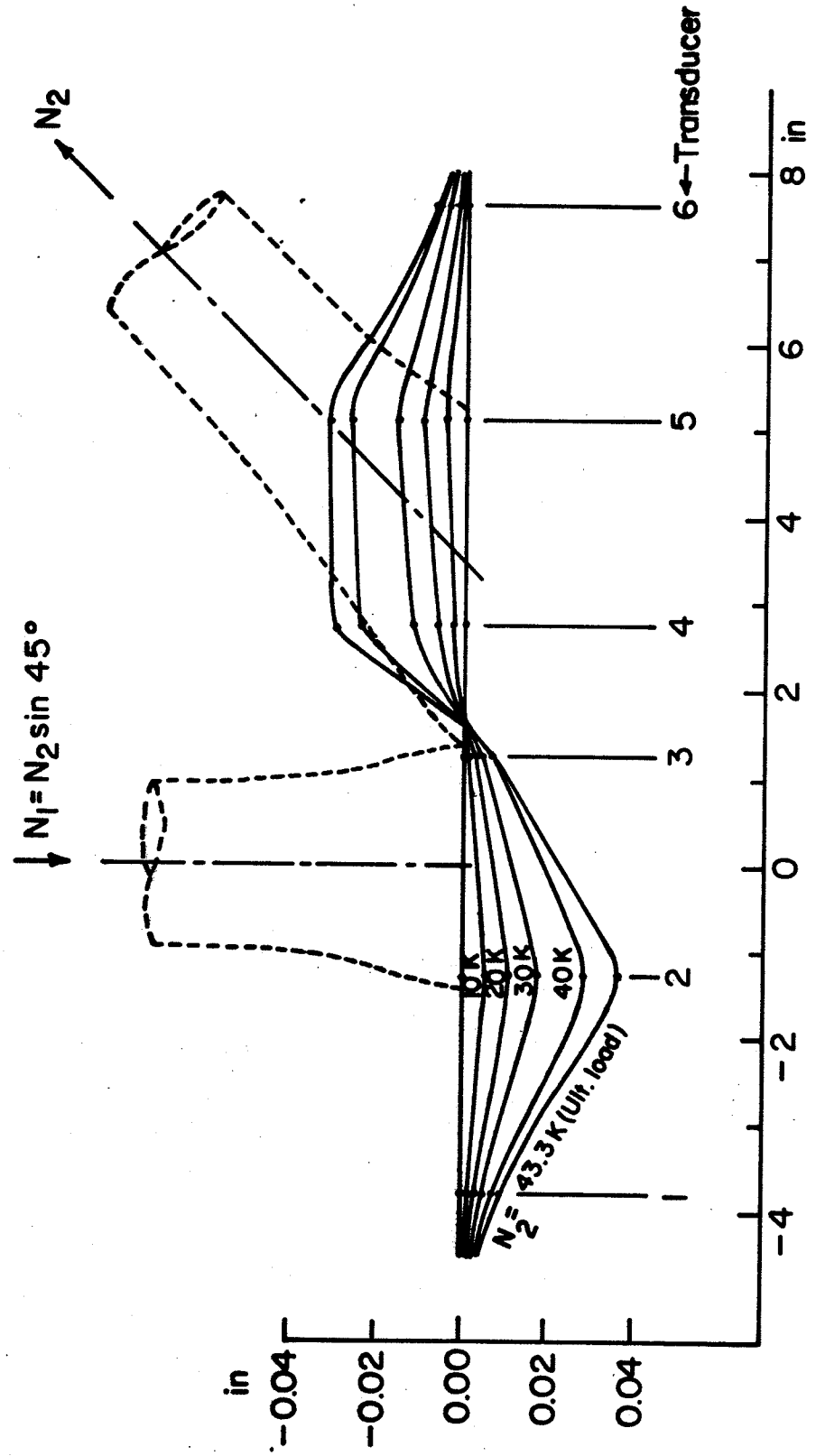

Fig. 3.3. Deformation of Loaded Chord Face of Specimen 5B00.

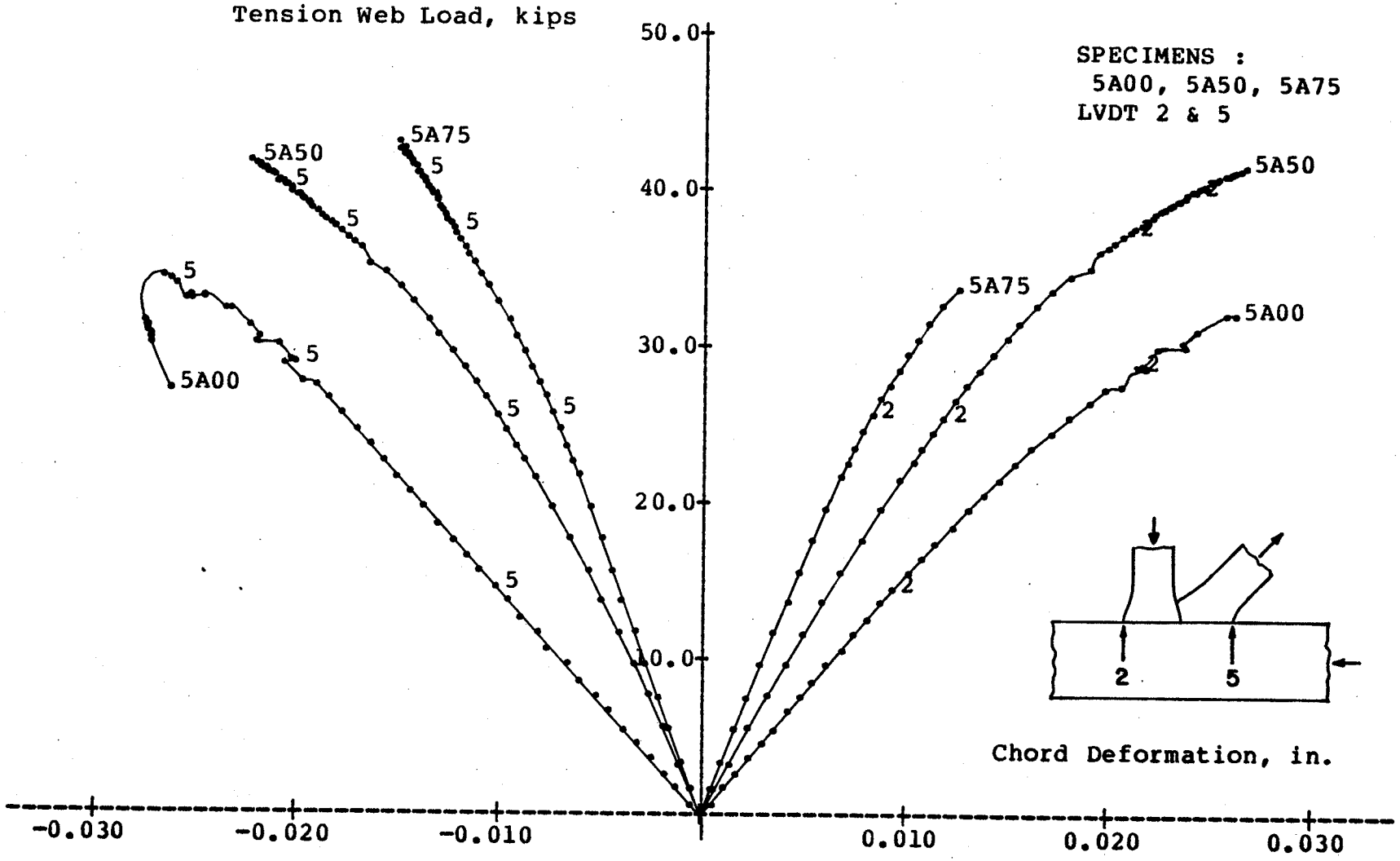

Fig. 3.4 Maximum Deformations of Loaded Chord Faces of Specimens 5A00, 5A50, and 5A75

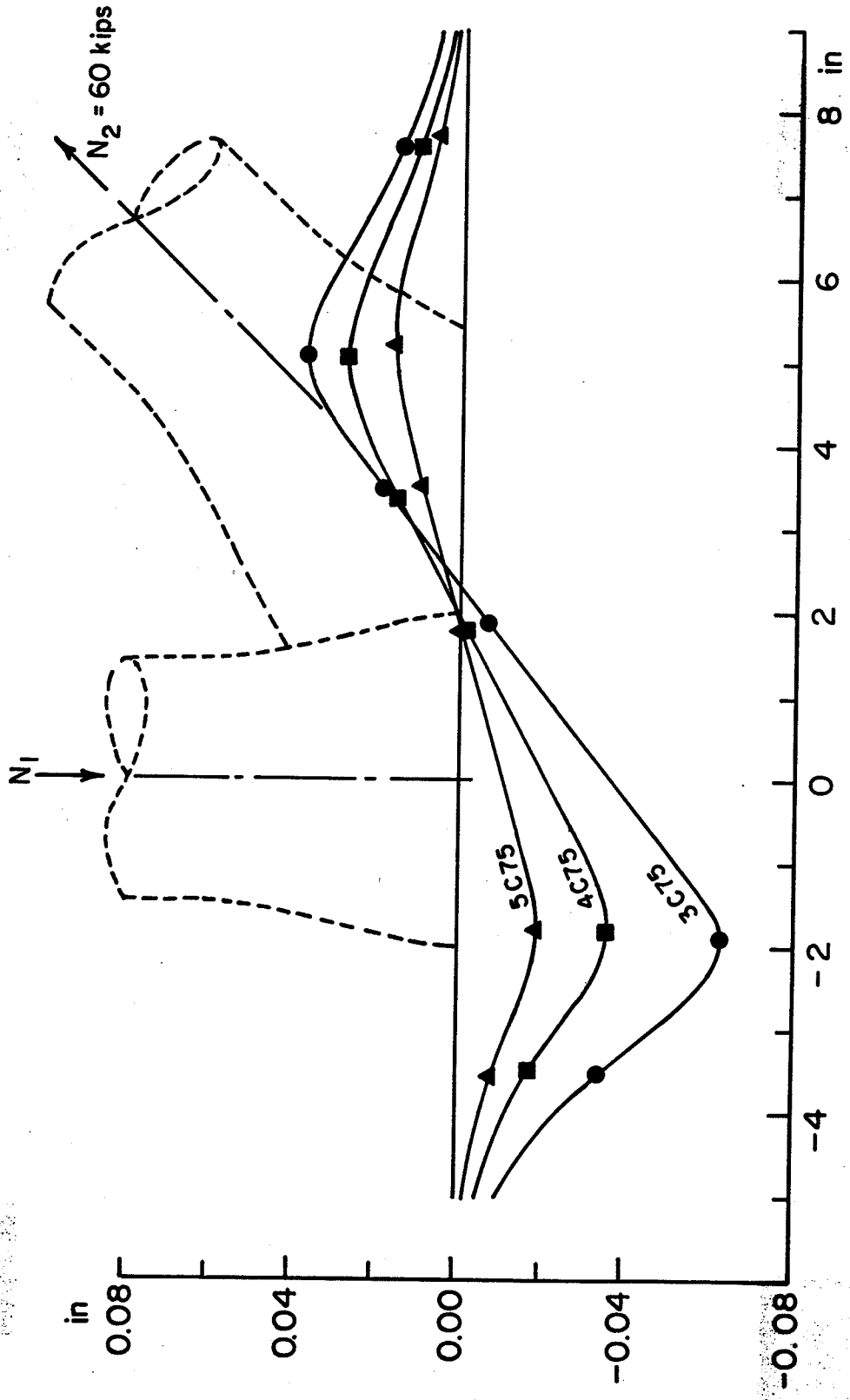

Fig. 3.5. Deformations of Loaded Chord Faces of Specimens 3C75, 4C75, and 5C75.

but their t_0/b_0 were 0.0442, 0.0600, and 0.0782, respectively. Finally, the local deformations of the chord faces were decreased by an increase in d/b_0, which allowed the loads on the chord faces to be distributed more favorably. This is illustrated in Fig. 3.6, using specimens 4A50, 4B50, and 4C50, which were similar but had d/b_0 equal to 0.418, 0.475, and 0.720, respectively.

The load-deformation characteristics of the joints can be summarized in terms of their stiffnesses; this is presented in Section 3.8.

3.2. Buckling of Compression Web Members

Because of the rotational deformation of the loaded chord face, the compression web tended to bend when it was loaded. If the web was slender, buckling usually occurred when the ultimate load was reached. This is illustrated in Fig. 3.7, which shows the load-deflection curves of the compression web of specimen 3A50. When the load was small, the bending in the web was small. When the ultimate load was reached, the bending became very large and buckling occurred. After this, the bending increased as the load decreased.

Buckling of the compression webs of the specimens always occurred in the plane of the specimens. This is because the moments at the ends of the webs were in this plane. In addition, the support conditions tended to prevent out-of-plane buckling. For an actual truss, the compression webs could also buckle out of the plane of the truss.

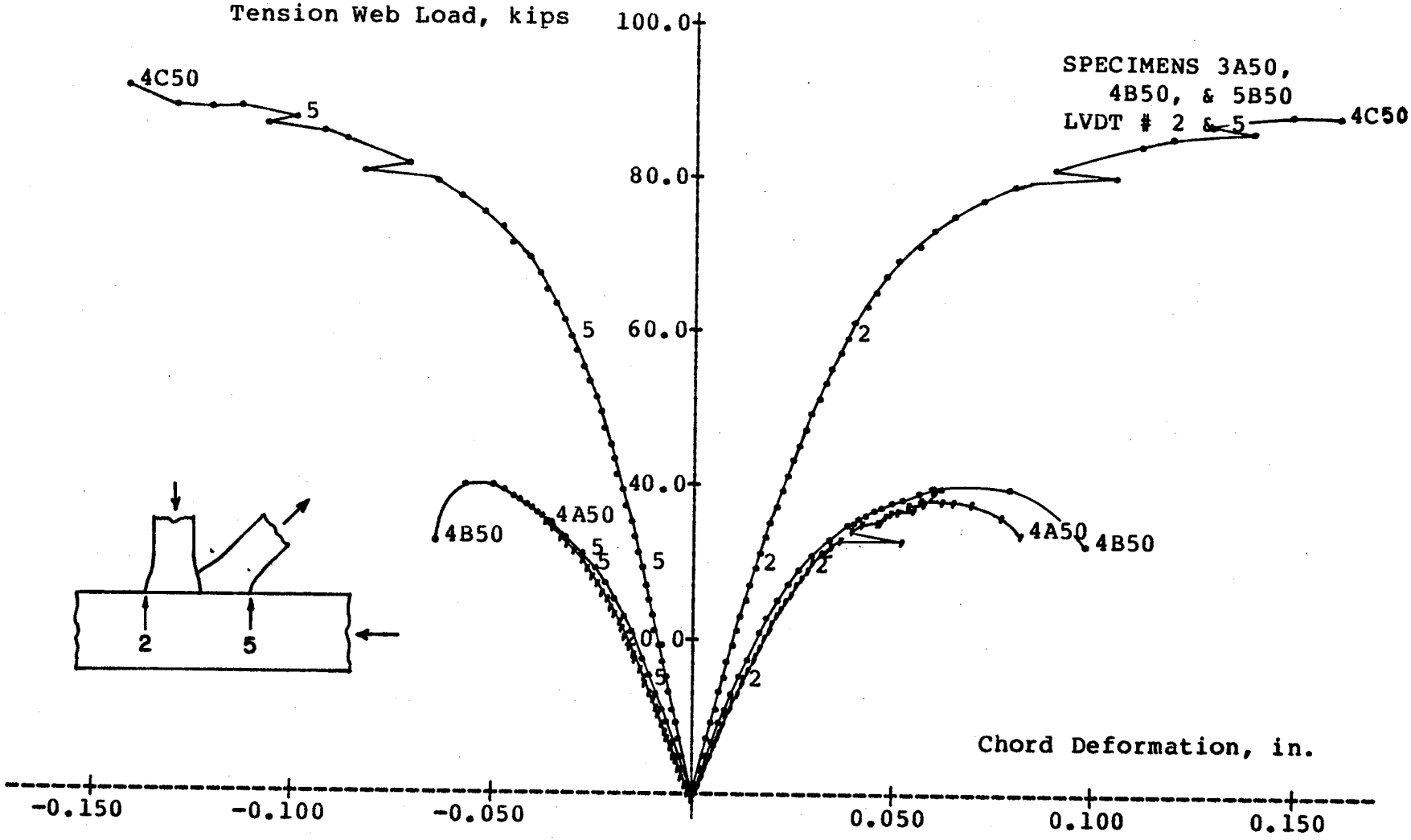

Fig. 3.6. Maximum Deformations of Loaded Chord Faces of Specimens 3B50, 4B50, and 5B50

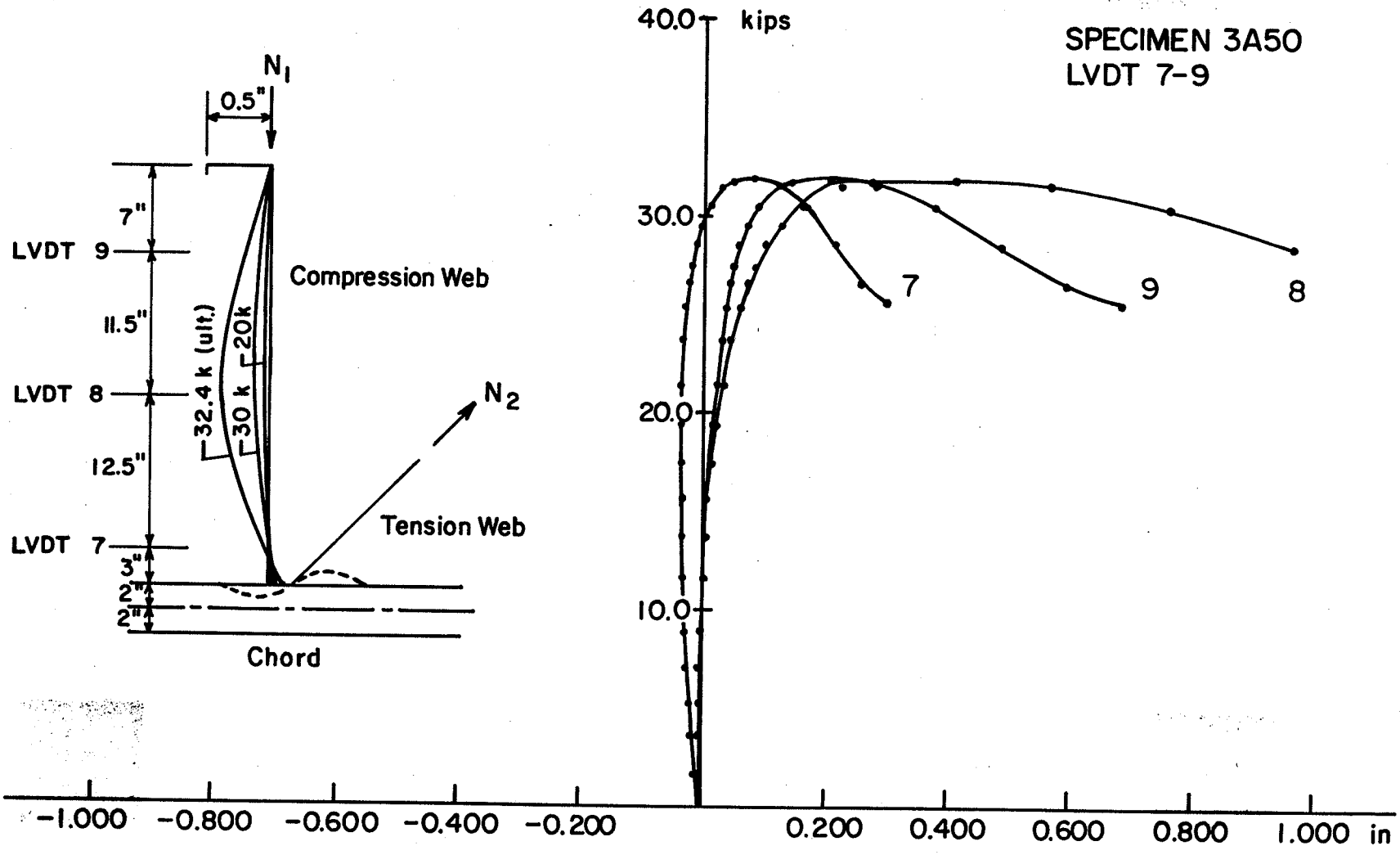

Fig. 3.7 Load-deflection Curves of Compression Web Member of Specimen 3A50.

The direction of bending and buckling was usually away from the tension web, as illustrated in Fig. 3.7, because the end moment was in that direction.

If the compression webs were relatively stocky, they deflected but usually did not buckle at the ultimate loads.

3.3. Strains of Chord Faces

Because of local bending, the strains of the chord faces near the joints were much larger than those at some distance away. This is illustrated in Fig. 3.8, which shows longitudinal strains of specimen 5B75 at a load of 20.1 kips (89.4 kN) or a stress of 30 ksi (207 N/mm^2) in the tension web. The maximum strains at section B, near the joint, were as large as 1.6 times the maximum strains at section C, at 10.85 in. (276 mm) away. The strains at section C were rather uniform and agreed well with the average axial strain calculated by dividing the axial stress by Young's modulus.

Fig. 3.9 illustrates strains in the transverse direction of the chord faces of specimen 5B75. The transverse strains were highly non-uniform and were more critical than the longitudinal strains. The maximum transverse strain was about six times as large as the corresponding longitudinal strain, and was smaller than the yield value (0.17%).

A plot of transverse strains of the loaded chord face near the weld of specimen 5B75 against the load in the tension web is shown in Fig. 3.10. The locations of the strain gauges have been shown in Fig. 2.8b. The strains were relatively large near the extremities of the

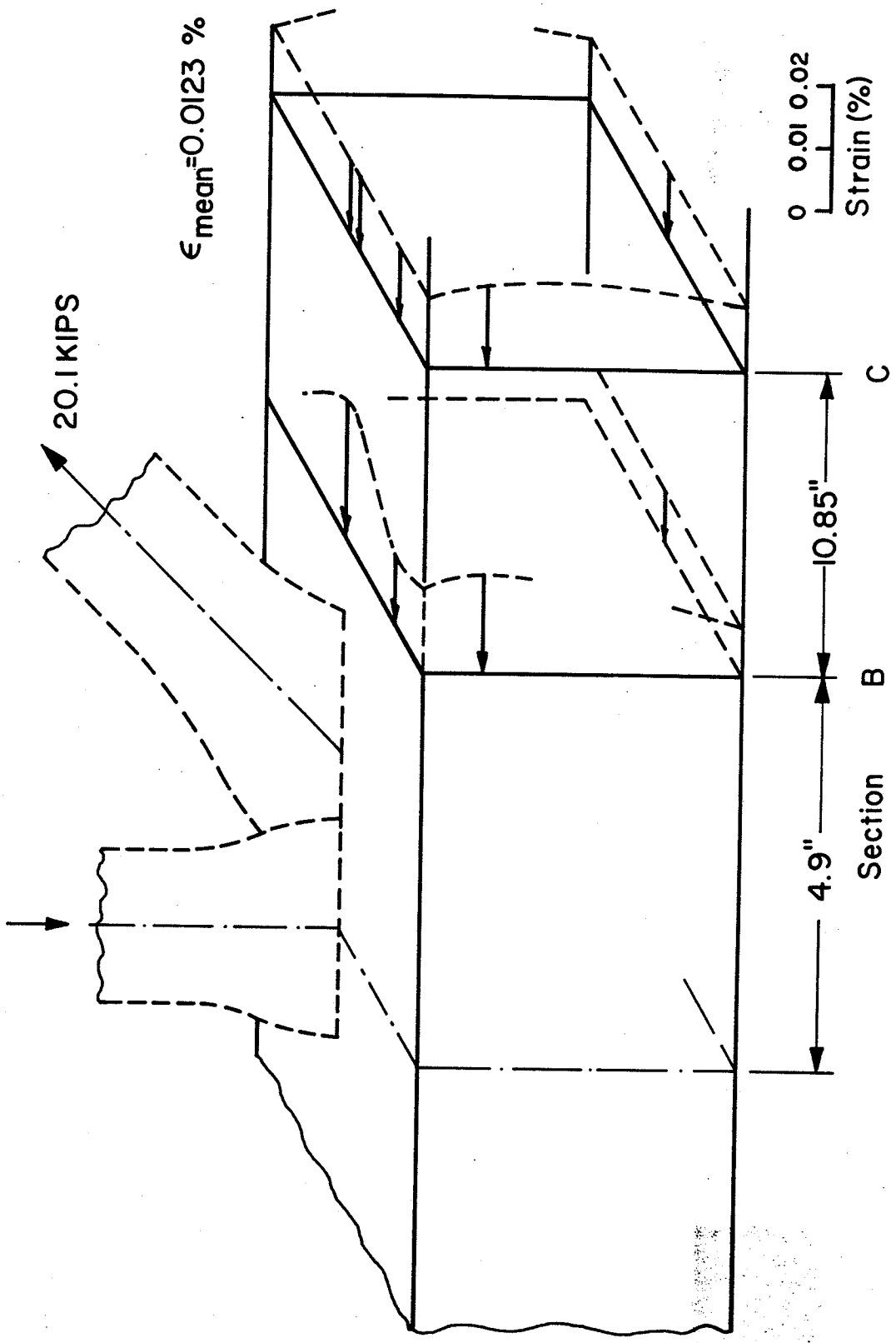

Fig. 3.8. Longitudinal Strains on Chord Faces of Specimen 5B75

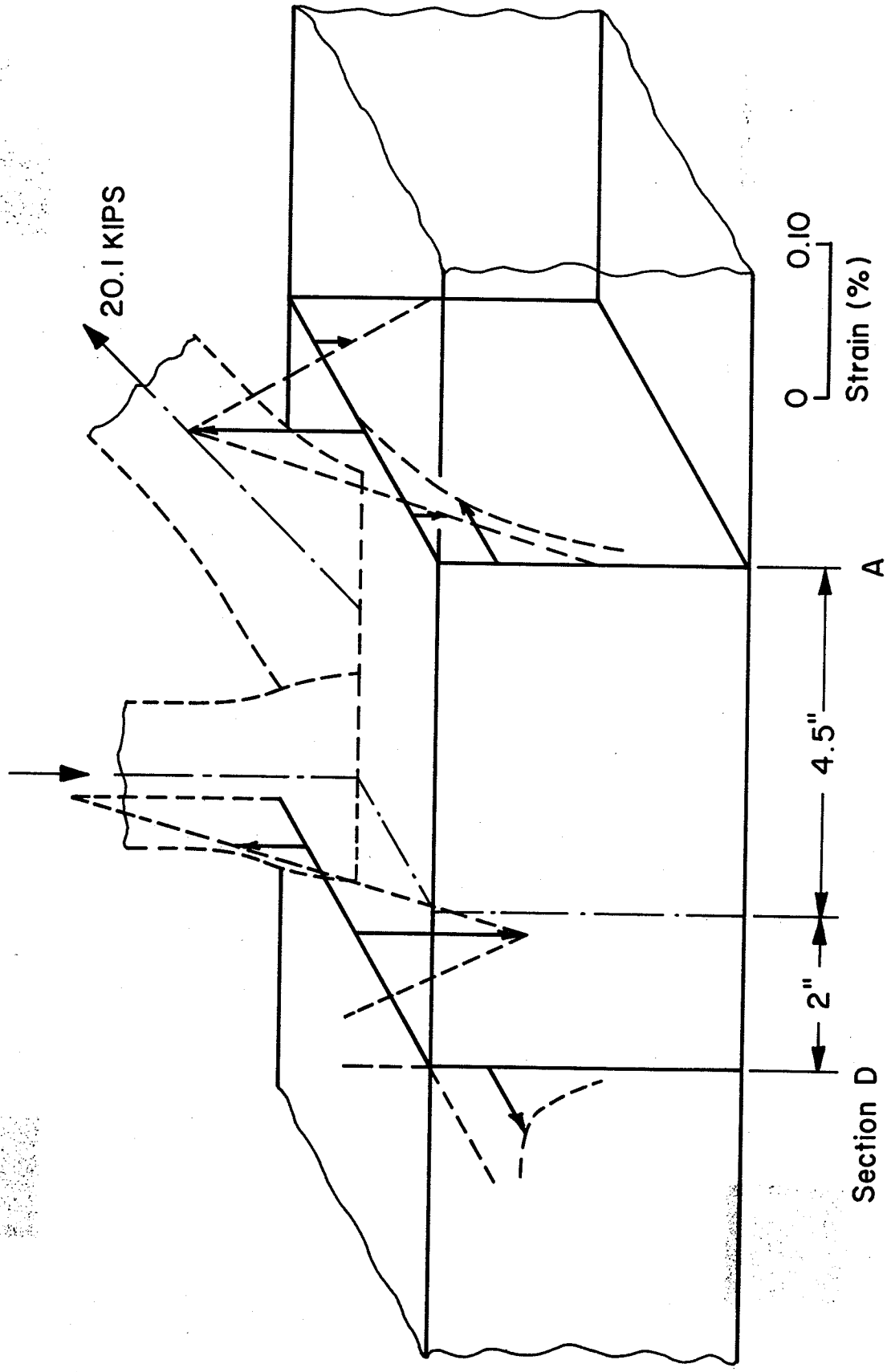

Fig. 3.9. Transverse Strains on Chord Faces of Specimen 5B 75

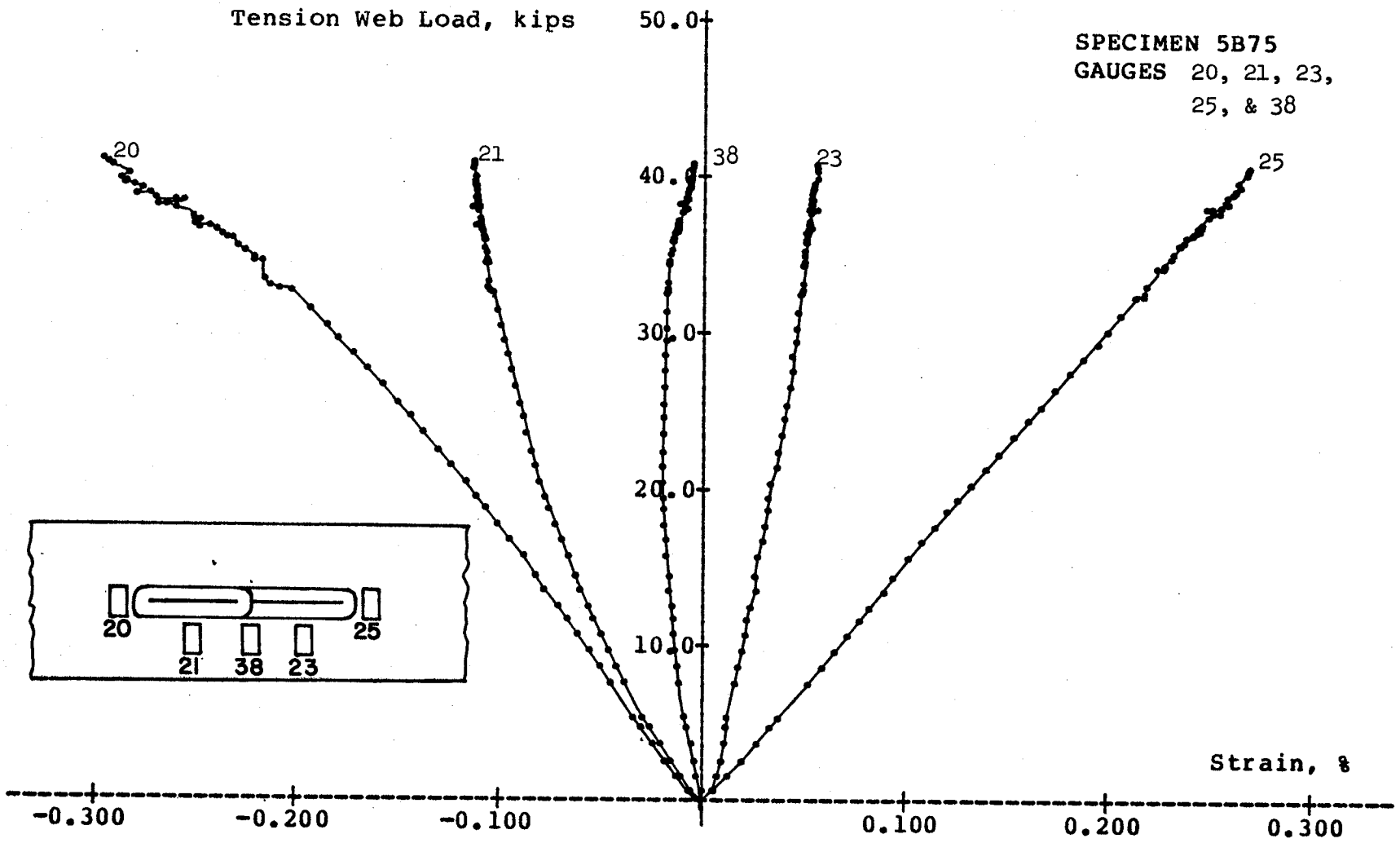

Fig. 3.10. Loads vs. Transverse Strains near the Weld on Loaded Chord Face of Specimen 5B75

webs and small near the overlap. At the working load of the tension web (about 20.1 kips), the strains were approximately linear, because the stiffness of the chord wall (t_0/b_0) was large. Therefore, a linear analysis may still be valid up to this load.

The transverse strains of the loaded chord face were usually larger than those of other faces. As a result, plastic deformation often concentrated on the loaded face. Thus the strength of the joint could significantly depend on the thickness and width of this face.

As t_0/b_0 was decreased, the maximum transverse strains of the loaded chord face were increased and became non-linear at a low load. This is illustrated in Fig. 3.11, which shows the maximum transverse strains of specimens 3B75, 4B75, and 5B75. At the working load of the tension web (20.1 kips or 89.4 kN), only the strains of specimen 3B75 exceeded the nominal yield strain of 0.17% that corresponds to the nominal yield stress of 50 ksi (344 N/mm^2) for the joint materials. It may be estimated from the Figure that, at the working load of these webs, t_0/b_0 of larger than 0.05 probably results in maximum strains which are smaller than the yield strain.

The transverse strains of the loaded chord faces of specimens 5B00, 5B50, and 5B75 are shown in Fig. 3.12. At the working load of 20.1 kips, the strains were approximately linear and smaller than the yield strain. This shows that a zero-lap joint, which is easier to fabricate than a lap joint, has acceptable deformations at the working load if t_0/b_0 is relatively large. In this case, t_0/b_0 was larger than 0.07.

The strains of the chord face near the joint of specimen 1B75

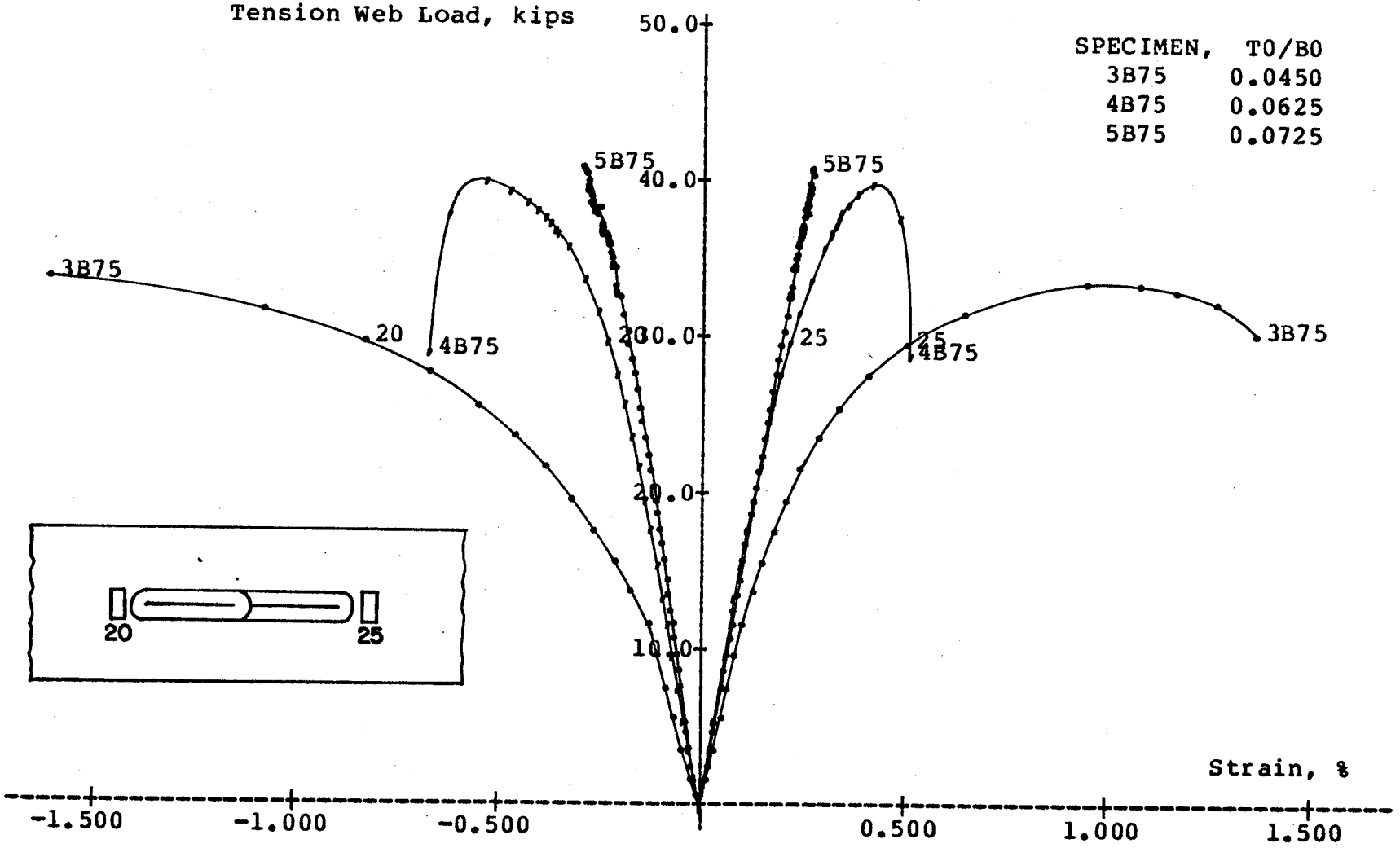

Fig. 3.11. Transverse Strains on Loaded Chord Faces of Specimens 3B75, 4B75, and 5B75

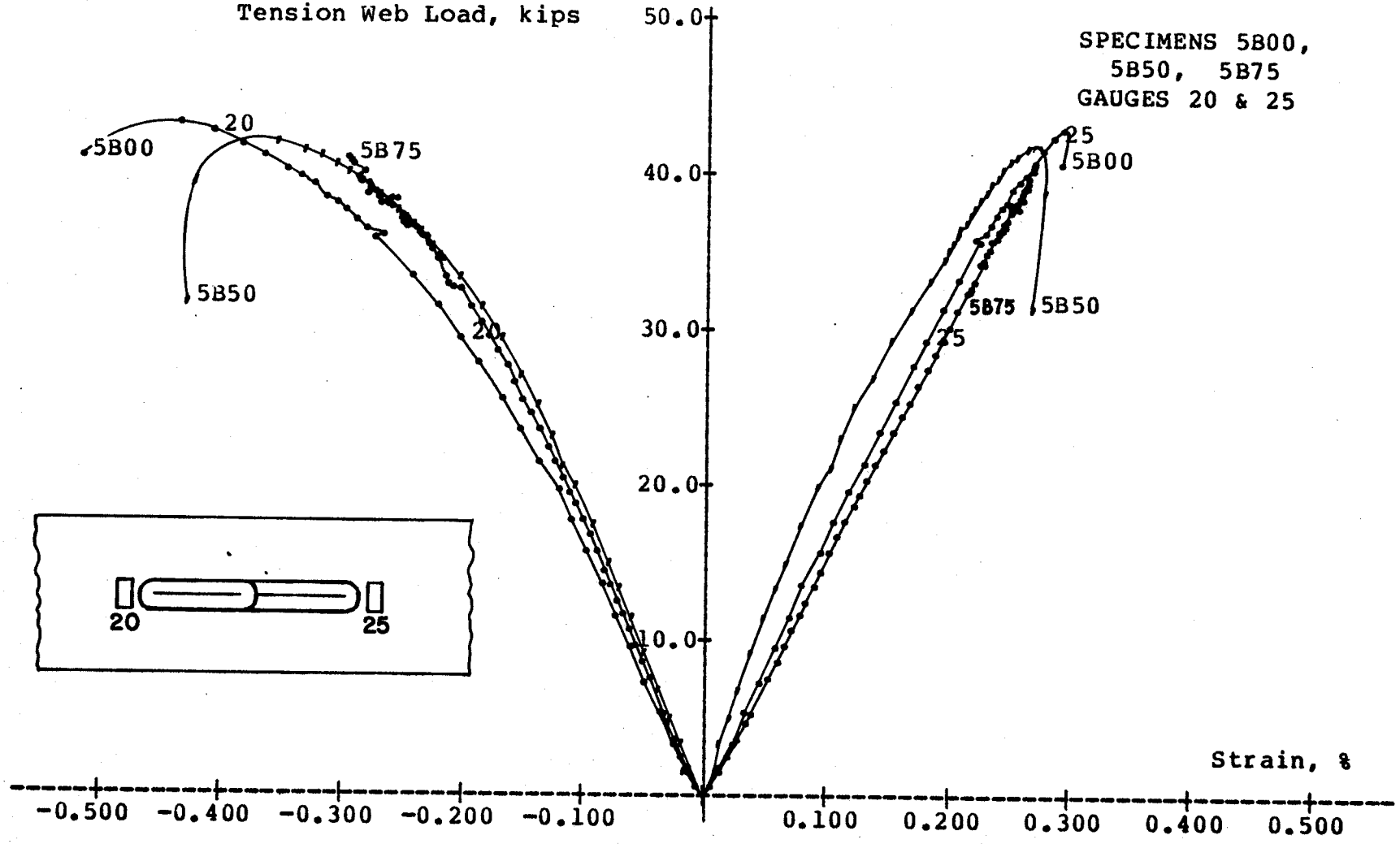

Fig. 3.12. Transverse Strains on Loaded Chord Faces of Specimens 5B00, 5B50, and 5B75

are shown in Fig. 3.13. The specimen had t_0/b_0 of only 0.0313 and a working load in the tension web of 59.9 kips (267 kN). At this load, the chord face had very large deformations. The ultimate load of the specimen was only 80.7 kips (358 kN), which corresponded to an axial stress of 40.4 ksi (278 N/mm^2) in the tension web. Consequently, the working load in the tension web of such a specimen, which had a small t_0/b_0, should be reduced.

3.4. Strains in Compression Web Members

The longitudinal strains at a cross-section of a compression web usually were non-uniform, indicating bending or stress concentration in the web. This is illustrated in Fig. 3.14, which shows such strains for specimen 5B75 at a tension web load of 20.1 kips (89.4 kN). The strain near the lap was relatively large; it had the order of the yield strain and was much larger than the strain on the opposite side. The strain distributions at different sections on the compression web show that the web bent away from the tension web. Although out-of-plane bending was larger than in-plane bending in this case, the latter usually predominated if buckling occurred.

The average of the strains at the top section shown in Fig. 3.14 was 0.068%. In comparison, the average axial strain calculated by dividing the axial stress by Young's modulus was (0.707 x 20.1 kips)/ (0.671 $in.^2$ x 29000 ksi) = 0.073%, a difference of 8%.

When a compression web buckled, the difference in longitudinal strains on the opposite sides of the web in the plane of buckling became

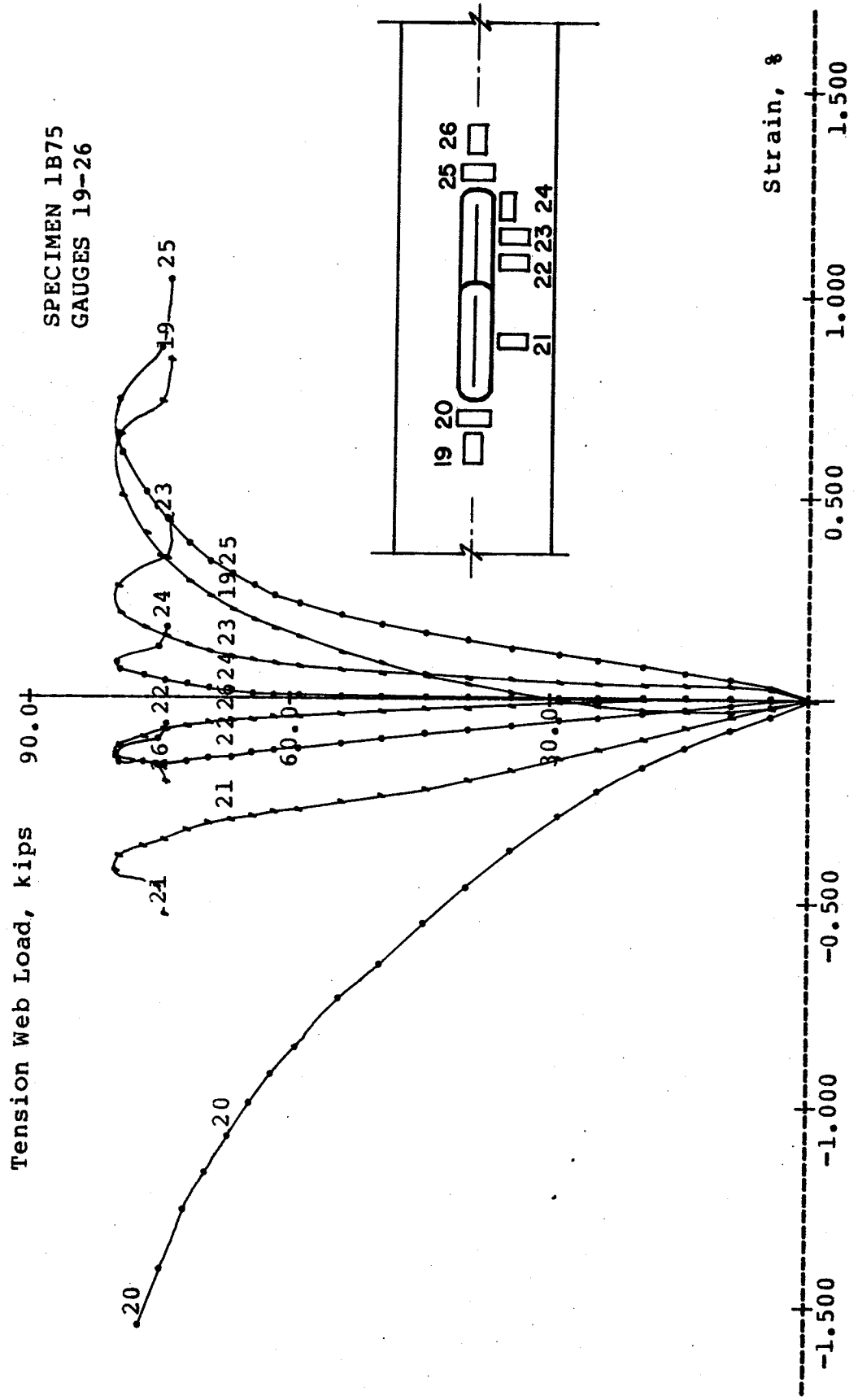

Fig. 3.13. Strains on Loaded Chord Face of Specimen 1B75

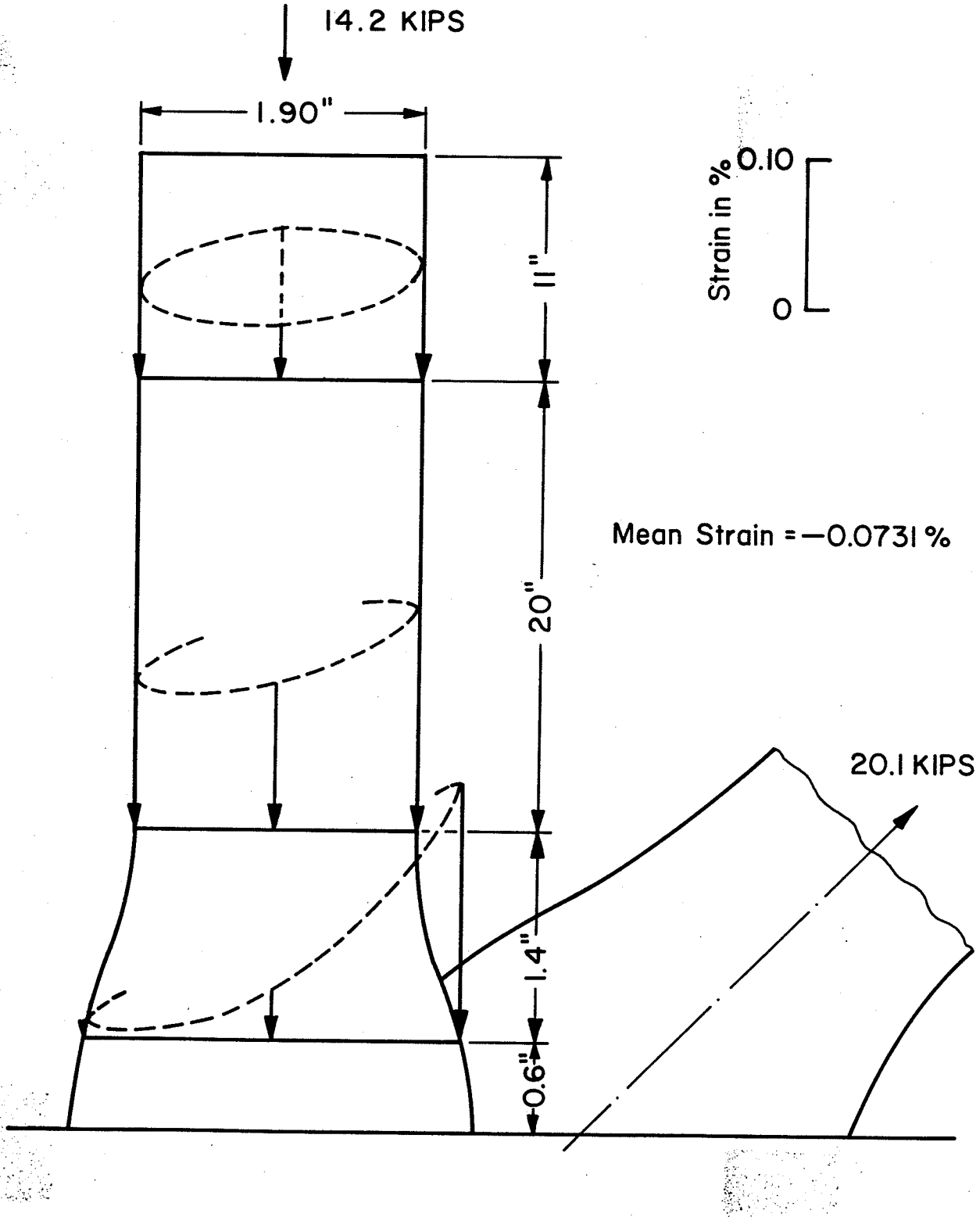

Fig. 3.14. Longitudinal Strains on Compression Web Member of Specimen 5B75.

very large. This is illustrated by the strains at the mid-length of the compression web of specimen 5B50 in Fig. 3.15. Initially, the strain differences of the opposite faces were relatively small and increased steadily with the load. When the ultimate load was reached, the difference in strains of gauges 1 and 3, which were in the plane of the specimen, became very large. The difference in strains of gauges 2 and 4, which were in the plane perpendicular to the plane of the specimen, remained approximately constant. This indicates that the compression web buckled in the plane of the specimen and in the direction away from the tension web. Such buckling behavior was typical of most other specimens.

The direction of bending at the mid-length of the compression web was sometimes reversed at the ultimate load. This happened to specimens 4C75, 5C50, and 5C75, all of which had large t_0/b_0, d/b_0, and laps. It is illustrated by the strains of gauges 1 and 3 of specimen 5C75 in Fig. 3.16. When the ultimate load was reached, the strains of the compression web were still smaller than the yield value (0.17%), although the tension web and the loaded chord face had yielded locally and excessively.

When t_0/b_0 was small, the compression web near the lap usually bent and buckled away from the tension web, as the chord face was deformed plastically. This is illustrated in Fig. 3.17, which shows the longitudinal strains near the lap of the compression web of specimen 1B75.

On the other hand, when t_0/b_0 was large, the compression web

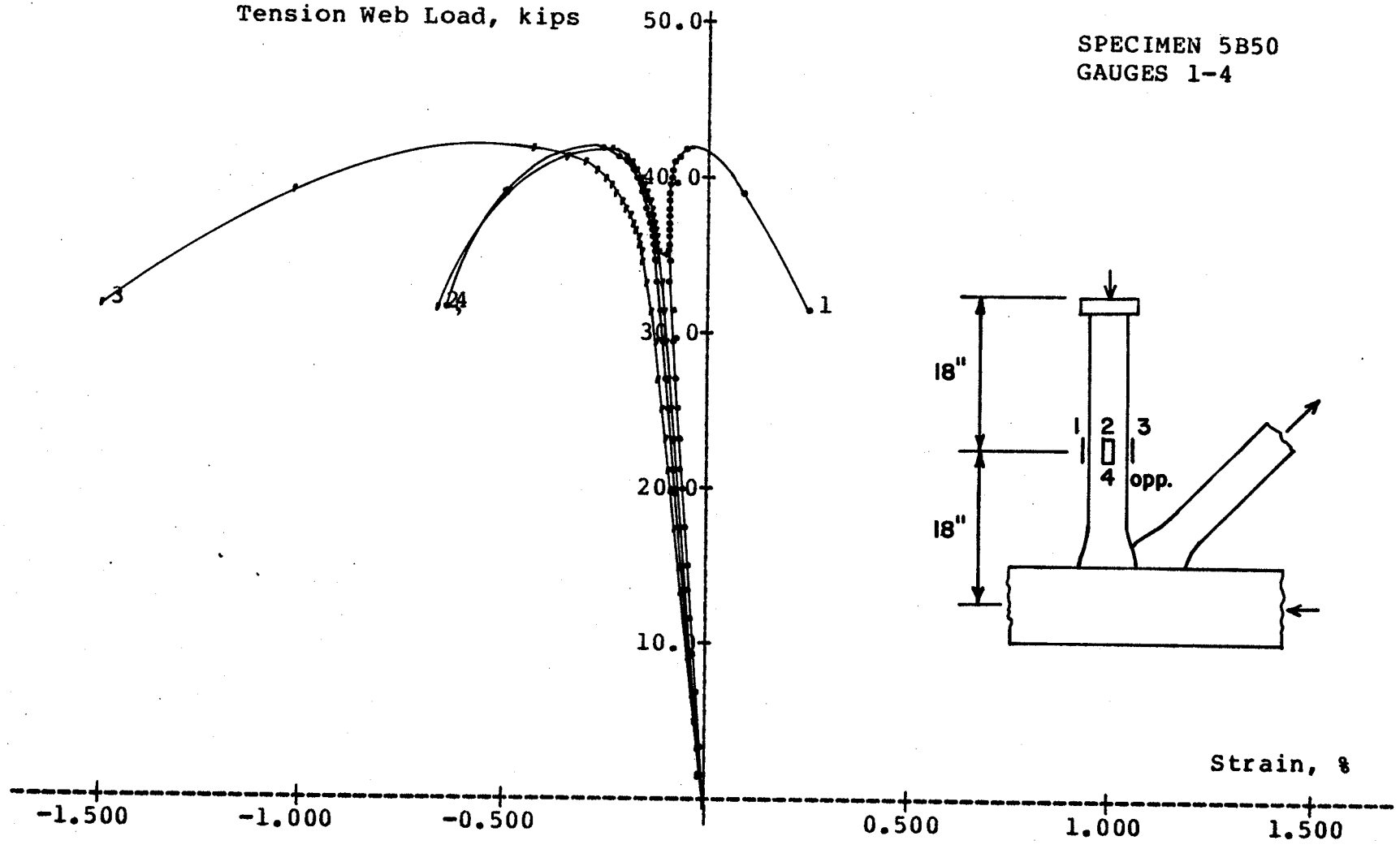

Fig. 3.15. Longitudinal Strains on Compression Web Member of Specimen 5B50

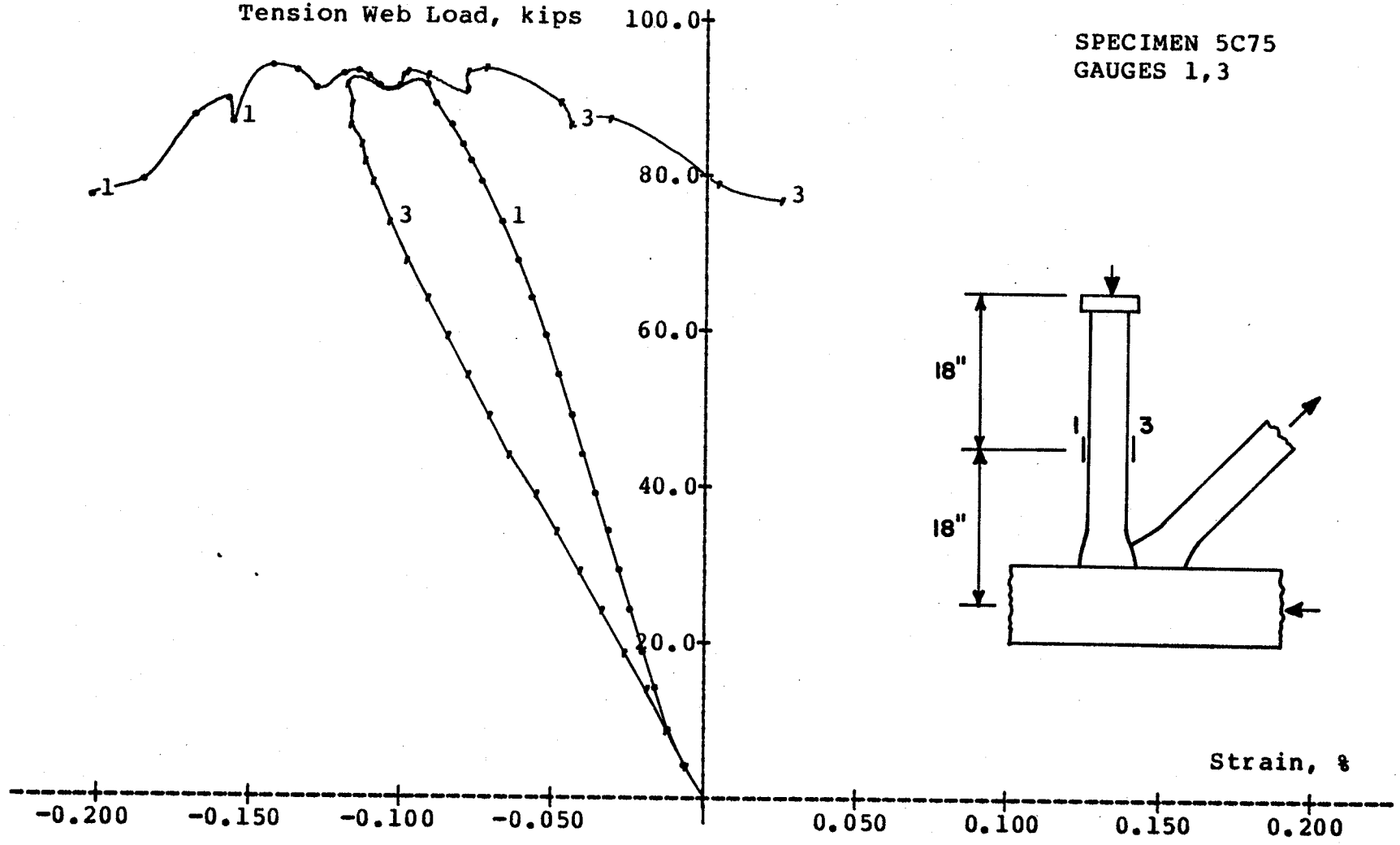

Fig. 3.16. Longitudinal Strains on Compression Web Member of Specimen 5C75

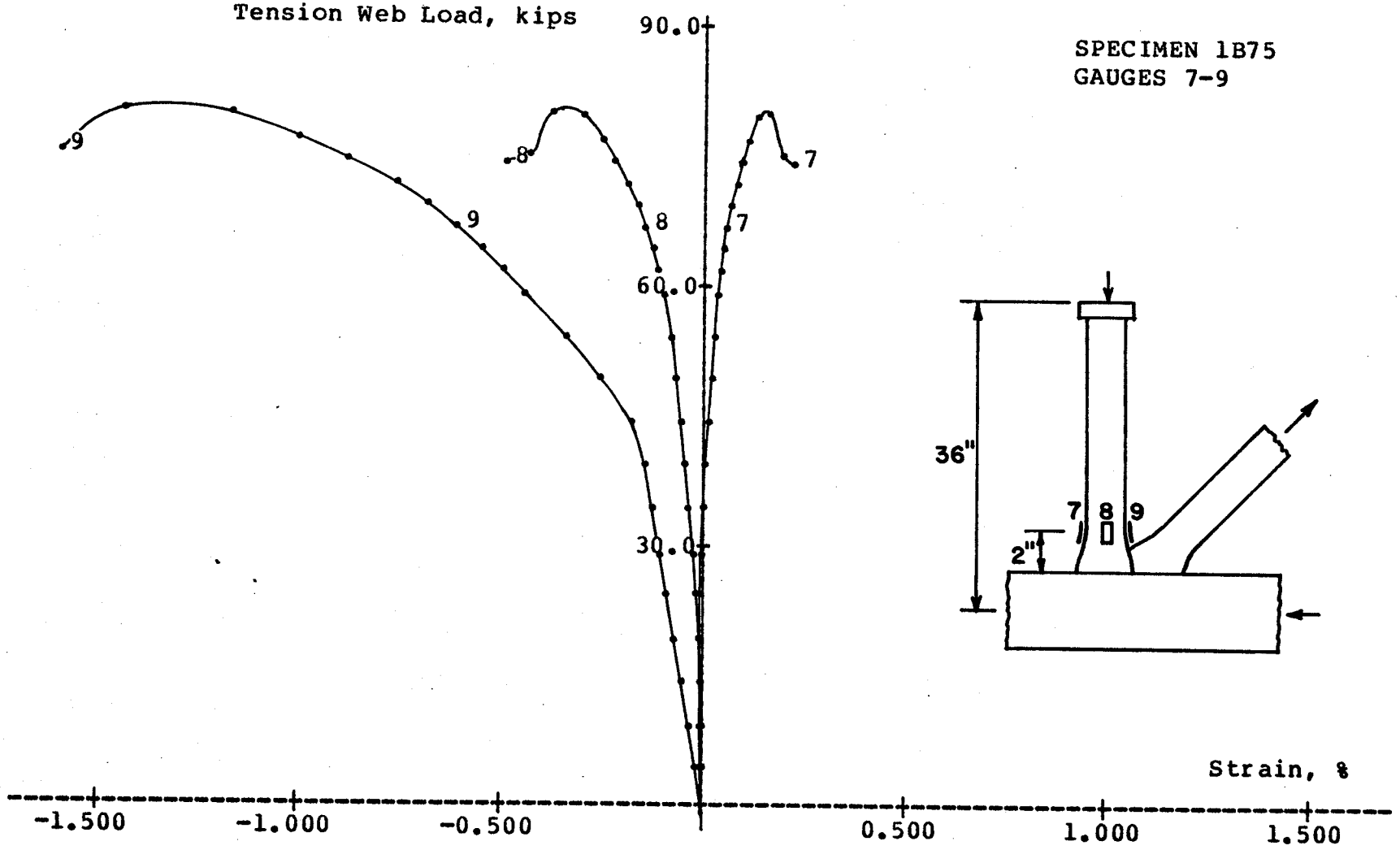

Fig. 3.17. Longitudinal Strains on Compression Web Member of Specimen 1B75

near the lap usually bent away from the tension web but reversed the direction of bending when the ultimate load was reached. This is illustrated using specimen 4B75 in Fig. 3.18. Such behavior resulted in a point of inflection near the lap, which reduced the effective length of the compression web and increased the buckling load. It was found in such specimens as 3B75, 4B75, 5B00, 5B50, and 5C75, all of which had t_0/b_0 of larger than 0.04. Thus a chord wall having t_0/b_0 of larger than about 0.04 approximated a fixed-end condition for the compression web.

3.5. Strains in Tension Web Members

The longitudinal strains at the mid-length of a tension web member were usually uniform, indicating that there was little or no bending at this section in the member. This is illustrated by the strains of gauges 15-18 of specimen 5A75 in Fig. 3.19a. The average of these strains usually agreed very well with the average strain calculated from the measured load.

The strains near the joint of a tension web were less uniform, being relatively large near the lap and on the opposite side. This is illustrated in Fig. 3.19b, which shows that the strains of gauges 12 and 14 were sometimes as large as twice the strain of gauge 13. As a result, tearing in the tension web usually started near the lap.

Figure 3.20 illustrates that when specimen 5A75 reached the ultimate load, the tension web yielded excessively, while the compression web bent but did not buckle, and the chord had small strains.

Figure 3.21 shows that when specimen 4B75 reached the ultimate

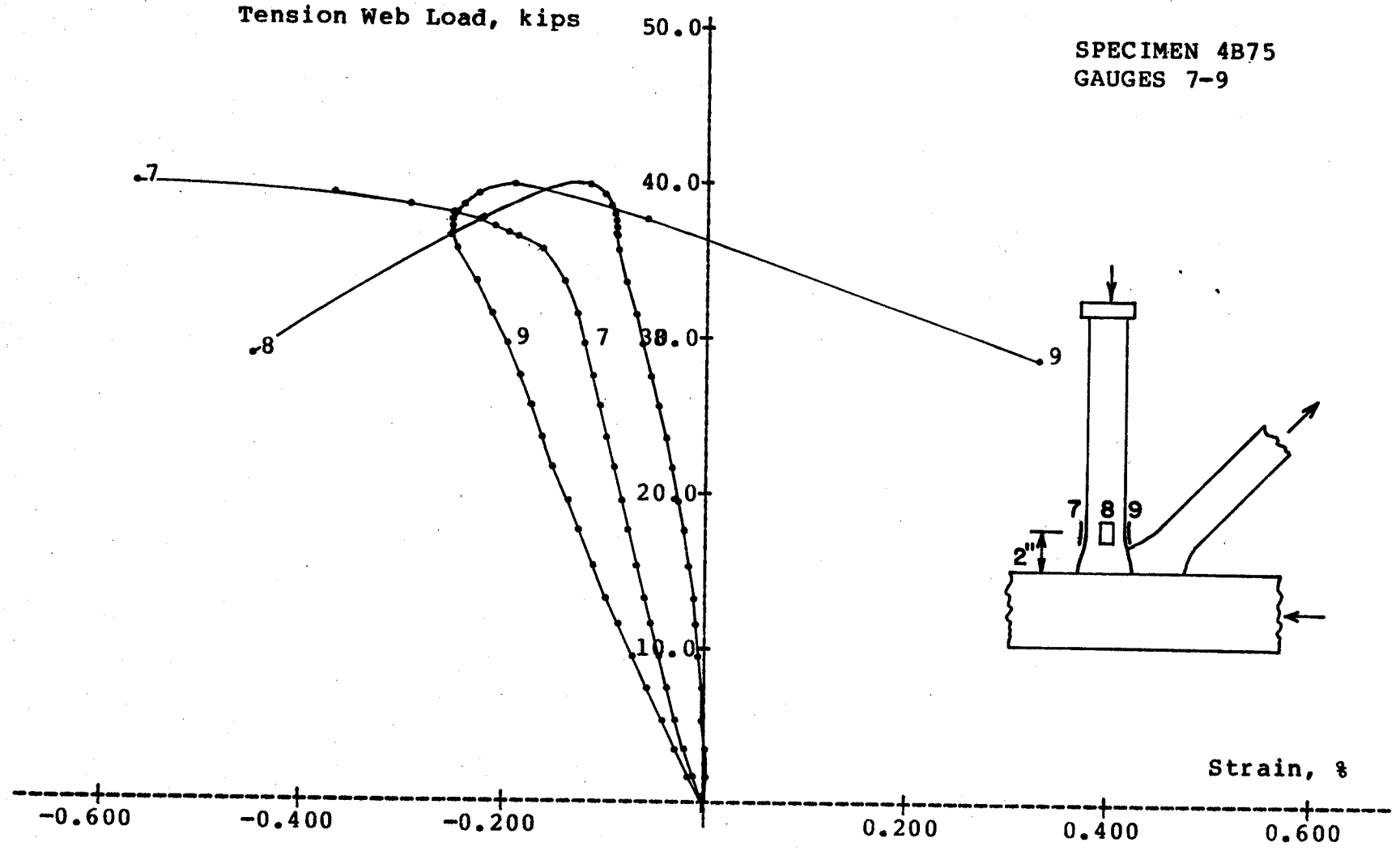

Fig. 3.18. Longitudinal Strains on Compression Web Member of Specimen 4B75

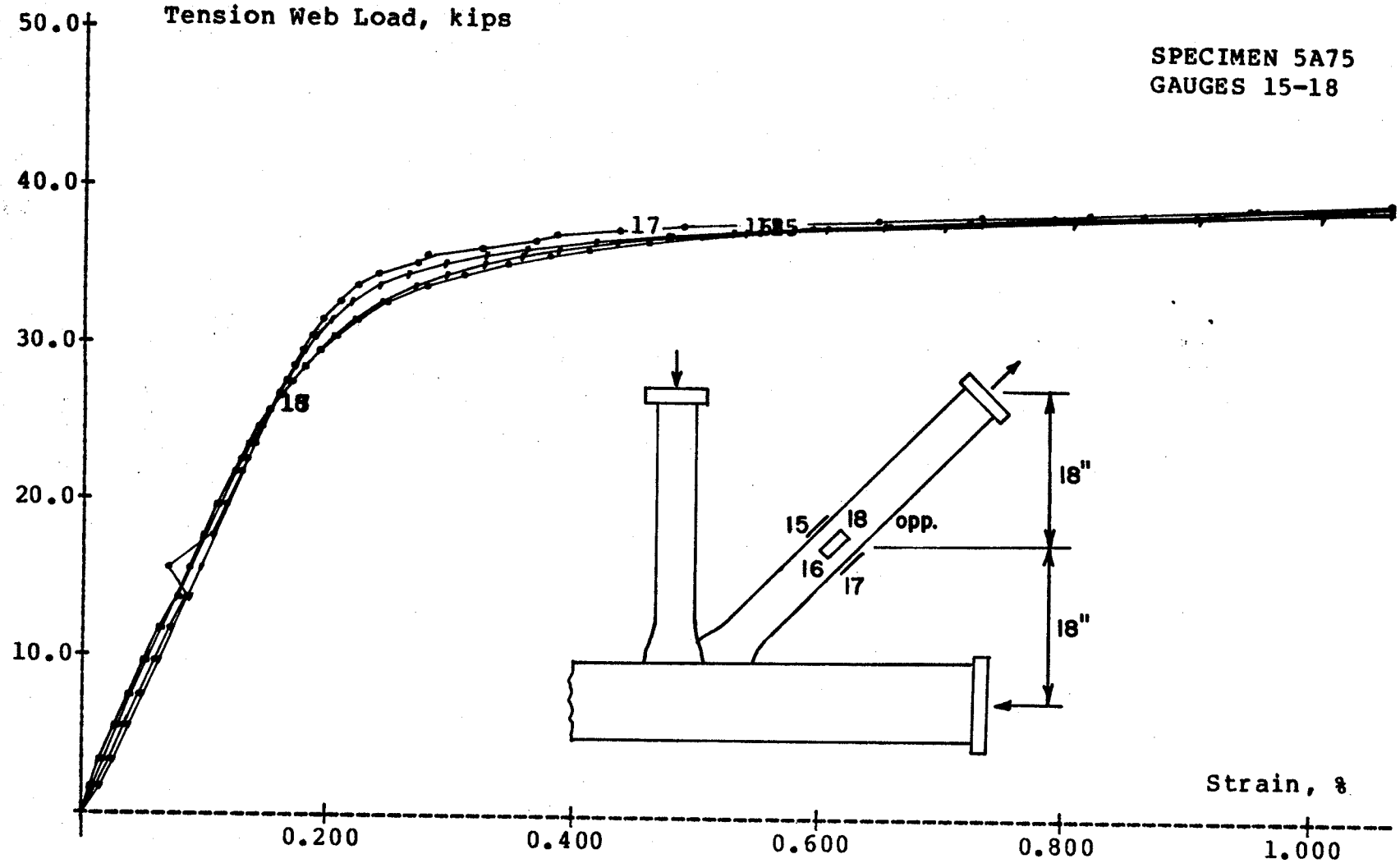

Fig. 3.19a. Longitudinal Strains on Tension Web Member of Specimen 5A75

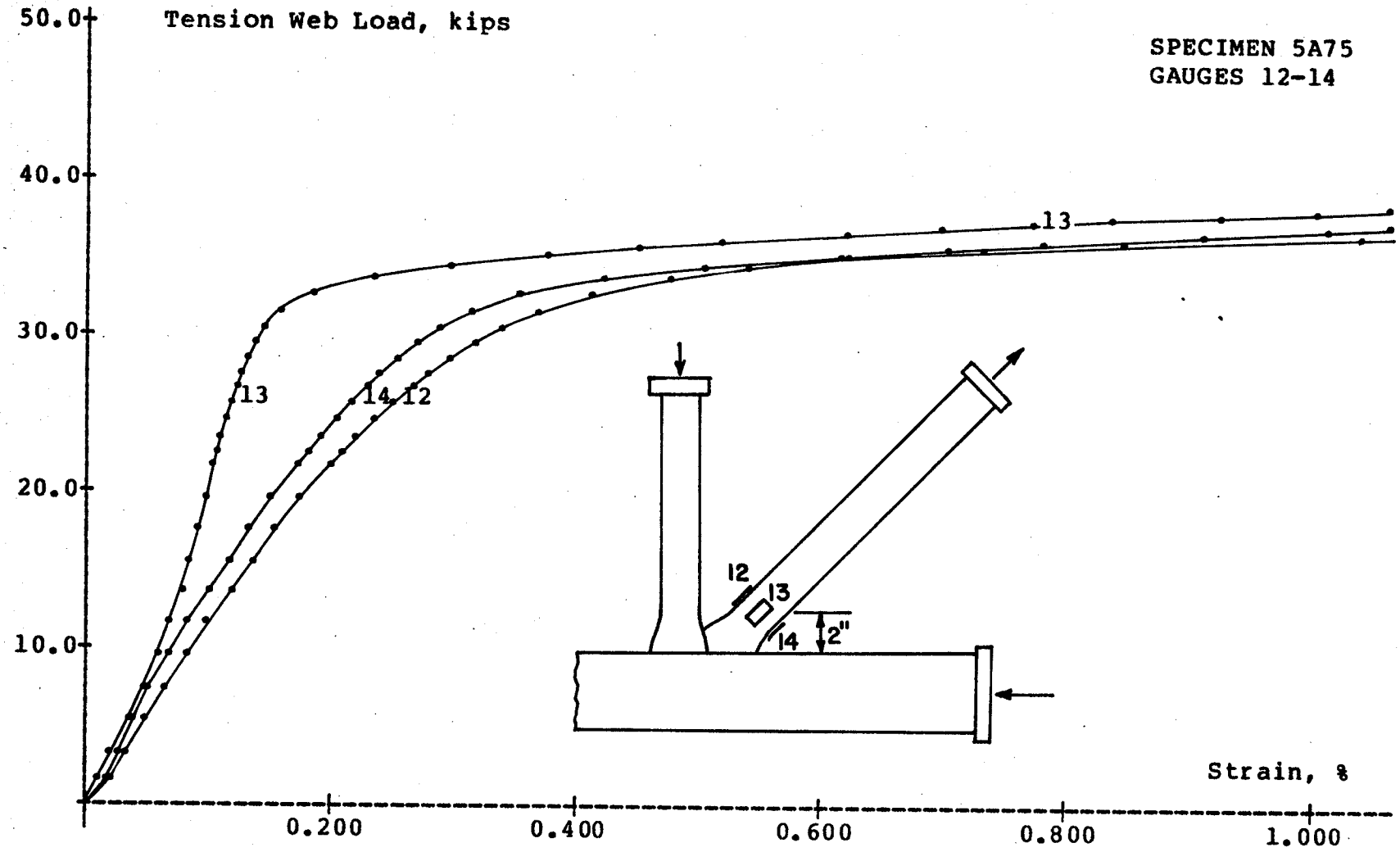

Fig. 3.19b. Longitudinal Strains on Tension Web Member of Specimen 5A75

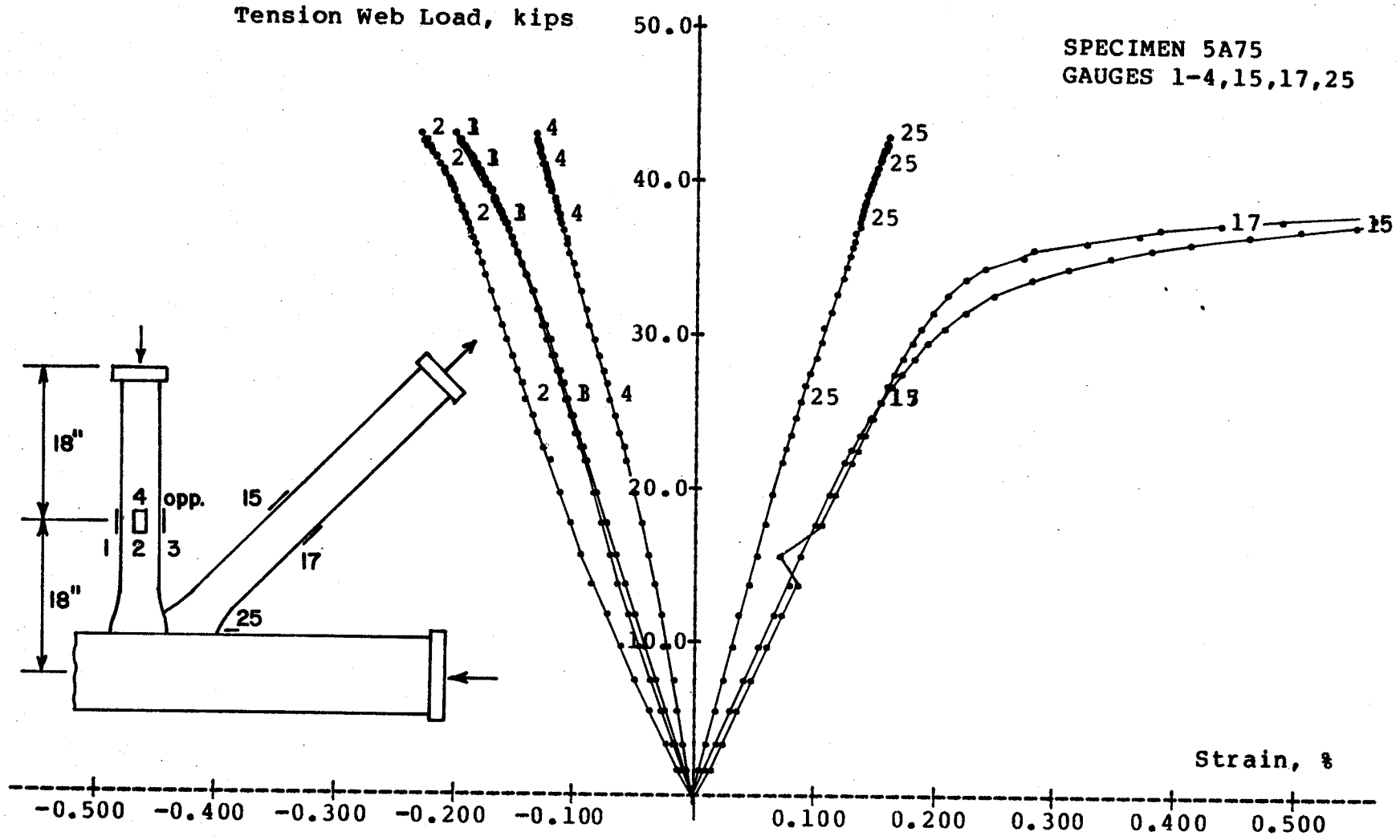

Fig. 3.20. Strains on Specimen 5A75

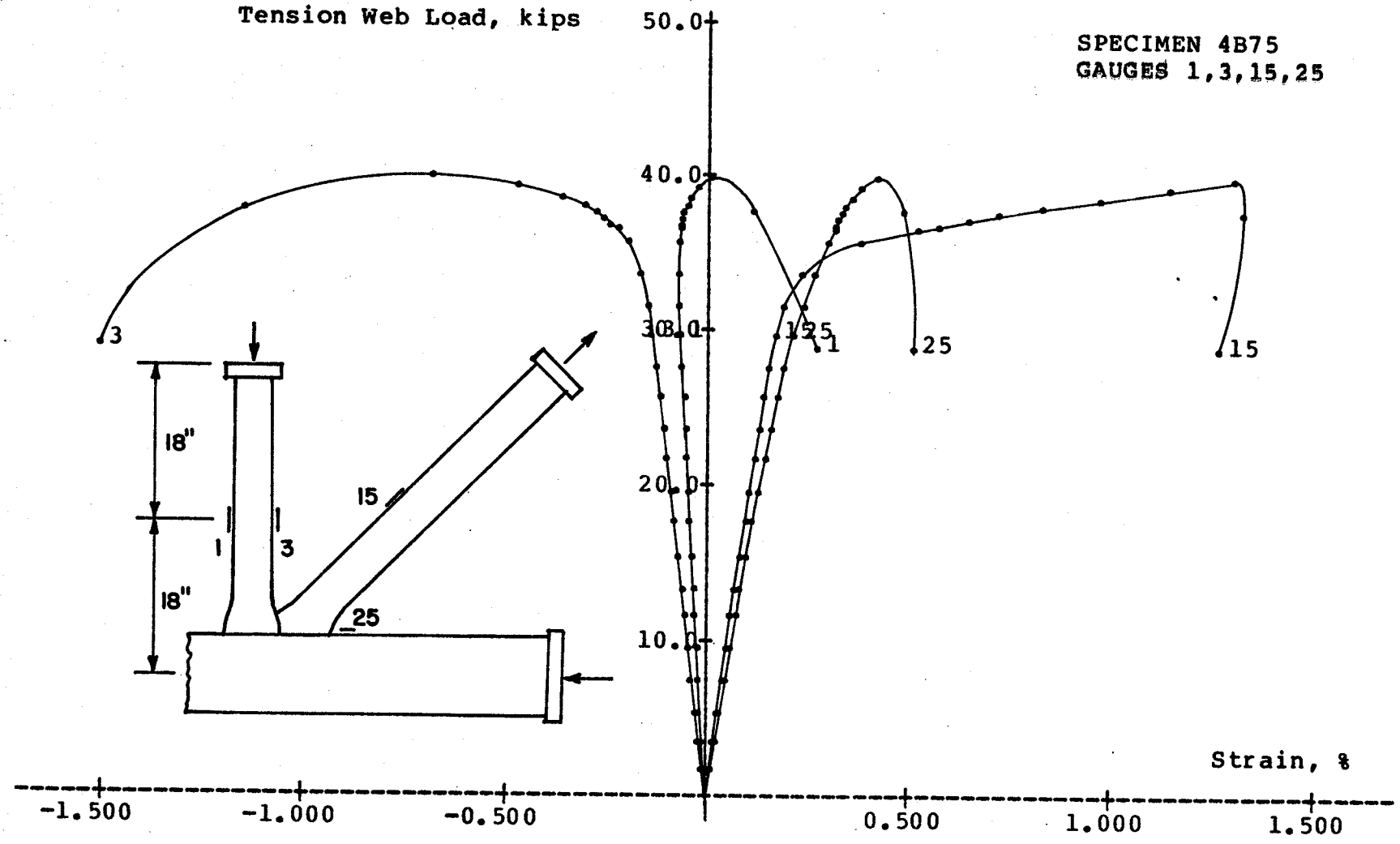

Fig. 3.21. Strains on Specimen 4B75

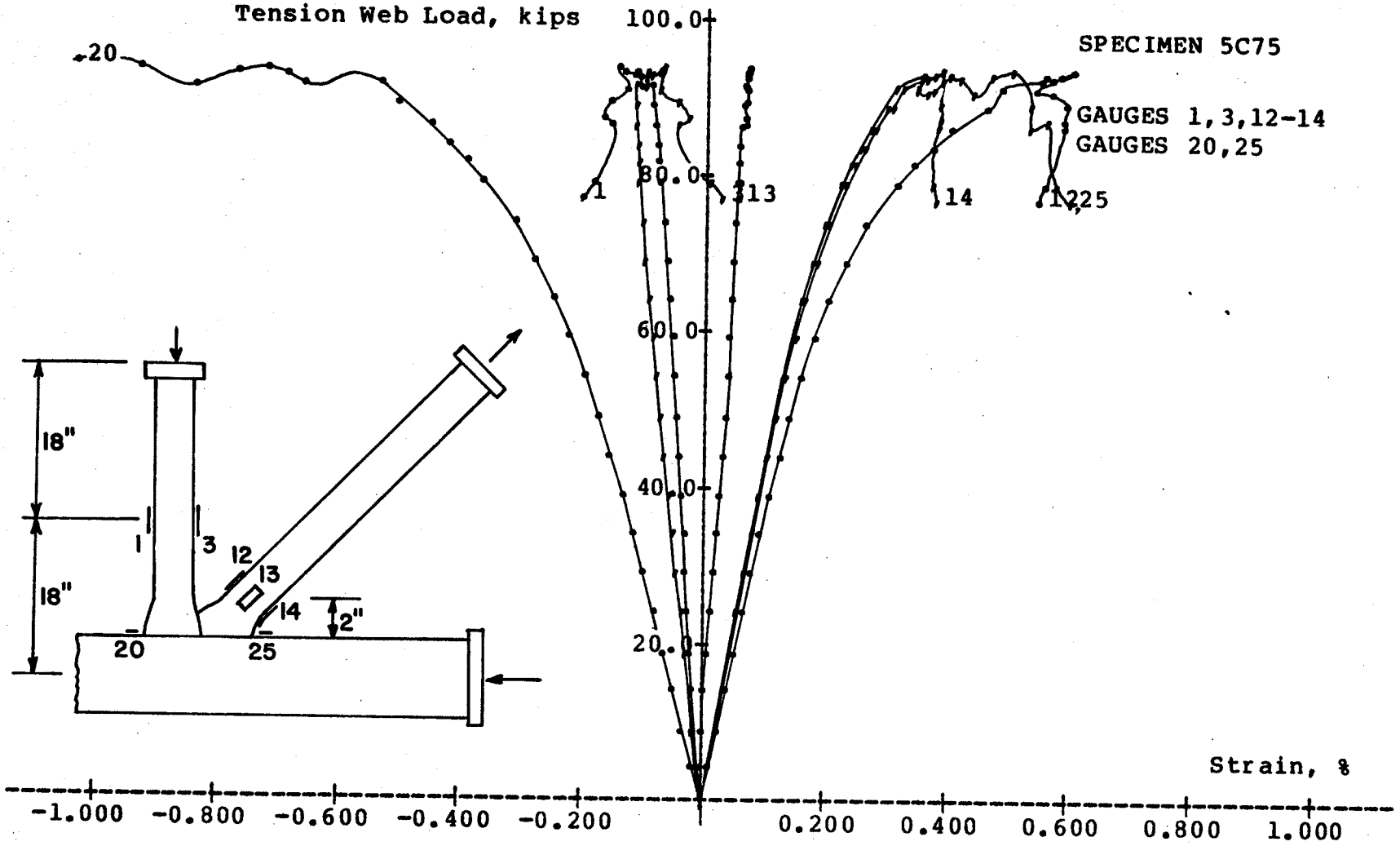

Fig. 3.22. Strains on Specimen 5C75

load the tension web yielded excessively, the compression web buckled, and the chord strains were small.

Figure 3.22 shows that when specimen 5C75 reached the ultimate load the tension web and the chord yielded locally and the compression web bent. The strains in the compression web did not increase substantially when the load dropped.

3.6. Failure Modes

Failure of a specimen was said to occur when the ultimate load, representing the limit of usefulness of the joint, was reached. Failure of the specimens was divided into three main modes, corresponding to failure in one of the three members forming the joint. The three modes of failure are: failure by excessiye local deformation of the loaded chord face, failure by buckling of the compression web, and failure by tearing of the tension web. These failure modes have been designated A, B, and C, respectively, in Table 3.1. The Table shows that a specimen could fail in one or more of the three modes.

Failure by excessive deformation of the chord face (mode A) is illustrated in Fig. 3.23. It usually occurred when the chord wall was relatively flexible compared to the web members. The local deformation was arbitrarily considered large if its maximum value exceeded about 2% of the chord width. This mode of failure usually occurred with other mode(s).

Failure by buckling of the compression web (mode B) is shown in Fig. 3.24. It occurred in most specimens, as shown in Table 3.1. Only

Table 3.1. Test Results

Specimen	N_{2u}	$\frac{J_u}{t_0 b_0 \sigma_e}$	$\frac{J_u}{t_0 \sigma_e}$	$\frac{N_{2u}}{A_2 \sigma_{2e}}$	$\frac{J_u}{N_{1b}}$	Failure Modes
	kips		in.	%	%	
1	34.5	0.677	2.71	99.4	179	A B C
2	29.8	0.585	2.34	85.9	155	A B
3	54.3	1.096	4.39	127.0	124	A B
4	33.4	0.418	2.51	96.2	174	A B
5	49.6	0.621	3.73	116.0	113	A B
1A50	57.4	0.644	3.86	95.5	97.4	A B C
1A75	58.1	0.652	3.91	96.7	98.7	A B
2A50	59.9	0.545	3.27	99.7	102	A B
2A75	62.7	0.571	3.42	104.3	106	A B
3A50	32.4	0.636	2.54	84.4	226	A B C
3A75	32.7	0.641	2.57	85.1	228	A B
4A50	40.3	0.557	2.23	104.9	281	B
4A75	38.5	0.532	2.13	100.2	268	B C
5A00	34.7	0.389	1.55	90.4	242	B
5A50	42.0	0.470	1.88	109.4	293	B
5A75	43.2	0.484	1.94	112.5	301	B C
1B50	84.2	1.021	6.13	77.0	75.9	A B C
1B75	80.7	0.978	5.87	73.8	72.9	A B C
3B50	27.7	0.578	2.31	73.2	132	A B
3B75	33.9	0.707	2.83	89.5	161	A B
4B50	40.5	0.559	2.24	107.6	194	B
4B75	40.2	0.555	2.22	106.8	193	B
5B00	43.3	0.451	1.81	115.0	207	B
5B50	42.3	0.456	1.82	112.4	202	B
5B75	45.2	0.504	2.01	120.1	217	B
1C50	103.3	1.294	7.76	47.7	41.4	A
1C75	88.5	1.108	6.65	40.9	35.4	A C
3C50	95.8	1.858	7.43	87.7	86.4	A B
3C75	99.5	1.930	7.72	87.7	86.8	A B
4C50	104.2	1.476	5.90	95.7	94.5	A C
4C75	93.6	1.326	5.30	84.1	82.8	A
5C00	91.7	1.063	4.25	83.0	81.9	A C
5C50	97.1	1.039	4.16	90.2	88.9	A
5C75	94.8	1.018	4.07	86.7	85.5	A

Note: A = Failure by excessive deformation of loaded chord face,
B = Failure by buckling of compression web member,
C = Failure by tearing of tension web member.

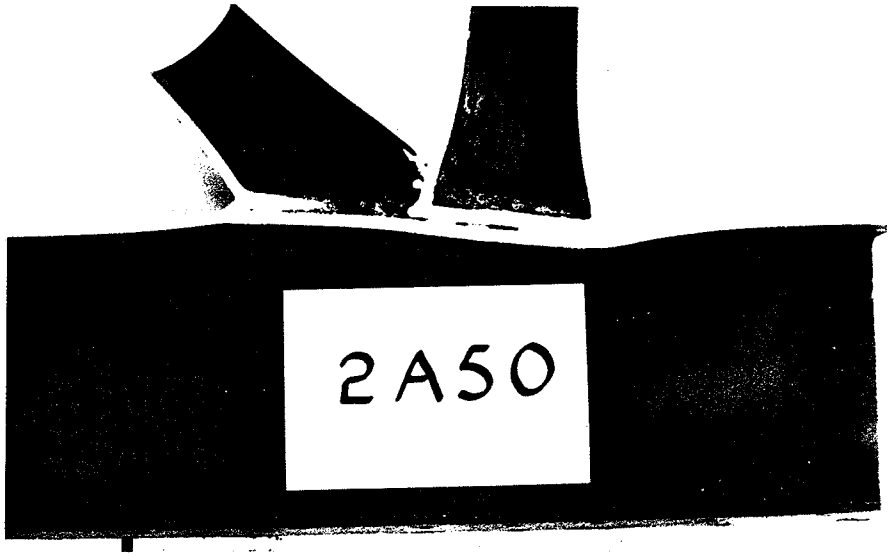

(a)

(b)

Fig. 3.23. Failure Mode A - Large Deformation of Loaded Chord Face

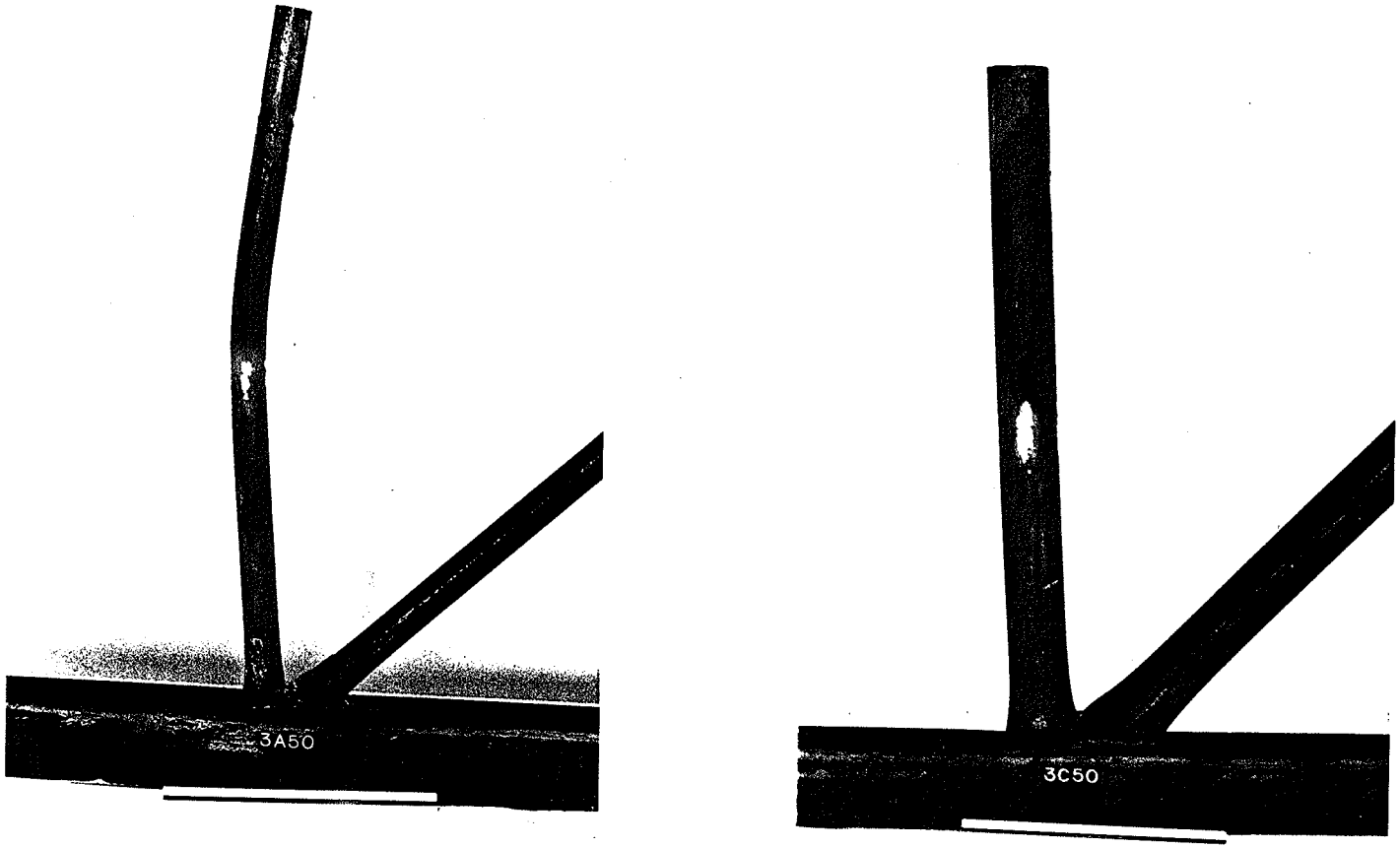

(a) (b)

Fig. 3.24. Failure Mode B - Buckling of Compression Web Member

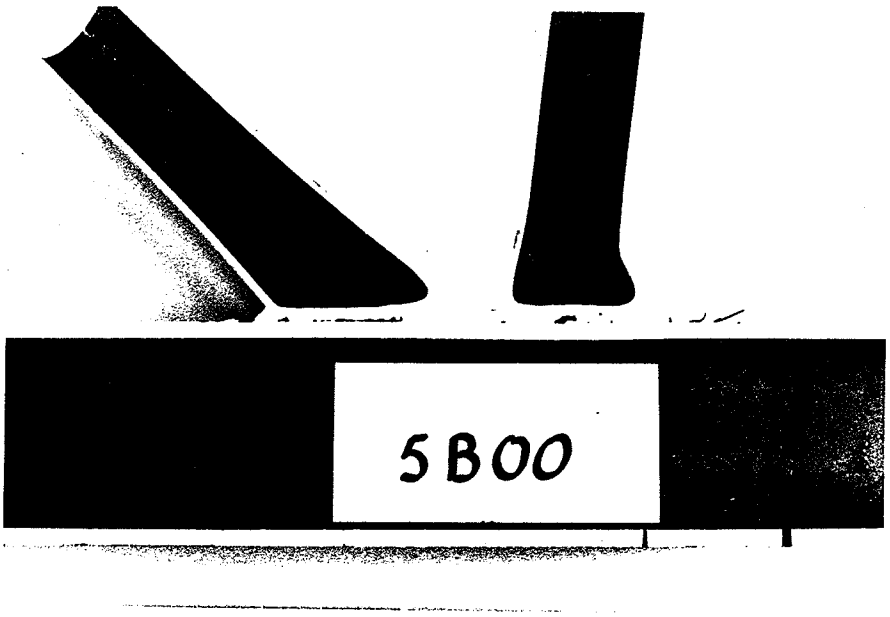

Fig. 3.24c. Failure Mode B - Buckling of Compression Web Member

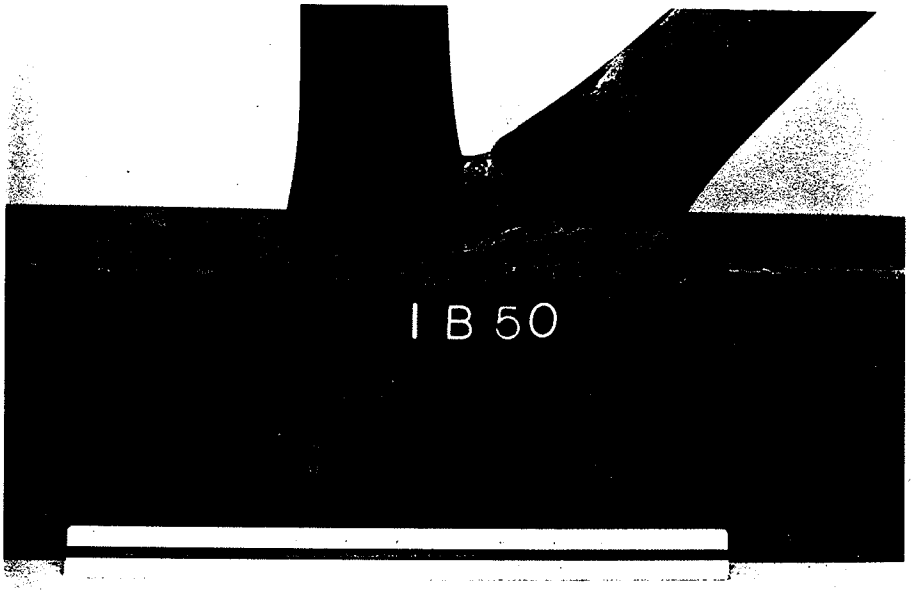

Fig. 3.25a. Failure Mode C - Tearing of Tension Web Member

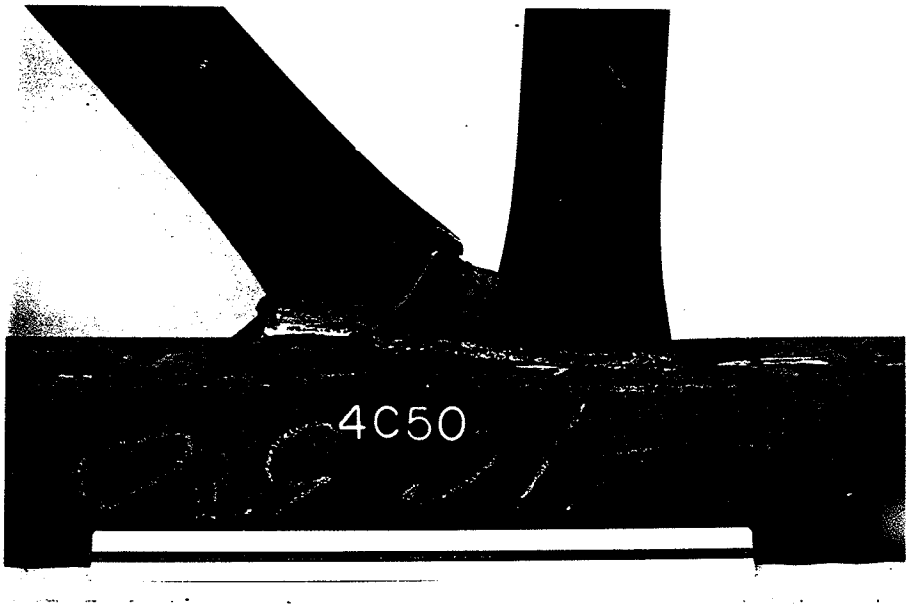

(b)

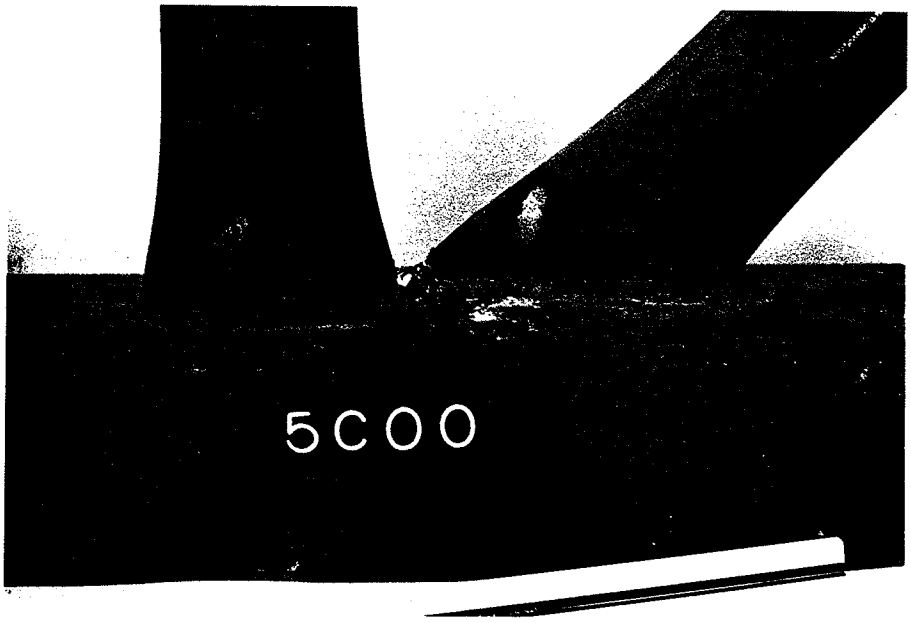

(c)

Fig. 3.25. Failure Mode C - Tearing of Tension Web Member

inelastic buckling having large plastic deformation is included in the Table. Elastic buckling occurred to almost all specimens. As previously mentioned, buckling was in the plane of the specimen and usually in the direction away from the tension web, as it was induced by an end moment.

When buckling failure occurred in the compression web alone, the actual joint strength might be slightly larger than the measured load.

Besides the overall buckling, local buckling or crippling of the end of the compression web occurred in specimens 5A00, 5B00, and 5B50, as illustrated in Fig. 3.24b. These specimens had a stiff chord wall and a slender compression web. The crippling was caused by the overall buckling of the compression web and the restraint of the chord wall. As it was dependent on the overall buckling, it was regarded as a secondary buckling failure.

Failure by tearing of the tension web (mode C) is illustrated in Fig. 3.25. Tearing of the web usually started near the lap close to the weld because of stress concentration and local yielding there. It occurred more often in specimens with a 50% lap than in those with a 75% lap, indicating that an increase in overlap improved the stress distribution.

If loading was continued after tearing in the tension web had occurred, tearing in the chord face could result. This happened to specimen 4C50.

When welding was designed and done properly, tearing in the weld rarely occurred. It happened near the overlaps of specimens 1 and 1B75, but could be considered as tearing in the tension web.

Specimens 1C50 and 1C75 were not fabricated and welded properly, thus were not included in the following analyses. The latter failed prematurely in the weld.

When specimen 1A75 reached the ultimate load, the tension web yielded excessively. Tearing or buckling would likely result if loading were continued.

3.7. Joint Strength

The strength of a cropped-web joint is measured by the ultimate web-force component normal to the chord. For the Pratt or N-truss geometry used in the tests, this is equal to the ultimate load in the compression web (N_{1u}), or 0.7071 times the ultimate load in the tension web (N_{2u}) given in Table 3.1.

The strength of a cropped-web joint having no gap can be estimated using the following empirical formula:

$$J_u = t_0 b_0 \sigma_e (0.504 + 6.10(d/b_0)^3 - 43.3(d/b_0)^2(t_0/b_0)) \qquad (3.1)$$

where J_u = ultimate web-force component normal to the chord,

t_0 = thickness of chord wall,

b_0 = outside width of chord,

σ_e = yield stress at 0.2% offset of chord material,

d = average outside diameter of web members.

Alternatively, the equation can be written non-dimensionally as:

$$J_u/t_0 b_0 \sigma_e = 0.504 + 6.10(d/b_0)^3 - 43.3(d/b_0)^2(t_0/b_0) \qquad (3.2)$$

The experimental values of $J_u/t_0b_0\sigma_e$ are given in Table 3.1 and plotted against d/b_0 and t_0/b_0 in Fig. 3.26. Also shown in the Figure are curves of $J_u/t_0b_0\sigma_e$ calculated from Eq. 3.2 for a number of d/b_0 and t_0/b_0 values. It can be seen that the experimental and calculated values agree very well. The curves show that, for a given value of t_0/b_0, $J_u/t_0b_0\sigma_e$ is approximately constant when d/b_0 is small, but increases sharply when d/b_0 is large. For a given d/b_0, $J_u/t_0b_0\sigma_e$ increases as t_0/b_0 decreases.

Equation 3.2 has been obtained by means of a stepwise multiple regression analysis and checked by a multiple regression analysis (Libson and Sheth 1973, Kennedy and Neville 1976, Chebib et al. 1976). According to the analyses, the equation relating the variables in this form is statistically significant at the 0.1% level. In other words, the probability that all the true partial regression coefficients are equal to zero is equal to 0.1%. Thus, the dependent variable $J_u/t_0b_0\sigma_e$ significantly relates to the independent variables $(d/b_0)^3$ and $(d/b_0)^2(t_0/b_0)$. The coefficients of the independent variables are also significant at the 0.1% level; thus these variables significantly influence the dependent variable. The former variables account for 96% of the variation in the latter.

Some results of the regression analyses are given and explained in more details in Appendix A.

The overlap is not included in Eq. 3.1 and 3.2 for the sake of simplicity and because the effect of overlap was inconsistent. An increase in overlap usually resulted in an increase, but occasionally a

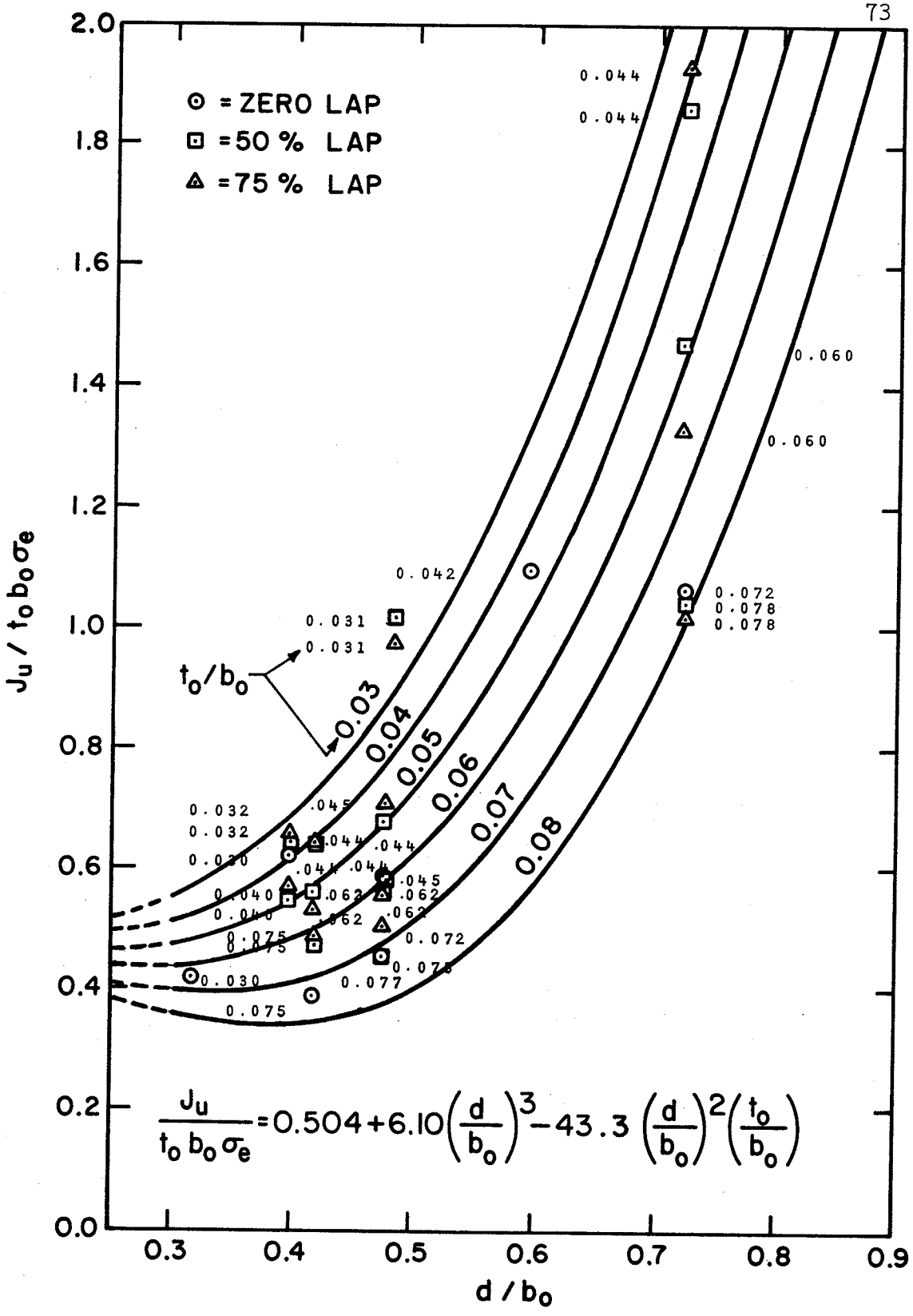

Fig. 3.26 . Strength of Cropped-Web Joints

decrease, in joint strength, as can be seen in Fig. 3.26. The increase in strength due to overlap was usually smaller than 5 to 10%, although sometimes was 20% when d/b_0 was smaller than 0.50. A decrease in strength was usually smaller than 5%, but a 10% decrease occurred when d/b_0 was equal to 0.72.

For design purposes, the strength of a cropped-web joint may be calculated from Eq. 3.1 or 3.2, or from Fig. 3.26, as illustrated in the following examples. Suppose that the joint has the following members:

chord: RHS 4 x 4 x 0.250 in. (102 x 102 x 6.35 mm),

tension web: CHS 1.90 x 0.125 in. (48.3 x 3.18 mm).

compression web: the same as tension web.

All members have a minimum yield stress σ_e of 50 ksi (344 N/mm^2). Thus,

$d/b_0 = 1.90/4 = 0.475$, and $t_0/b_0 = 0.250/4 = 0.0625$.

Using Eq. 3.1,

$$J_u = (0.25 \text{ in.})(4 \text{ in.})(50 \text{ ksi})(0.504 + 6.10 \times 0.475^3 - 43.3 \times 0.475^2 \times 0.0625)$$

$$= 27.4 \text{ kips (122 kN)}.$$

Alternately, using Fig. 3.26, for $d/b_0 = 0.475$ and $t_0/b_0 = 0.0625$, $J_u/t_0 b_0 \sigma_e$ is approximately 0.55. Thus,

$$J_u = 0.55(0.25 \text{ in.})(4 \text{ in.})(50 \text{ ksi}) = 27.5 \text{ kips (122 kN)}.$$

If the limit state design approach (CISC 1977) is used, the joint strength calculated should be reduced by a performance factor ϕ of 0.9 or smaller. Thus, the factored joint resistance is:

$$J_r = \phi J_u \qquad (3.3)$$

where J_u is given by Eq. 3.1.

For the example given above, assuming that $\phi = 0.9$, the factored joint resistance is:

$J_r = 0.9 \times 27.4 = 24.7$ kips (110 kN).

This should be compared with a factored design load. Assume that the latter load is smaller than the factored resistances of the webs. Using CISC 1977, the factored tensile resistance of the tension web is:

$T_r = \phi A_2 \sigma_e = 0.9(0.697 \text{ in.}^2)(50 \text{ ksi}) = 31.4$ kips (140 kN).

If the tension web is 45° inclined to the chord, the normal force component is 0.707 x 31.4 kips or 22.2 kips (98.8 kN). Assume that the compression web is vertical and has a length L of 6 feet (1.83 m) and an effective length factor K of 1.0. Then,

$$\lambda = (KL/r)(\sigma_e/\pi^2 E)^{0.5}$$
$$= (1 \times 72 \text{ in.}/0.629 \text{ in.})(50 \text{ ksi}/3.14^2 \times 29000 \text{ ksi})^{0.5}$$
$$= 1.51$$

The factored compressive resistance of the compression web is given by:

$$C_r = \phi A_1 \sigma_e(-0.111 + 0.636\lambda^{-1} + 0.087\lambda^{-2})$$
$$= 0.9(0.697 \text{ in.}^2)(50 \text{ ksi})(-0.111 + 0.636 \times 1.51^{-1} + 0.087 \times 1.51^{-2})$$
$$= 10.9 \text{ kips } (48.5 \text{ kN}).$$

Since the factored resistance of the compression web (10.9 kips) is smaller than both the factored resistance of the tension web in the normal direction (22.2 kips) and that of the joint (24.7 kips), the compression web, not the joint, controls the design. If the factored

resistance J_r was smaller than the factored design load, other member sizes would have to be chosen.

If a working stress design approach (CISC 1973) is used, the maximum allowable load normal to the chord of a cropped-web joint is:

$$J_w = J_u/F.S. \tag{3.4}$$

where J_u is given by Eq. 3.1 and F.S. is a factor of safety. The normal force components of the webs applied to the chord should not exceed this allowable load J_w.

Using the same joint illustrated above, with a safety factor of 1.7, the allowable load of the joint is:

$$J_w = J_u/F.S. = 27.5/1.7 = 16.2 \text{ kips } (72.1 \text{ kN}).$$

The allowable load in the tension web is:

$$N_{2w} = 0.6A_2\sigma_e = 0.6\ (0.697 \text{ in}^2)(50 \text{ ksi}) = 20.9 \text{ kips } (93.0 \text{ kN}).$$

This corresponds to a normal load of 0.707 x 20.9 kips = 14.8 kips (65.9 kN). Since the slenderness ratio of the compression web is $(KL/r)_1 = 1(72 \text{ in.})/(0.629 \text{ in.}) = 114$, the allowable load of this web is:

$$N_{1w} = A_1\sigma_{1a} = A_1\pi^2E/1.92(KL/r)_1^2 = 8.0 \text{ kips } (35.6 \text{ KN}).$$

Again, assume that N_{1w} and N_{2w} are, respectively, larger than the load each web is required to carry. Since the load in the compression web (8.0 kips) is smaller than that in the tension web in the normal direction (14.8 kips) and smaller than the allowable load of the joint (16.2 kips), the compression web again controls the design.

In order to compare the strength of lapped cropped-web joints with

that of joints but with sawn webs and a weld gap between them (Eastwood and Wood 1970), $J_u/t_0\sigma_e$ values are plotted against d/b_0 in Fig. 3.27. The Figure shows that the strengths of the cropped-web joints were comparable to those of the sawn web joints, provided that t_0/b_0 is smaller than about 0.07. It also shows that if the suggested working load curve used for the sawn-web gap joints is applied to the cropped-web lap joints, the results will be unconservative when t_0/b_0 is larger than 0.07, and excessively conservative in many cases when t_0/b_0 is small. The equations for calculating the suggested working loads shown in the Figure have the disadvantage that their coefficients vary with the system of units used; in this case, the term $J_u/t_0\sigma_e$ has been expressed in inches.

The strength of a tubular truss joint has also been expressed in many other ways, including in terms of joint efficiency and joint load factor. These and other parameters have been used to relate the strength of cropped-web joints to various independent parameters, but the results have not been so satisfactory as that given by Eq. 3.2.

For example, the joint efficiency, previously defined as the ratio of the ultimate load to the yield load in the tension web ($N_{2u}/A_2\sigma_{2e}$), is plotted against t_0/b_0 in Fig. 3.28. It can be seen that the efficiency inconsistently relates to t_0/b_0, d/b_0, and o_v. This is probably because the yield stresses of some tension webs (σ_{2e}) were larger than those of some chords and did not control the ultimate loads. In addition, the yield load in the tension web did not govern the ultimate load when failure primarily occurred in other members.

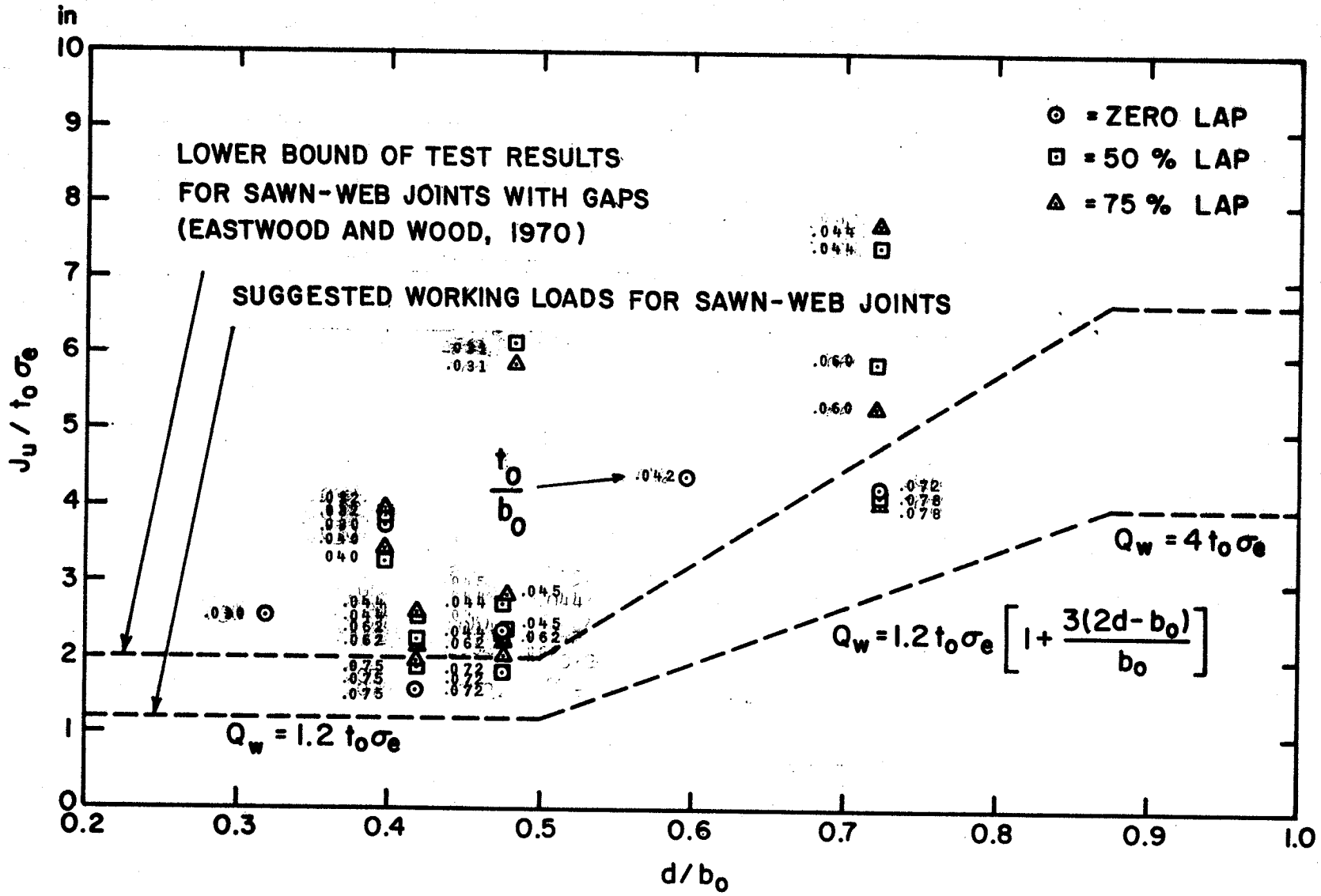

Fig. 3.27. Comparative Strengths of Cropped– and Sawn-Web Joints .

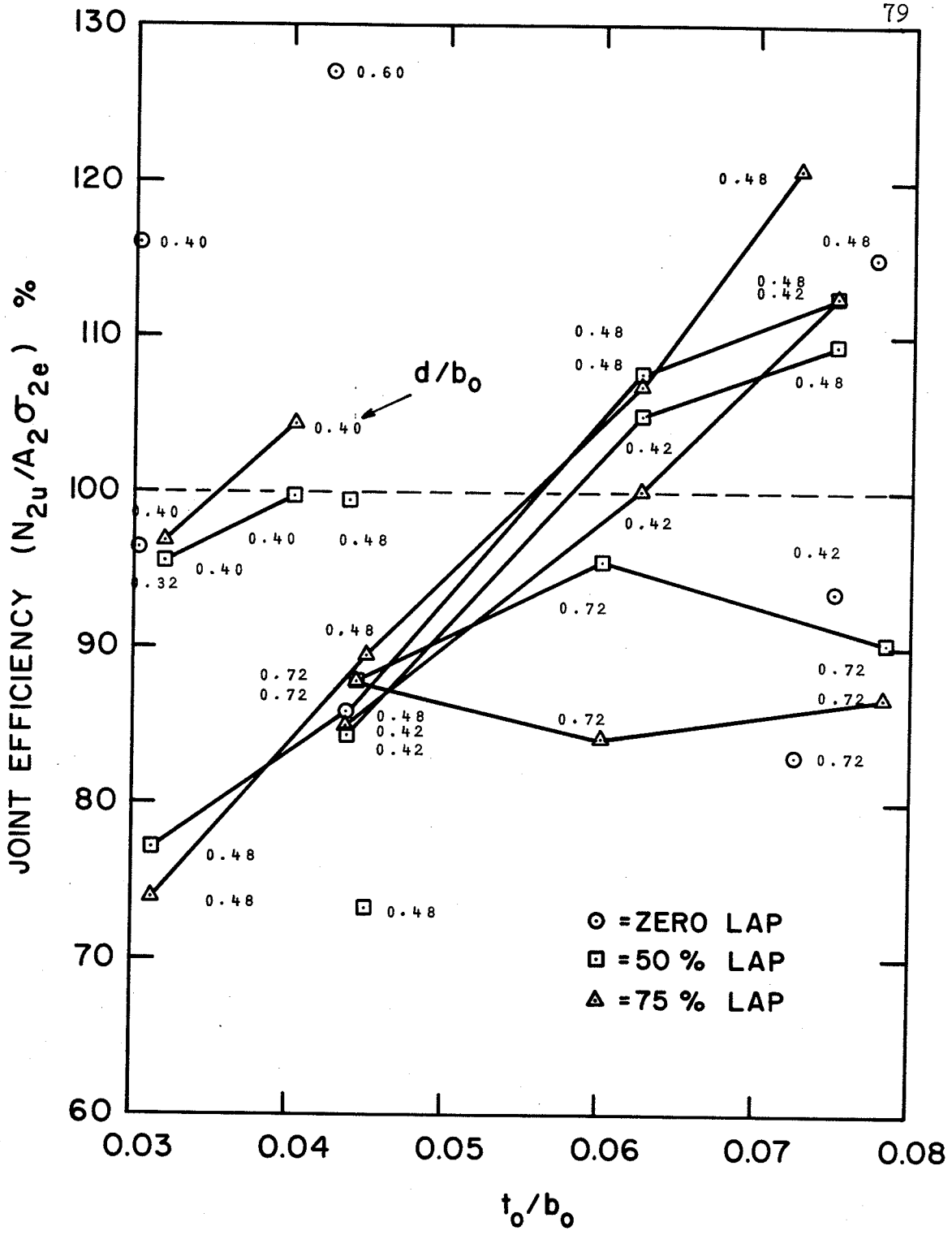

Fig. 3.28. JOINT EFFICIENCY

Despite these limitations, Fig. 3.28 suggests that the cropped-web joints tested had an efficiency ranging from 73% to 127%. The efficiency of most of the joints was larger than 84%. A 100% efficiency was obtained for joints having d/b_0 about 0.40 to 0.50, t_0/b_0 larger than about 0.05, and a 50% to 75% overlap. A large d/b_0 or a small t_0/b_0 often led to a low efficiency.

In comparison, Bouwkamp (1968) found that a 100% efficiency was obtained for a profiled joint having circular hollow members with a chord diameter d_0, if the joint had t_0/d_0 of larger than about 0.05 and had no eccentricity, or if it had t_0/d_0 of larger than about 0.03 and a negative eccentricity. A tension web having diameter about half of the chord diameter also gave a relatively high efficiency (Cran et al. 1971).

The strength of a cropped-web joint is compared to the buckling strength of the compression web (N_{1b}) as shown in Fig. 3.29. The buckling load N_{1b} was calculated using the CSA Standard S16-1969 and assuming that the compression web had a length of six feet and an effective length factor of 1.0. When the ratio of joint strength to the buckling strength of the compression web (J_u/N_{1b}) exceeded 1.0, the joint was stronger than the compression web and was very efficient. Figure 3.29 shows that this usually occurred when the slenderness ratio of the compression web $(KL/r)_1$ was larger than about 90. In addition, an increase in d/b_0 or $(KL/r)_1$ generally decreased J_u/N_{1b}. Finally, an increase in t_0/b_0 usually increased J_u/N_{1b} but only when inelastic buckling of the compression web was involved.

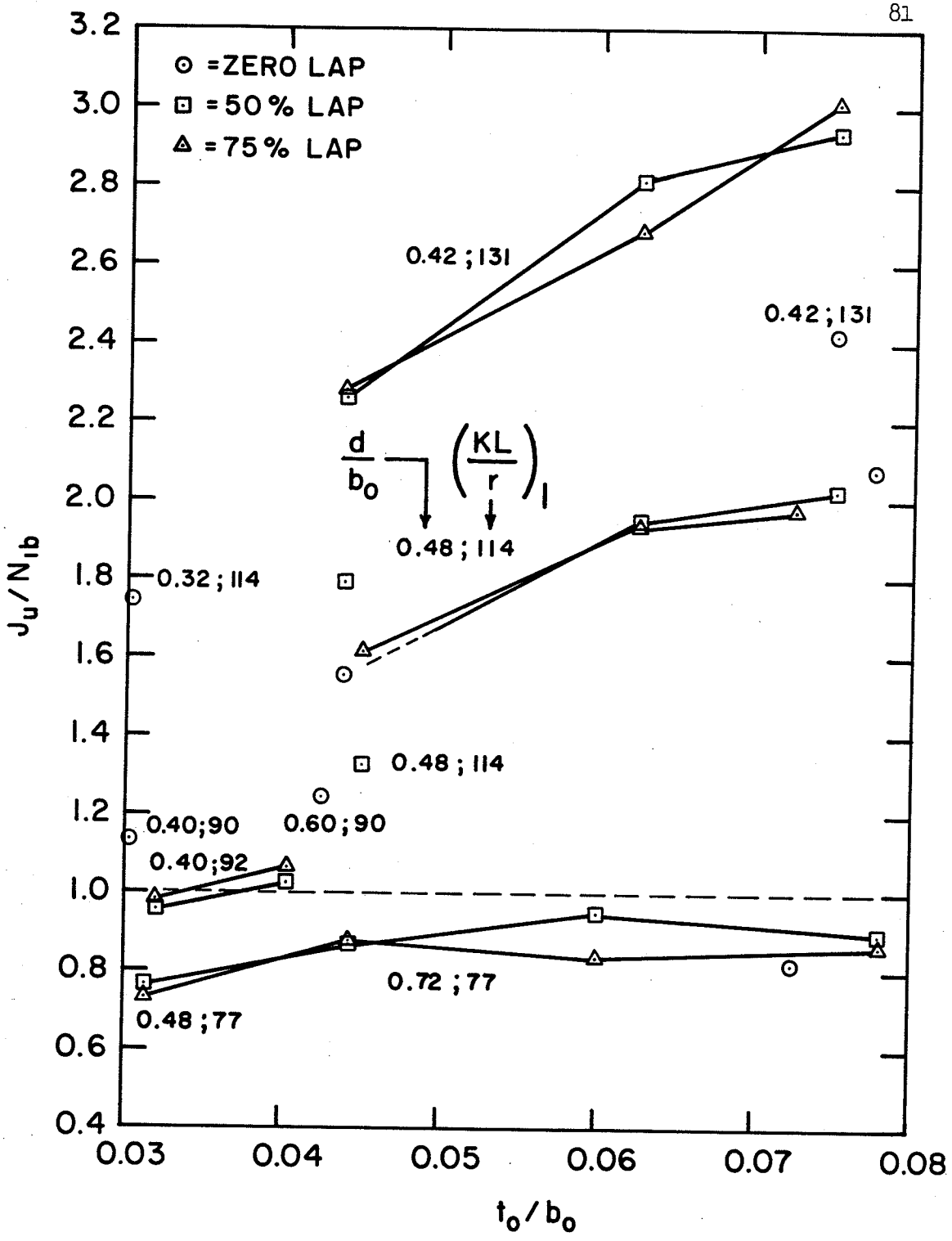

Fig. 3.29. Ratio of Joint Strength to Compression – Web Strength

In summary, the strength of a cropped-web joint with a zero to 75% overlap can be accurately estimated using Eq. 3.1. Examples illustrating the calculations of the joint strength by the limit state design or the working load design methods have been provided. The calculation can be facilitated by using a design chart or table, which can be easily produced. The strengths of the cropped-web joints were generally comparable to those of similar joints with sawn webs and gaps, provided that t_0/b_0 was smaller than about 0.07. They were usually larger than 85 to 100% of the yield loads in the tension webs or the buckling loads in the compression webs, provided that t_0/b_0 was larger than about 0.04. For efficient design, the web diameters should range about 0.4 to 0.6 times the width of the chord, and the slenderness ratio of the compression web should be larger than about 90. The effect of an increase in overlap was usually small. The strengths of the cropped-web joints are generally acceptable and the joints can be safely used in a tubular truss under static loads. The strengths may also be acceptable when a small weld gap is provided between the web members.

3.8. Joint Stiffness

The stiffness of a cropped-web joint along the compression web axis is defined as $k_1 = N_1/\delta_1$, where N_1 and δ_1 are, respectively, the force and displacement in the linear range along the compression web axis at the loaded chord face, as illustrated in Fig. 3.30. Similarly, the stiffness along the tension web axis is defined as $k_2 = N_2/\delta_2$, where N_2 and δ_2 are, respectively, the force and displacement in the linear range

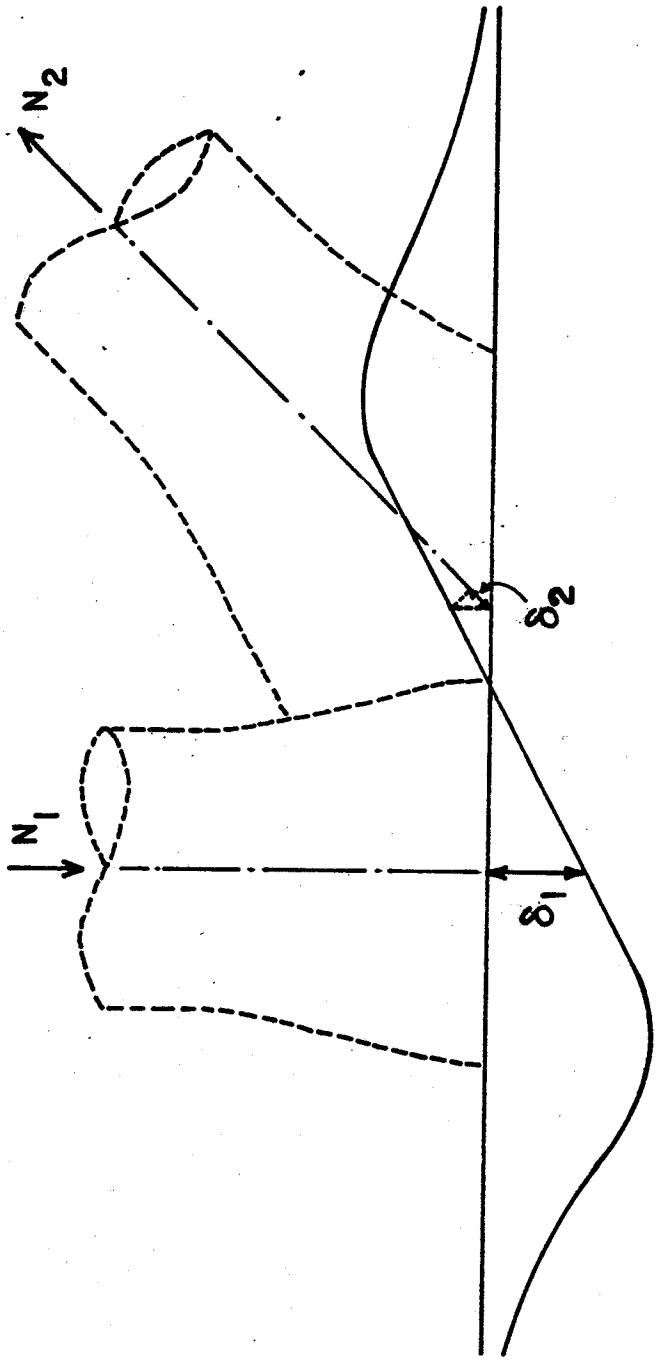

$k_1 = N_1/\delta_1$ $k_2 = N_2/\delta_2$

Fig. 3.30. Joint Stiffnesses

along the tension web axis at the loaded chord face. The values of k_1 and k_2 for the joints tested usually remained approximately constant until the loads were equal to about half the ultimate loads of the joints or near the working loads of the web members. These values are given in Table 3.2 in terms of k_1/Ed and k_2/Ed, where E is the modulus of elasticity (29000 ksi or 20000 N/mm^2) and d is the average outside diameter of the web members.

The estimated values of k_2/Ed were generally less accurate than those of k_1/Ed. This is because the axes of the tension webs, associated with k_2/Ed, were more difficult to locate accurately. In addition, the deformation components of the tension web along the chord axes were not measured and were neglected. Furthermore, the determination of the deformation at the tension web axis usually involved an interpolation, as no transducer was installed at the axis location because of limited available space.

The stiffness k_1 can be estimated from the following equation:

$$k_1/Ed = 0.0012 + 67.4(t_0/b_0)^3 + 6.91(t_0/b_0)^2 o_v \qquad (3.5)$$

The k_1/Ed values obtained from this equation and those obtained from experiments are plotted for comparison in Fig. 3.31. It can be seen that the experimental and calculated values agree quite well. The curves show that, for a given value of overlap o_v, k_1/Ed increases rapidly as t_0/b_0 becomes large. For a given value of t_0/b_0, k_1/Ed increases with o_v.

Equation 3.5 has been obtained by means of a stepwise multiple regression analysis and checked by a multiple regression analysis. According to the analyses, the equation relating the variables in this

Table 3.2. Joint Stiffnesses and Truss Deflections

Specimen	k_1/Ed %	k_2/Ed %	Δ_j in.	Δ_m in.	Δ in.	Δ_j/Δ_m %
1	1.38	5.26	0.193	1.169	1.36	16.5
2	0.84	3.18	0.320	1.169	1.49	27.3
3	0.64	1.33	0.413	0.983	1.40	42.0
4	0.47	1.78	0.567	0.975	1.54	58.2
5	0.44	2.09	0.461	0.775	1.24	59.5
1A50	0.67	4.78	0.277	0.627	0.90	44.1
1A75	0.81	-19.27	0.175	0.627	0.80	28.0
2A50	1.28	6.77	0.154	0.570	0.72	26.9
2A75	1.32	6.77	0.150	0.570	0.72	26.3
3A50	1.73	5.86	0.181	1.182	1.36	15.3
3A75	2.17	7.83	0.142	1.182	1.32	12.0
4A50	2.95	6.26	0.126	1.042	1.17	12.1
4A75	4.17	14.74	0.074	1.042	1.12	7.1
5A00	3.10	7.23	0.116	0.992	1.11	11.7
5A50	5.90	13.92	0.060	0.992	1.05	6.1
5A75	9.17	23.54	0.038	0.992	1.03	3.8
1B50	0.67	14.44	0.201	0.507	0.71	39.6
1B75	0.67	-3.89	0.138	0.507	0.64	27.3
3B50	1.01	3.81	0.263	1.100	1.36	23.9
3B75	1.66	9.37	0.145	1.100	1.24	13.2
4B50	3.03	6.77	0.106	0.978	1.09	10.8
4B75	3.30	14.05	0.078	0.978	1.06	8.0
5B00	3.48	7.02	0.096	0.927	1.02	10.4
5B50	4.77	15.86	0.058	0.927	0.99	6.3
5B75	4.37	14.03	0.064	0.927	0.99	6.9
1C50	0.78	-6.02	0.083	0.415	0.498	19.9
1C75	1.00	-6.02	0.060	0.415	0.475	14.4
3C50	1.41	9.06	0.110	0.704	0.81	15.6
3C75	1.78	14.84	0.083	0.704	0.79	11.8
4C50	2.41	10.12	0.071	0.586	0.66	12.1
4C75	2.60	18.38	0.059	0.586	0.65	10.0
5C00	2.33	4.64	0.095	0.516	0.61	18.4
5C50	4.57	18.44	0.038	0.516	0.55	7.3
5C75	5.21	21.95	0.033	0.516	0.55	6.3

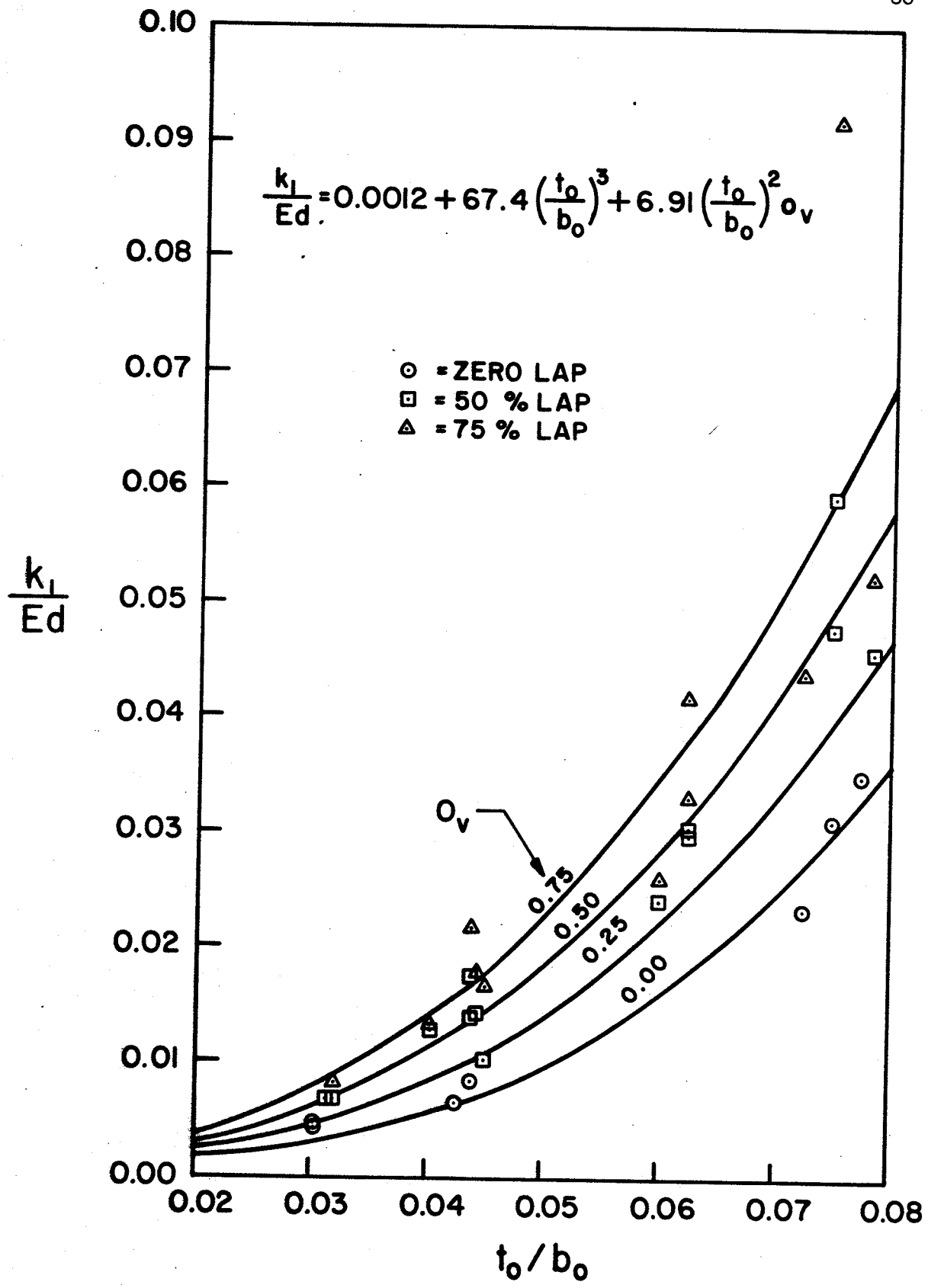

Fig. 3.31. Joint Stiffness Along Compression Web Axis

form is statistically significant at the 0.1% level. Thus k_1/Ed significantly depends on $(t_0/b_0)^3$ and $(t_0/b_0)^2 o_v$. The coefficients of the two independent variables are also significant at the 0.1% level. These two variables account for about 85% of the variation in the dependent variable. For simplicity, the parameter d/b_0 is not included in the equation.

In obtaining Eq. 3.5, the k_1/Ed values of specimens 1C50 and 1C75 were not included. These two specimens were not properly fabricated. Their welds were very poor and would be unacceptable in normal practice. Their overlaps were much larger than specified, being 114 and 131% instead of 50 and 75%. However, Eq. 3.5 predicted k_1/Ed values which agreed well with those of these two specimens. Thus the regression equation was not revised.

Both positive and negative values of δ_2, the displacement used to evaluate the stiffness k_2/Ed, were obtained for the joints tested. This observation, along with a consideration of the physical behavior of the joints, makes it clear that δ_2 equal to zero is possible, resulting in an infinite stiffness k_2/Ed. Curves involving k_2/Ed therefore possess a singularity and there are two regimes in which regression analysis could be applied, corresponding to δ_2 larger or smaller than zero, respectively. Since most of the joints had δ_2 larger than zero (i.e., very few negative values were obtained), curves were fitted only in the regime corresponding to positive δ_2, as shown in Fig. 3.32.

An alternative approach, which might have circumvented the problem of the singularity, would be to use the flexibility $1/k_2$ instead of the stiffness k_2. This was not tried.

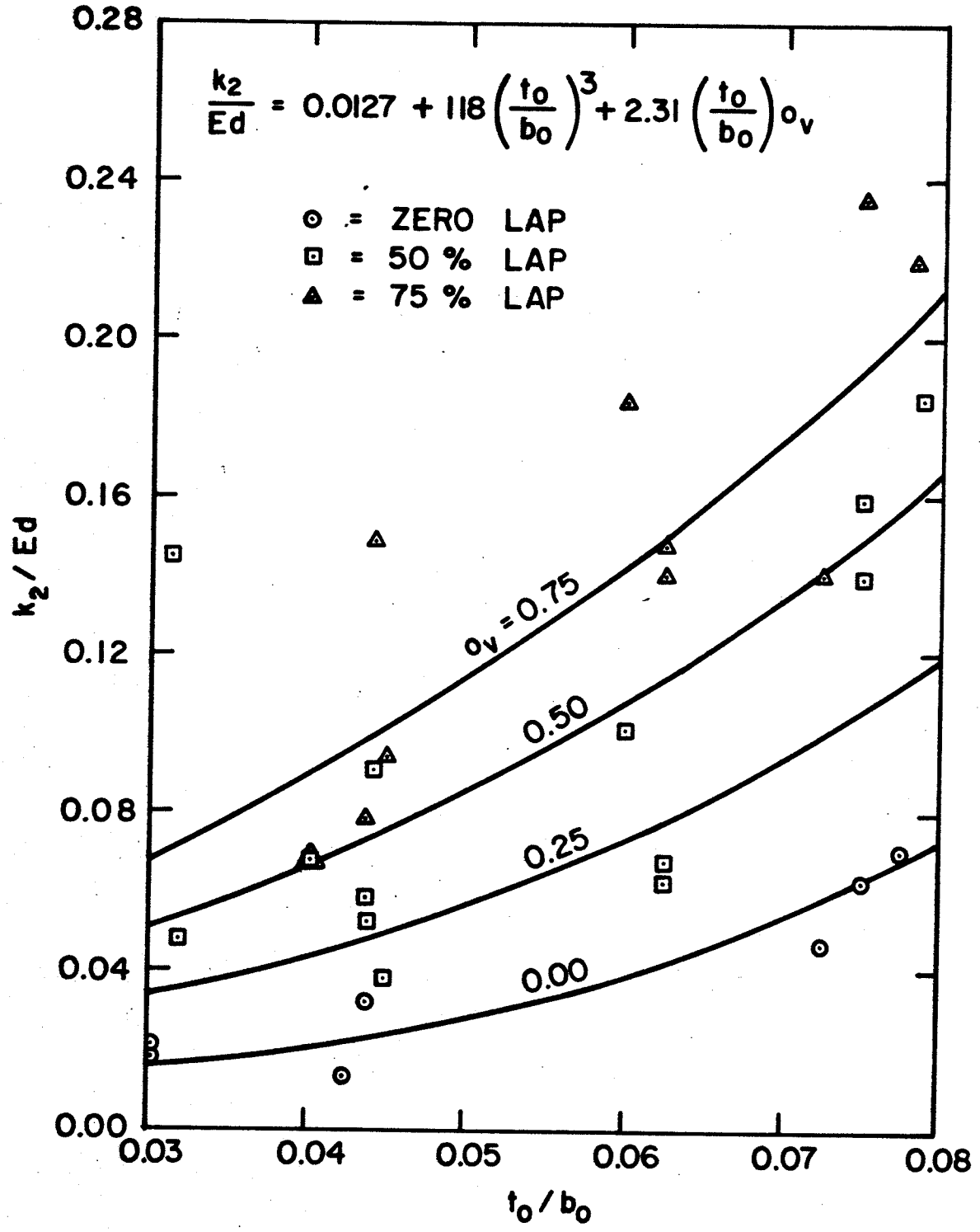

Fig. 3.32. Joint Stiffness along Tension Web Axis.

The stiffness k_2 along the axis of the tension web member can be estimated using the following empirical equation:

$$k_2/Ed = 0.0127 + 118(t_0/b_0)^3 + 2.31(t_0/b_0)o_v \qquad (3.6)$$

For comparison, the k_2/Ed values obtained from this equation and those obtained from the experiments are plotted against t_0/b_0 as shown in Fig. 3.32. It can be seen that they agree quite well. The stiffnesses k_2/Ed increase with increases in t_0/b_0 and overlap o_v.

The regression analyses used to obtain Eq. 3.6 showed that the equation is statistically significant at the 0.1% level. Thus the hypothesis that the regression is not significant is rejected; the stiffnesses k_2/Ed depend on the independent variables $(t_0/b_0)^3$ and $(t_0/b_0)o_v$. The coefficients of these two variables are significant at the 1.0% level. Finally, the regression of k_2/Ed on the two variables accounts for a significant amount (75.9%) of the variation in k_2/Ed.

Equation 3.6 does not predict k_2/Ed very well when t_0/b_0 is about 0.03 and overlap is 75% or larger. This is to be expected, because for these parameters, though the predicted values are positive, the experimental values are negative; thus the joints are outside the range of applicability of Eq. 3.6. Thus Eq. 3.6 can be used for prediction of k_2 only when t_0/b_0 is greater than about 0.03 and o_v is less than about 75%. The predicted values, however, can be used to conservatively estimate the increase in truss deflection due to joint deformation because a larger increase is obtained with the positive values.

The stiffnesses k_1 and k_2 can be used to estimate an increase in deflection of a tubular truss due to local deformations of the joints. Let Δ_j denote the truss deflection due to joint deformations, Δ_m the deflection due to changes in length of truss members, and $\Delta = \Delta_j + \Delta_m$ the overall deflection at midspan of the truss.

For practical trusses, the truss deflection due to joint deformations Δ_j is usually small compared to that due to changes in member lengths Δ_m. In other words, Δ_j/Δ_m is much less than 1.0. To illustrate this, a series of tubular trusses having geometry and loadings as shown in Fig. 2.1 was analyzed. The members and joints of each of these trusses were assumed to correspond to those of a particular test specimen. The method of virtual work (White, Gergely, and Sexsmith 1973) was used to calculate both Δ_j and Δ_m. The experimental values of k_1 and k_2 were used to calculate Δ_j. The calculated values of Δ_j, Δ_m, Δ, and Δ_j/Δ_m are given in Table 3.2. The Δ_j/Δ_m values are plotted against t_0/b_0 in Fig. 3.33. The Figure shows that Δ_j/Δ_m is usually smaller than 13% when t_0/b_0 is larger than 0.05, but can increase to 60% when t_0/b_0 is equal to 0.03.

The values of Δ_j/Δ_m shown in Fig. 3.33 represent an upper bound for most practical cases. This is because the trusses assumed have a large depth/span, thus small Δ_m and large Δ_j/Δ_m values, since Δ_j do not significantly vary with member lengths but Δ_m do. In addition, the Δ_j/Δ_m values are almost unaffected by a change in loading pattern or intensity, because both Δ_j and Δ_m vary with loads. Thus the values of

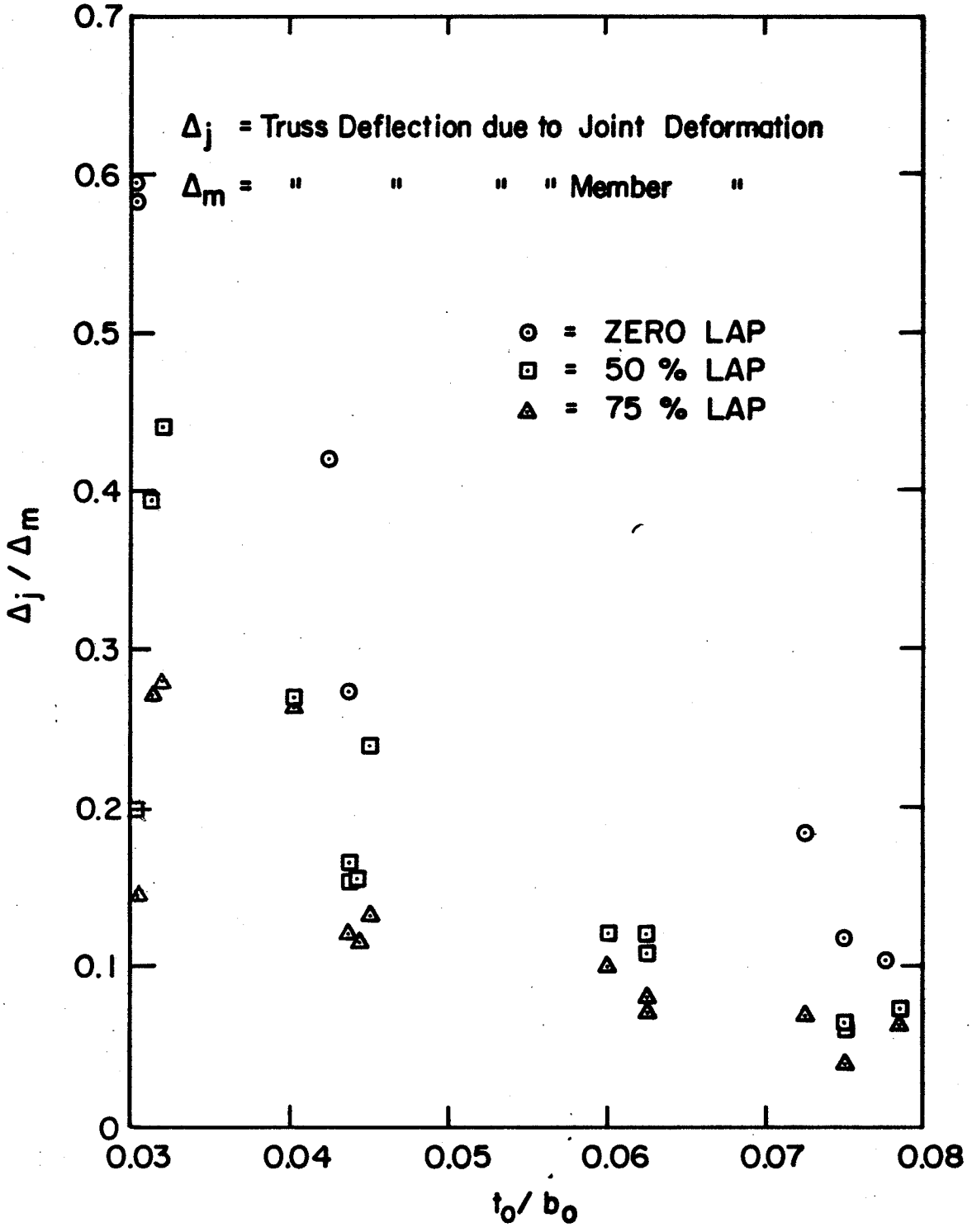

Fig. 3.33. Increase in Truss Deflection due to Joint Deformation.

Δ_j/Δ_m of typical trusses, which have a smaller depth/span, are usually smaller than the values shown in the Figure.

For example, if the span of the truss shown in Fig. 2.1 was doubled, keeping the same loading pattern and intensity, the Δ_j/Δ_m values shown could decrease by the order of 50%.

According to CSA Standard S16-1969, the maximum allowable deflection for the truss shown in Fig. 2.1 is span/180 = 3.2 in. (81 mm). This is larger than the calculated values of the total deflection Δ given in Table 3.2. Thus the truss deflections were acceptable.

In summary, the joint stiffnesses along the compression and tension web axes are given by k_1 and k_2 in Eq. 3.5 and 3.6. They can be used to estimate an increase in truss deflection due to joint deformations. The increase is generally small and may usually be neglected in most practical cases. However, if the truss deflection due to changes in member lengths is critical and t_0/b_0 is small (about 0.04 or lower), the increase in deflection due to joint deformations should be checked.

Chapter 4

THEORETICAL ANALYSIS

This chapter briefly describes the finite element method, computer programs, types of elements, and simplified models, used in the theoretical analysis of the cropped web joints.

4.1. The Finite Element Method

The finite element method, a powerful approximate numerical method for analyzing the forces and displacements in a structure, has been well covered in many books, including Przemieniecki 1968, Zienkiewicz 1971, Desai and Abel 1972. In this method, the structure is represented as an assemblage of finite elements interconnecting at nodes. The displacements at the nodes are usually chosen as primary unknown quantities, while the displacements in the elements are commonly assumed to vary according to some simple polynomial functions, called interpolation functions or displacement functions. Equations of equilibrium for each element are formulated in terms of a stiffness matrix and the displacements and forces at the nodes, using a variational principle such as the principle of minimum potential energy. The equations are combined into equilibrium equations for the whole structure. The nodal displacements are solved, and element strains and stresses computed.

4.2. The Computer Program Used

Based on the finite element method, many computer programs have been written to determine the forces and displacements in a structure under loads. One of these programs, written by Bathe, Wilson, and Peterson (1973), and called SAPIV (A Structural Analysis Program for Static and Dynamic Response of Linear System), was used in the analysis of cropped-web joints. The program contains many types of elements, three of which were used in the idealization of the joints. These three are a plane stress element, a thin plate (shell) element, and a boundary element.

The plane stress element, of a quadrilateral shape, was used to represent the web members. The element is isoparametric, that is, its geometry and displacements are described by the same parameters and have the same order. As a result, the displacements are compatible or conforming (continuous within and between elements) and complete (rigid body displacements and constant strain state of the element are possible).

The thin plate (shell) element, of a quadrilateral shape formed from four compatible triangles, was used to represent the chords. The membrane and bending behavior of the element are represented, respectively, by a constant strain triangle element and an "LCCT9" element.

The boundary element was used to idealize the supports of the specimens. It has one dimension and axial or torsional stiffnesses.

Data input for the analysis consisted of a heading card, a master control card, nodal point data cards, element data cards, concentrated load/mass data cards and element load multiplier cards. Data output included a print of input data for checking, nodal displacements/rotations, shell element stresses, stresses of the plane stress elements, and boundary element forces/moments.

4.3. Finite Element Models of Joints

A finite element model of cropped-web joints used in the study is shown in Fig. 4.1. Because of symmetry, only a half of each joint was used.

The chord, idealized by the thin plate elements, was assumed to have a width of $b_0 - t_0$, a depth of $h_0 - t_0$, and a thickness equal to the actual chord thickness t_0, where b_0 and h_0 are, respectively, the actual outside width and depth of the chord.

Each web member was idealized by the plane stress elements having the same cross-sectional area and moment of inertia as the member. The widths and thicknesses of the elements were assumed to be constant up to a point on the web axis one web diameter (d) above the cropped end, as illustrated in Fig. 4.2. Between this point and the cropped end, the width and thickness were assumed to vary linearly between the constant values and the values at the end, estimated by the formulas given in Fig. 4.2.

Two hinge supports at the chord and compression web ends were represented by two pairs of boundary elements, normal to each other, as

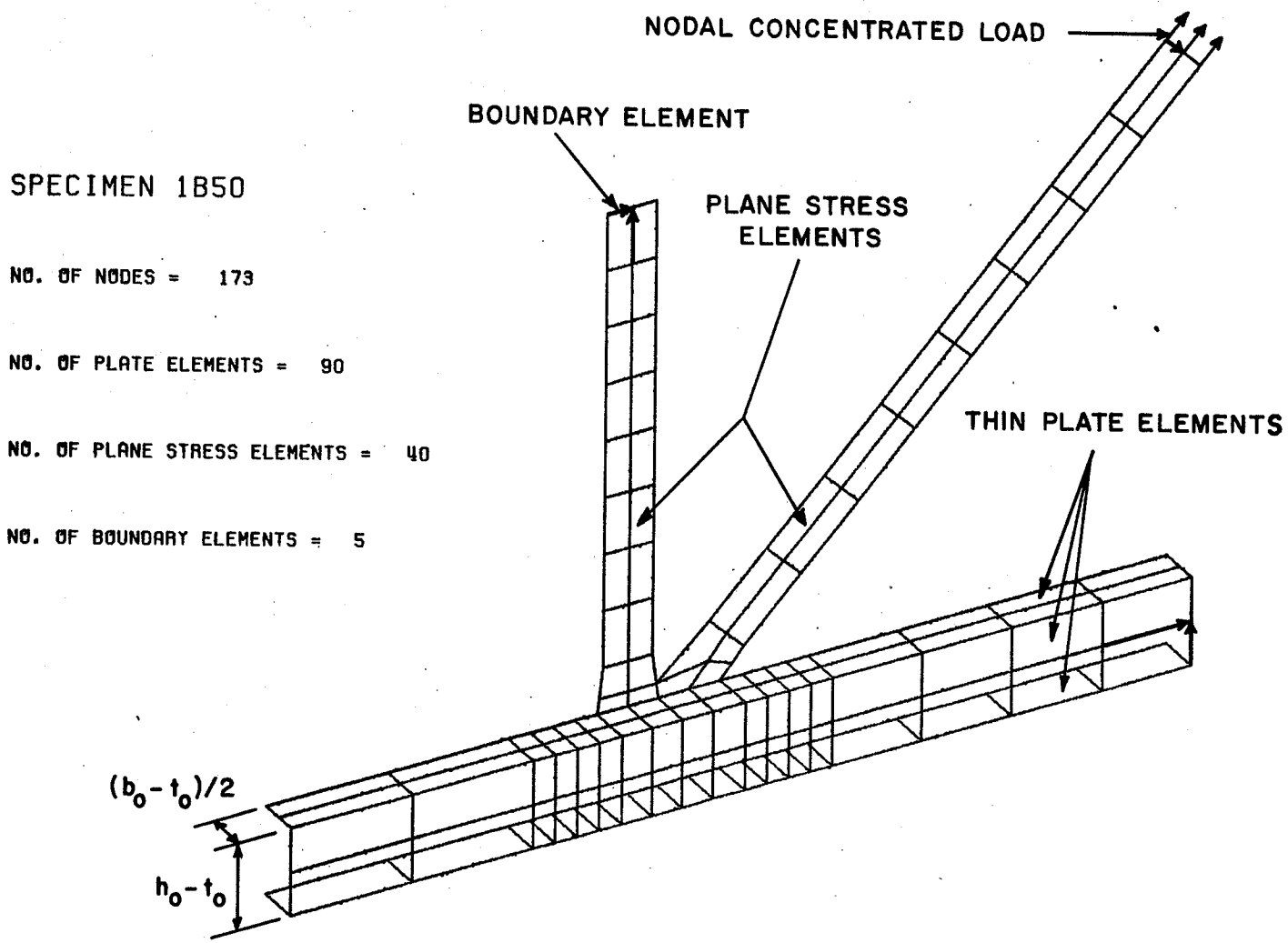

Fig. 4.1. Finite-Element Model of Cropped-Web Joints

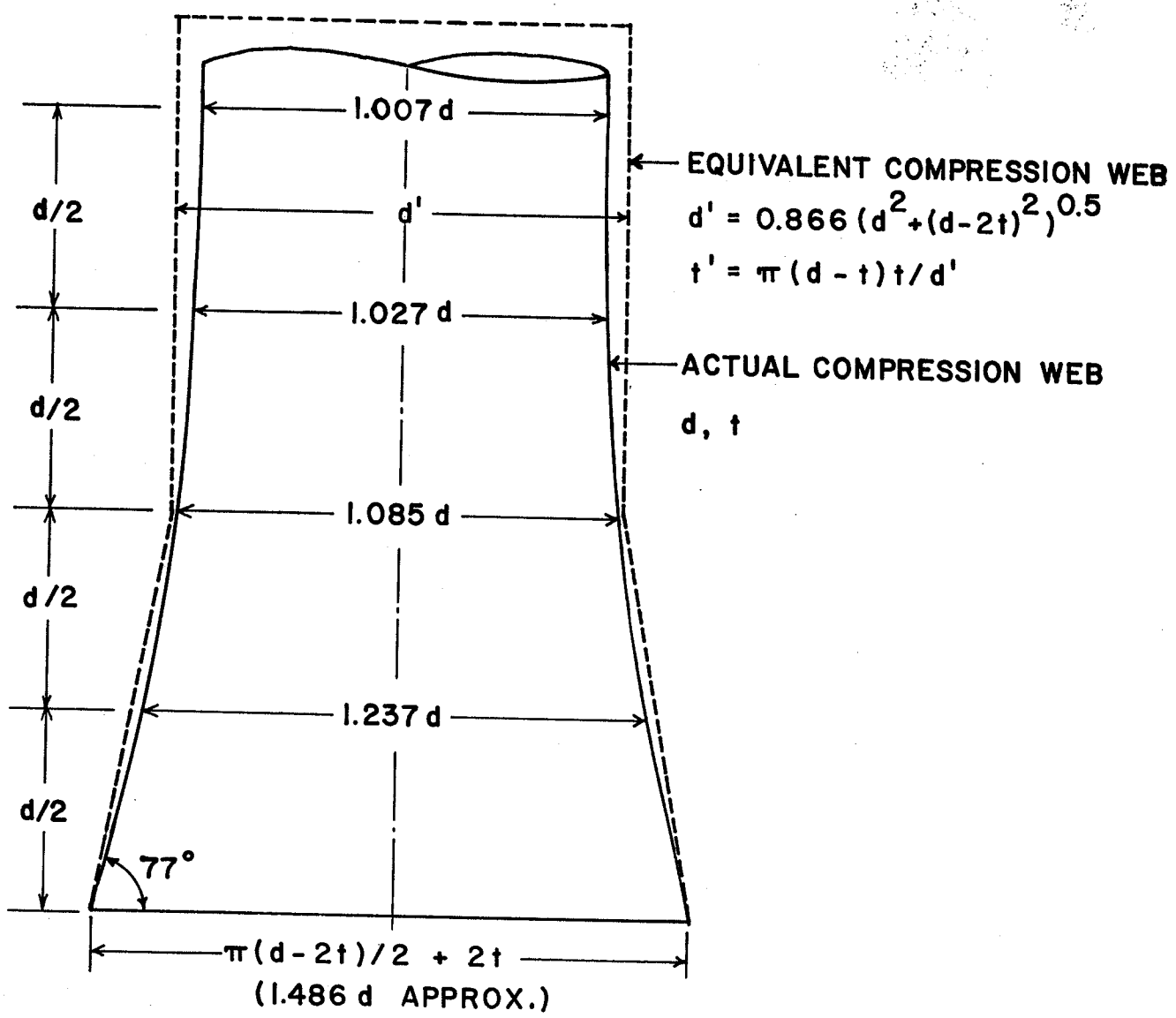

Fig. 4.2a. Compression Web Profiles

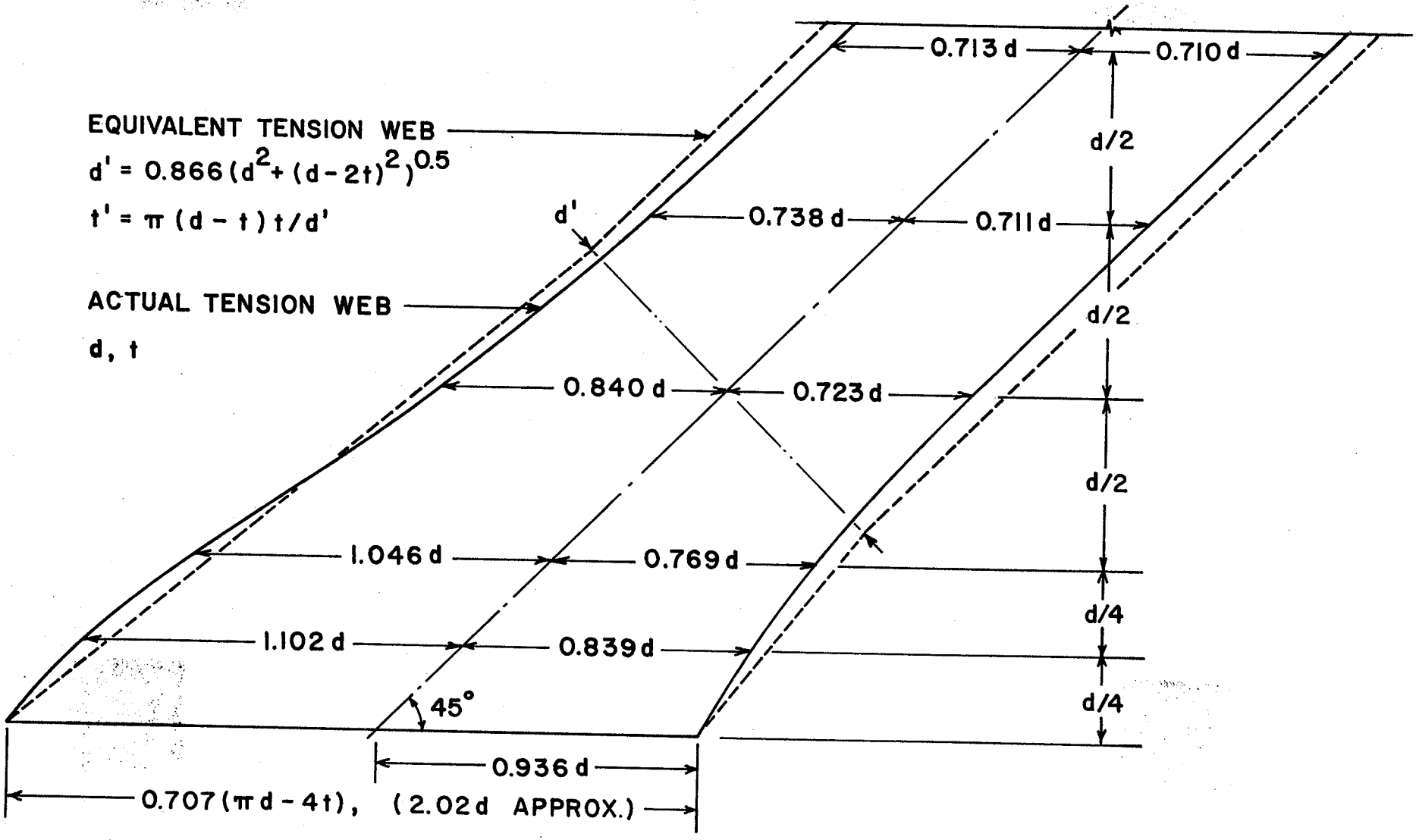

Fig. 4.2 b. Tension Web Profiles

shown in Fig. 4.1. A roller support at the tension web end was represented by another boundary element normal to the web axis.

An applied load producing an average stress of 30.0 ksi (207 N/mm^2) was assumed to distribute uniformly at the roller end of the tension web.

4.4. Data Generation Program

The amount of input data required for the finite element analysis of cropped web joints was quite large. The preparation and checking of the data was very tedious, although some of the data can be automatically generated by the SAPIV program. Thus, a computer program for generating the data was written.

The first input data card for the data generation program specifies the number of joints to be generated. The second card is a heading card identifying the joint. The third specifies the width, depth, thickness and length (b_0, h_0, t_0, and L_0) of the chord, the diameters, thicknesses, and lengths (d_1, t_1, L_1, d_2, t_2, and L_2) of the compression web and tension web, respectively, and also the percentage overlap (or percentage gap, negative of overlap) of the web members. The fourth card specifies the number of elements (N1 to N14) to be generated in 14 element fields, and the length factors YYL and YYR specifying the numbers of times of $(b_0 - t_0)/2$ to be used for the lengths adjacent to the compression and tension web members, respectively, as shown in Fig. 4.3. A set of cards similar to the second to the fourth cards is provided for each joint to be generated.

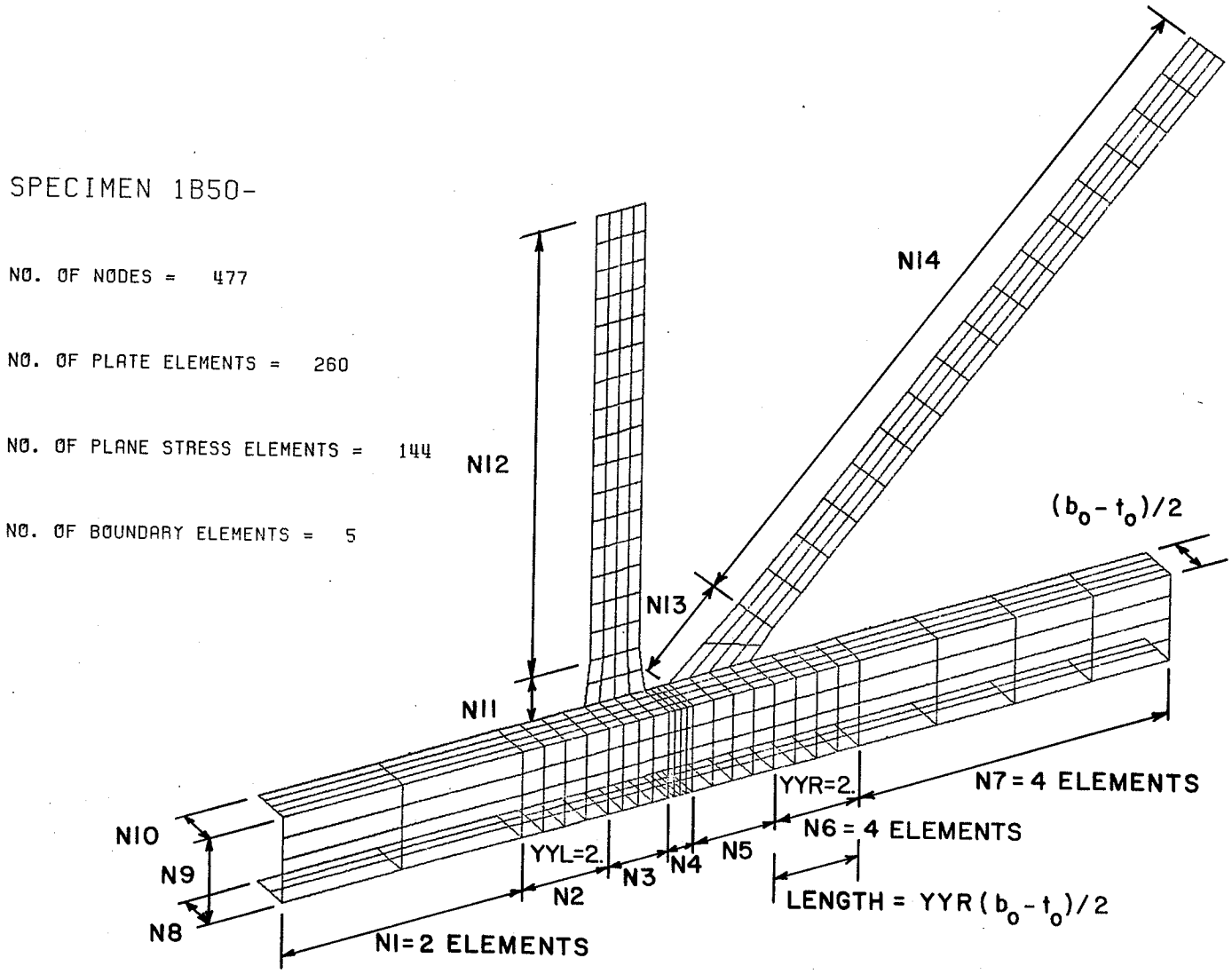

Fig. 4.3. Numbers of Elements and Length Factors

The program printed input and output data for checking. It also stored the output data on a permanent file for analysis by the SAPIV program.

A computer program was also written to read the joint data from the file and to plot the element meshes axonometrically, as illustrated in Fig. 4.1. The plots provide pictures of the joints and facilitate checking of the data.

Chapter 5

THEORETICAL RESULTS AND DISCUSSION

5.1. Deformations of Chord Faces

The deformations of the loaded chord face of a cropped-web joint, used to determine the stiffnesses of the joint, can be estimated quite accurately using a finite element analysis and a simplified model of the joint. The models used for specimen 5B00 are shown in Fig. 5.1. The deformations of the loaded chord face measured relative to those of the corners of the unloaded face of this specimen are shown in Fig. 5.2. Also shown is the deformation obtained from the experiment.

Figure 5.2 shows that the theoretical and experimental deformations agree quite well. The theoretical deformations increase as the numbers of nodes and elements are increased. They are generally smaller than the experimental deformations, as expected. However, they are slightly larger in some cases. This is probably because the weld, which distributes the loads more favorably on the chord face, was neglected in the theoretical models. In addition, the idealized models do not exactly represent the actual specimens. Moreover, the deformations vary considerably even with a slight change in chord thickness. Finally, there could have been errors in measurement.

The finite element models of specimens 5A00, 5A50, and of a similar specimen with a 50% gap (5A50-) are shown in Fig. 5.3. The deformations of the loaded chord faces of these specimens are shown in Fig. 5.4. It can be seen that the experimental and theoretical

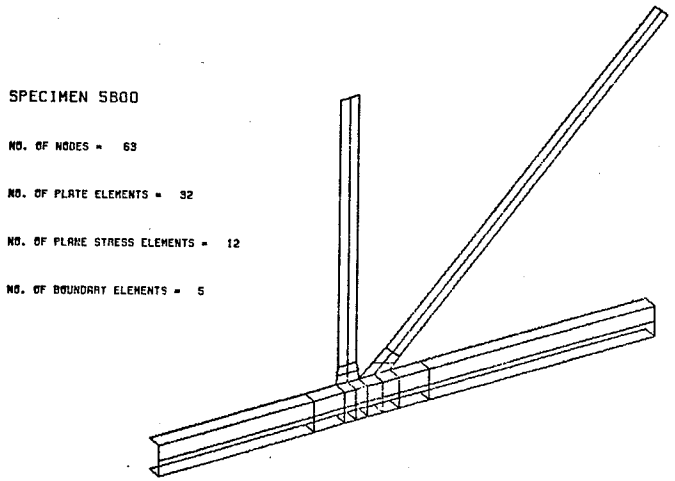

(a)

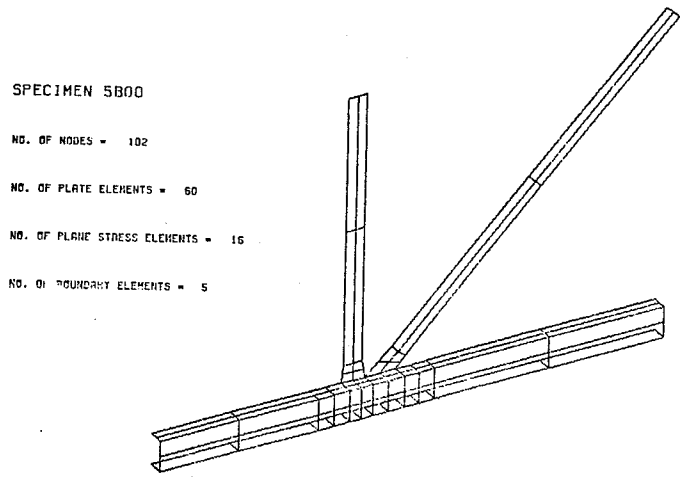

(b)

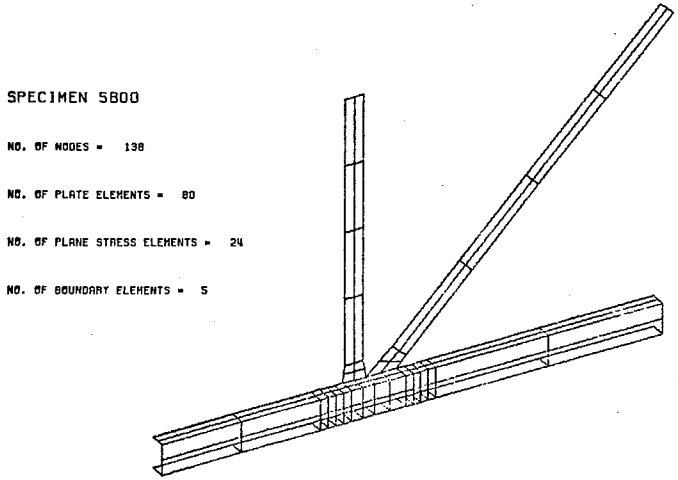

(c)

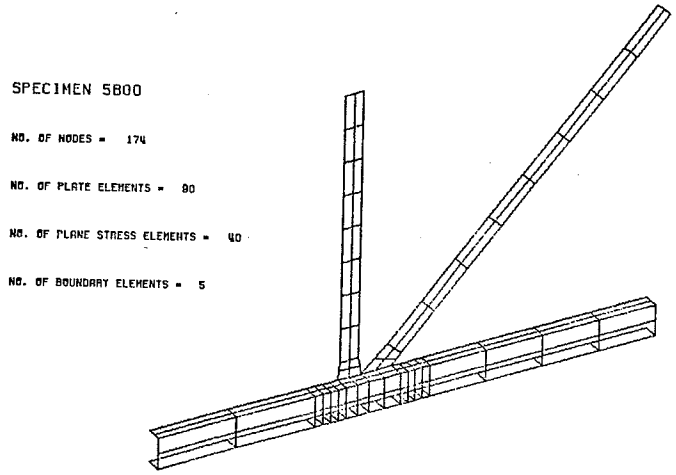

(d)

Fig. 5.1. Finite-Element Models for Specimen 5B00

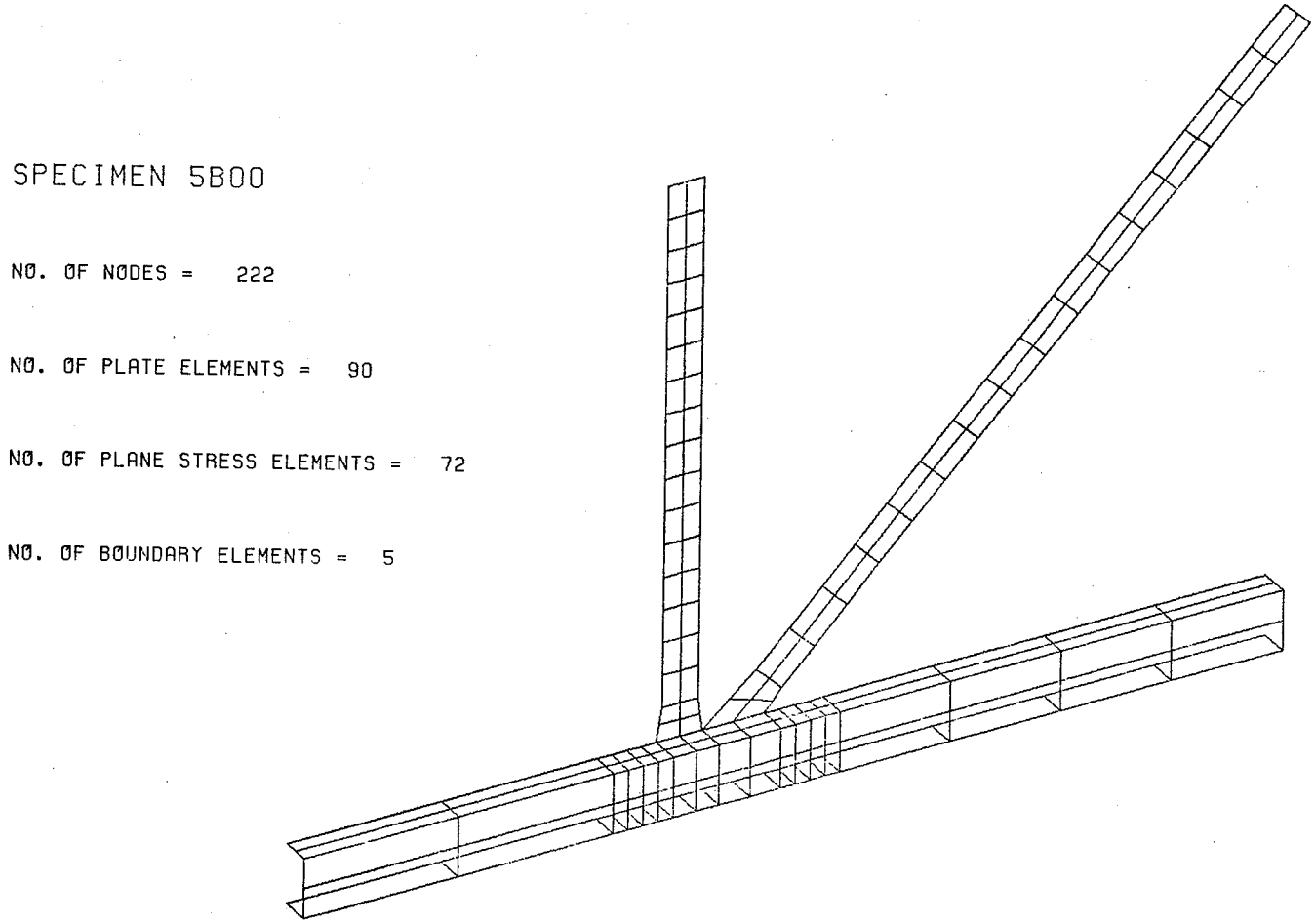

(e)

Fig. 5.1. Finite-Element Models for Specimen 5B00

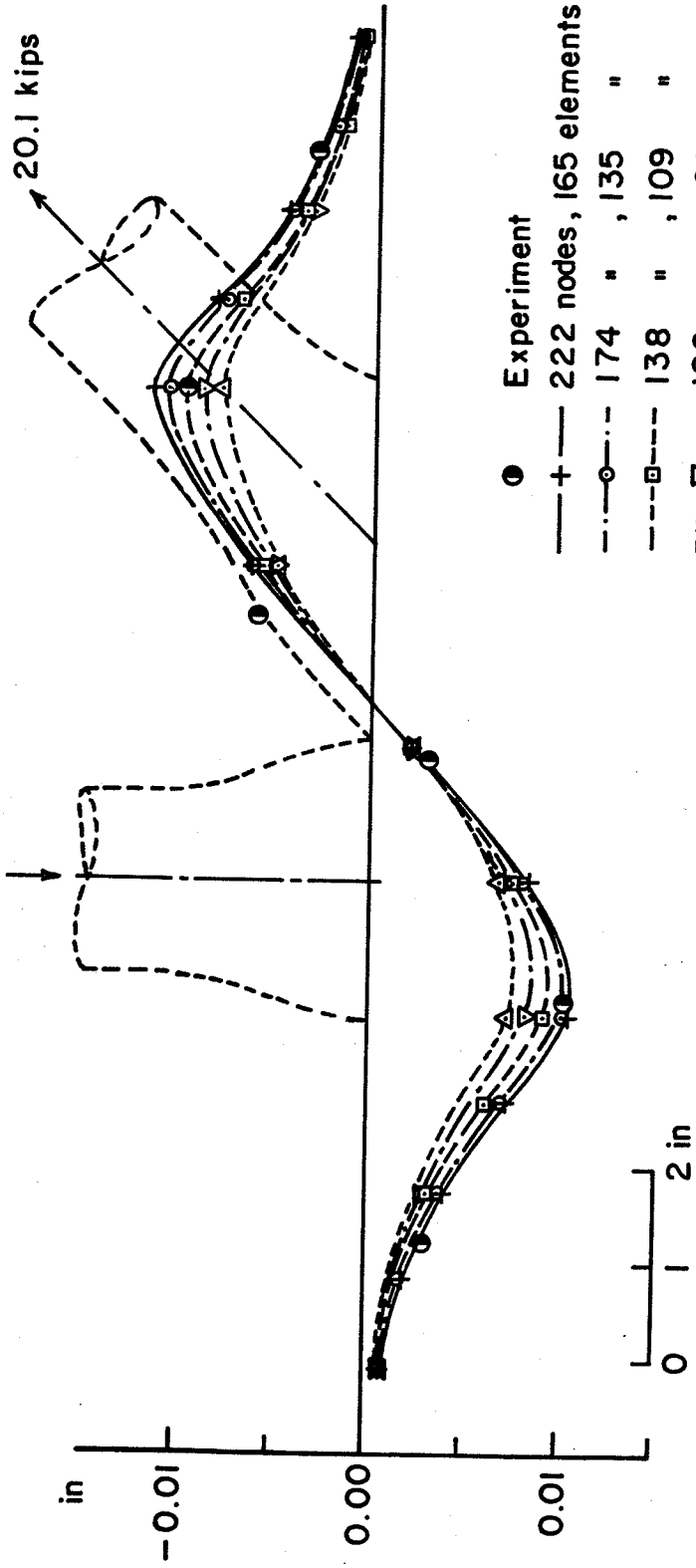

Fig. 5.2. Deformations of Loaded Chord Face of Specimen 5B00

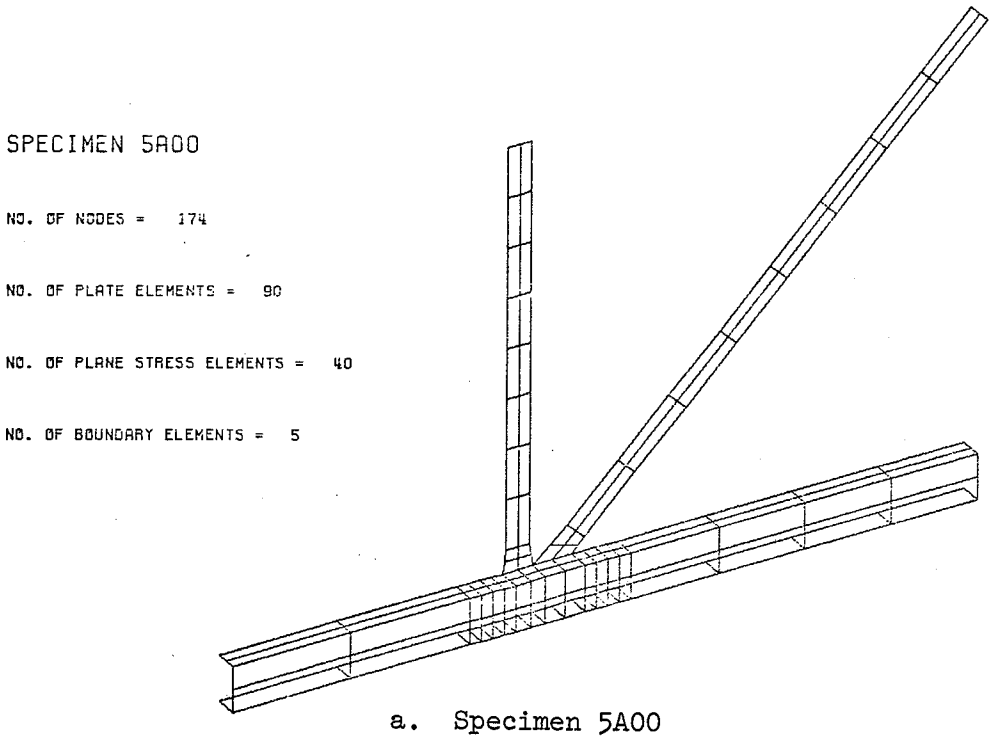

a. Specimen 5A00

Fig. 5.3. Finite-Element Models for Specimens 5A00, 5A50, and 5A50-

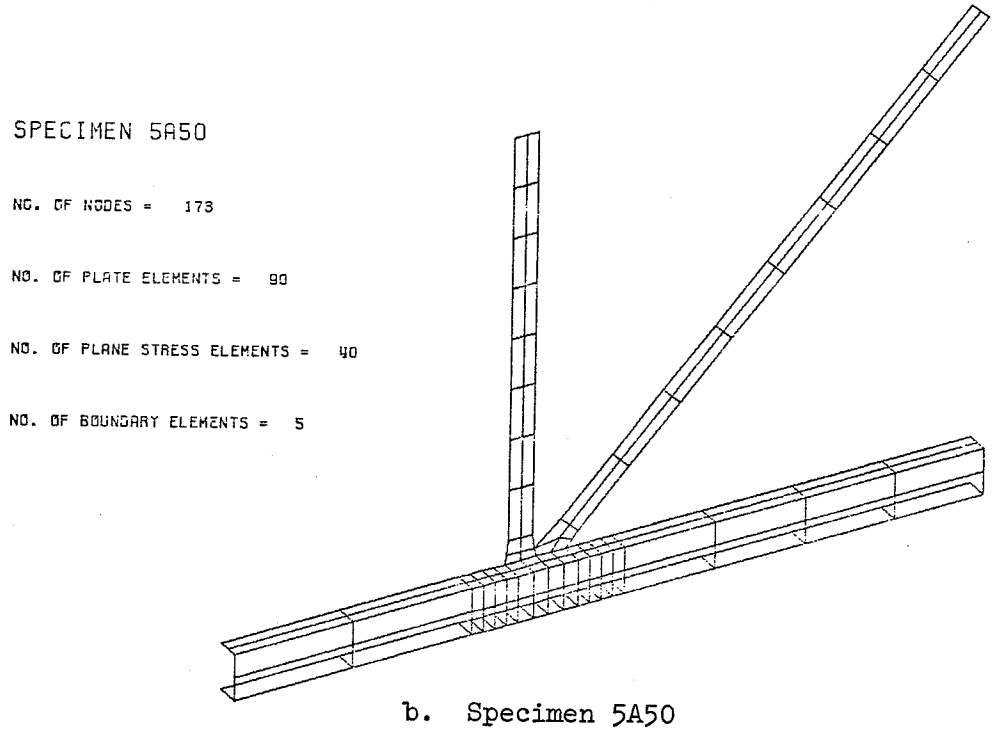

b. Specimen 5A50

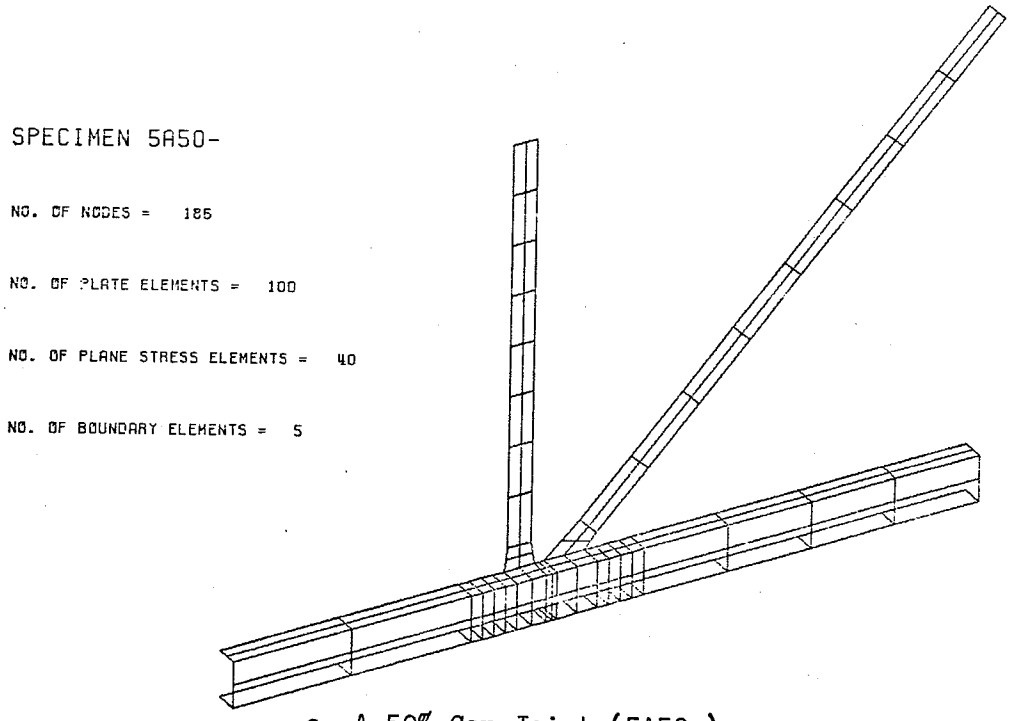

c. A 50%-Gap Joint (5A50-)

Fig. 5.3. Finite-Element Models for Specimens 5A00, 5A50, and 5A50-

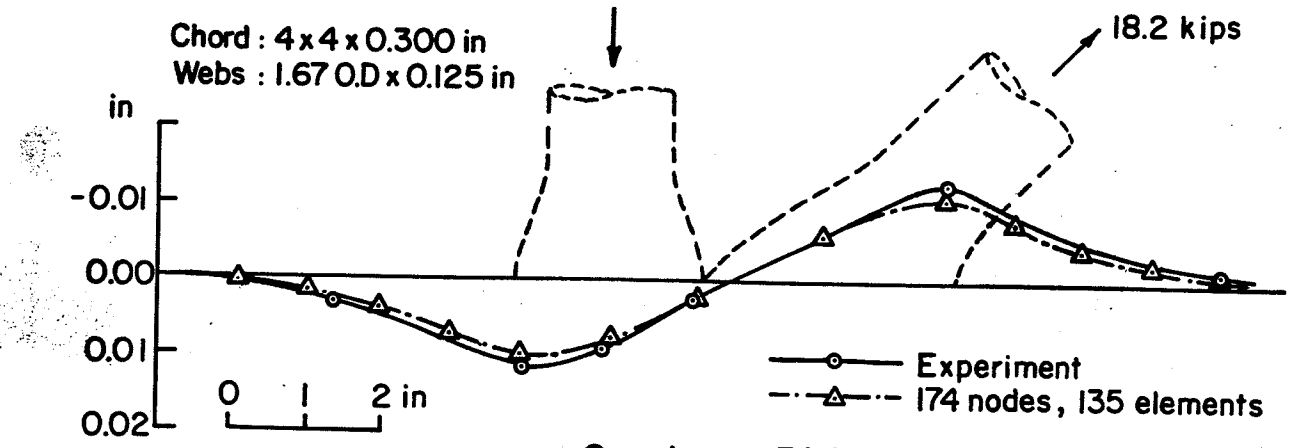

a. Specimen 5A00

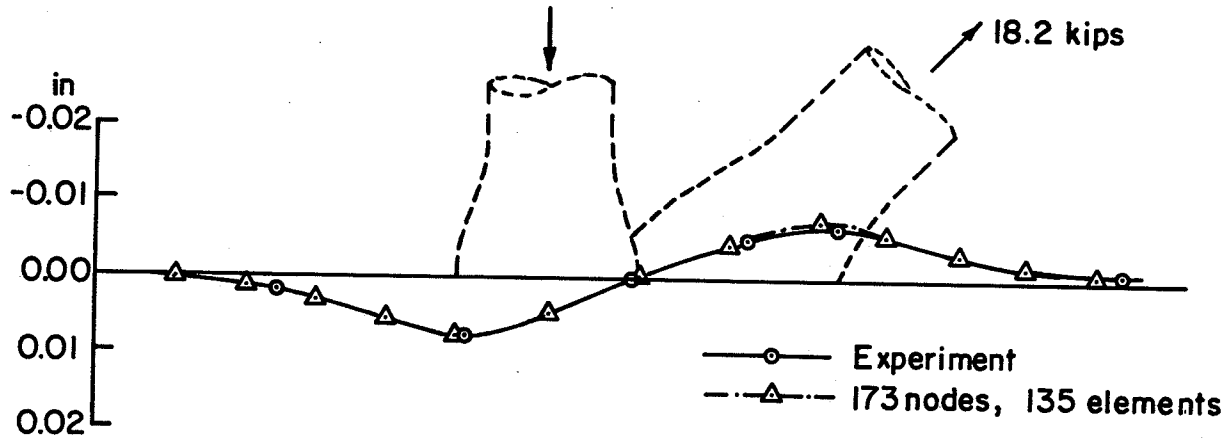

b. Specimen 5A50

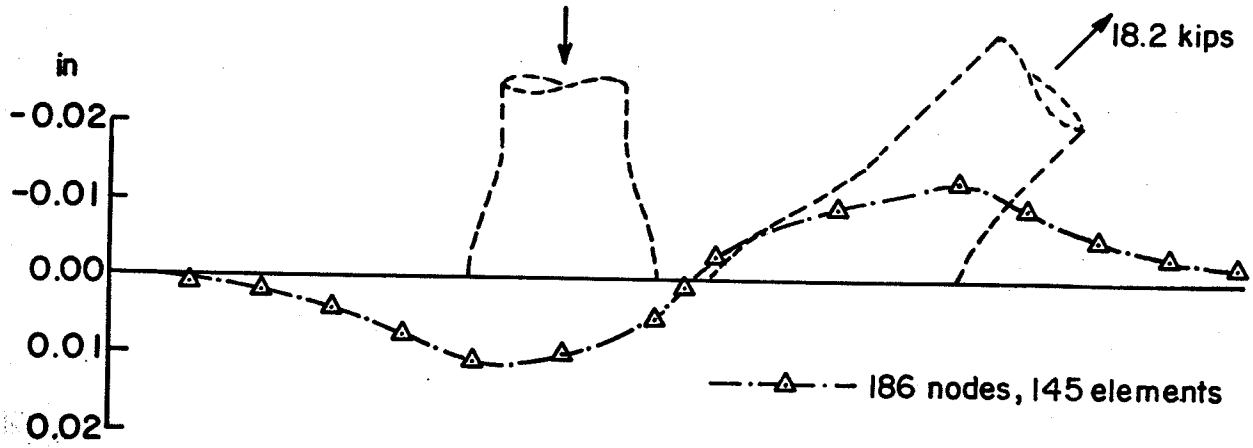

c. A 50%-gap joint (5A50-)

Fig. 5.4. Deformation of Loaded Chord Faces of Specimens 5A00, 5A50, and 5A50-.

deformations agree rather well. Furthermore, the deformations of a gap joint are generally larger than those of a lap joint.

The finite element models shown in Fig. 5.3, which have about 135 to 145 elements and 173 to 186 nodes, usually give satisfactory deformations with reasonable computational economy for joints having a chord width (b_0) of four inches (102 mm). For this chord width, the ratios of the theoretical deformation to the experimental deformation at the peak values of the chord face (δ_t/δ_e) usually vary from about 0.80 to 1.20, as shown in Table 5.1. Thus, an agreement between the theoretical and experimental deformations of the order of 20% is usually obtained for a joint with a chord width of four inches and having one of the models shown in Fig. 5.3.

When the chord width b_0 is six inches (152 mm), the models shown in Fig. 5.3 may result in large element sizes and small deformations. The ratios of the theoretical and experimental deformations for this chord size vary from 0.41 to 0.74, as shown in Table 5.1. The results can be improved by subdividing the elements, thus reducing the element sizes and increasing the numbers of nodes and elements. This is illustrated in Fig. 5.5 and 5.6. The former shows the models of specimen 1A50, while the latter shows the deformations of the chord face of this specimen, which has one of the poorest theoretical results. It can be seen that a discrepancy in deformation of 59% is reduced to 32% by increasing the numbers of elements from 135 to 259. Further improvements are possible if the elements are further subdivided, especially those in the vicinity of the joint.

Table 5.1. Ratios of Peak Theoretical and Experimental Deformations of Chord Faces, δ_t/δ_e, using 135-element Models

Specimen	b_0, h_0 in.	δ_t/δ_e at working load (approx.)
1	4.00	0.90
2	4.00	0.80
3	6.00	0.54
4	6.00	0.73
5	6.00	0.74
1A50	6.00	0.41
1A75	6.00	0.41
2A50	6.00	0.71
2A75	6.00	0.60
3A50	4.00	0.88
3A75	4.00	0.73
4A50	4.00	0.80
4A75	4.00	0.86
5A00	4.00	0.87
5A50	4.00	1.13
5A75	4.00	1.18
1B50	6.00	0.48
1B75	6.00	0.62
3B50	4.00	0.64
3B75	4.00	0.78
4B50	4.00	0.91
4B75	4.00	0.90
5B00	4.00	1.09
5B50	4.00	1.26
5B75	4.00	0.89
1C50	6.00	-
1C75	6.00	-
3C50	4.00	0.89
3C75	4.00	0.97
4C50	4.00	1.15
4C75	4.00	0.85
5C00	4.00	0.87
5C50	4.00	1.38
5C75	4.00	1.10

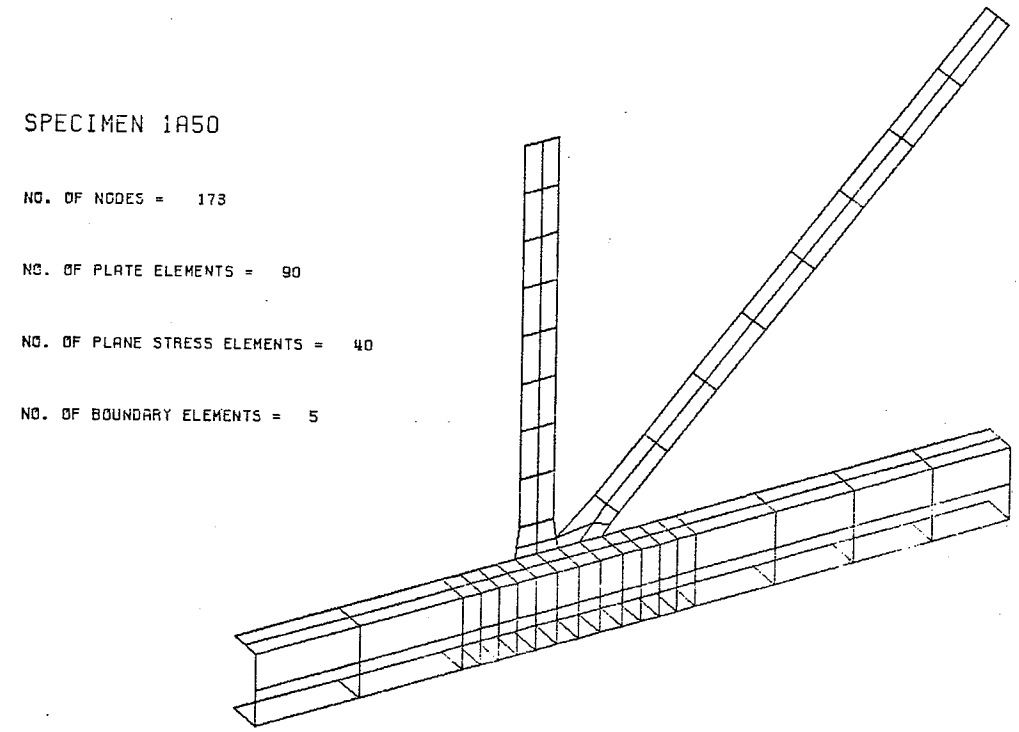

(a)

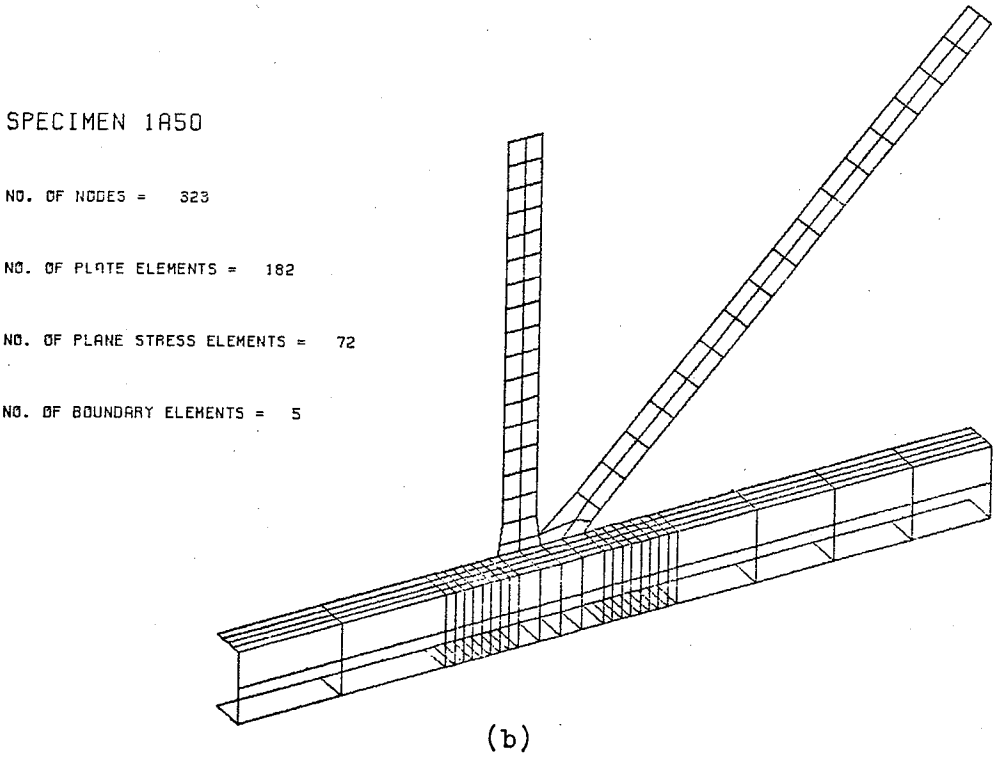

(b)

Fig. 5.5. Finite-Element Models for Specimen 1A50

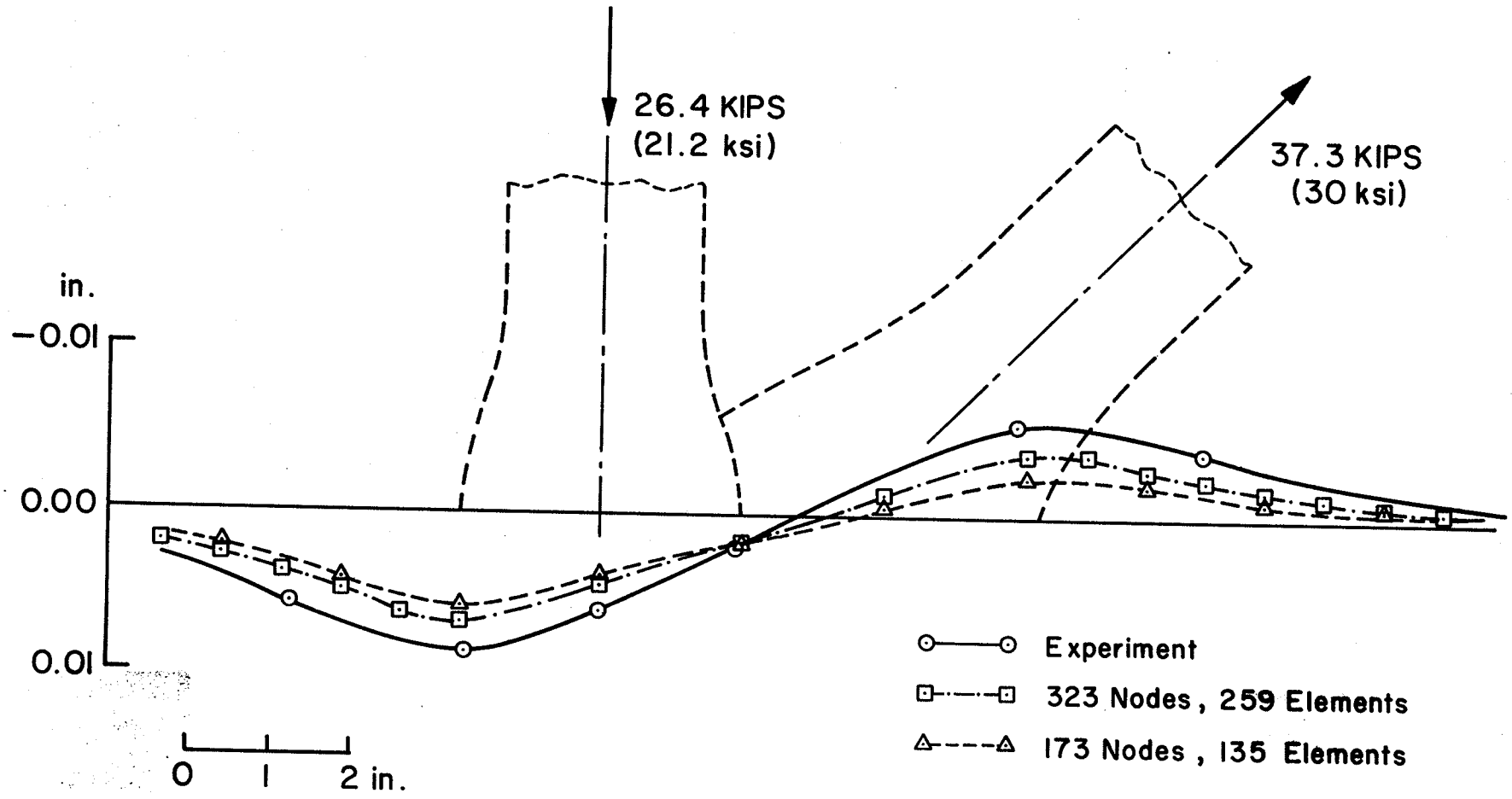

Fig. 5.6. Deformations of Loaded Chord Face of Specimen 1A 50

The theoretical deformations of the loaded chord faces increased more rapidly when incompatible bending modes were used for the plane stress elements representing the web members. However, such uses could result in theoretical deformations larger than experimental deformations, particularly when the chord widths were small. Thus the incompatible bending modes were suppressed in the analyses.

5.2. Deflections of Compression Webs

The deflections of the compression webs, indicating bending of the members, are also given by the finite element analysis. Illustrated in Fig. 5.7 are the theoretical deflections of the compression web axis of specimen 5B00 idealized as shown in Fig. 5.1. It can be seen that the deflections increase and converge as the elements along the web are subdivided.

Also shown in Fig. 5.7 is the experimental deflection which has been adjusted to account for a rigid body translation caused by initial movements of the pin supports at the ends. The experimental deflection agrees well with the theoretical deflection of the model which has 174 nodes. The theoretical deflection of model with 222 nodes appears larger than the experimental deflection. This is rather unreasonable and probably results from errors in measurement. If even one of the measurements of the deflections were inaccurate, the curvature of the experimental deflection curve would be significantly changed.

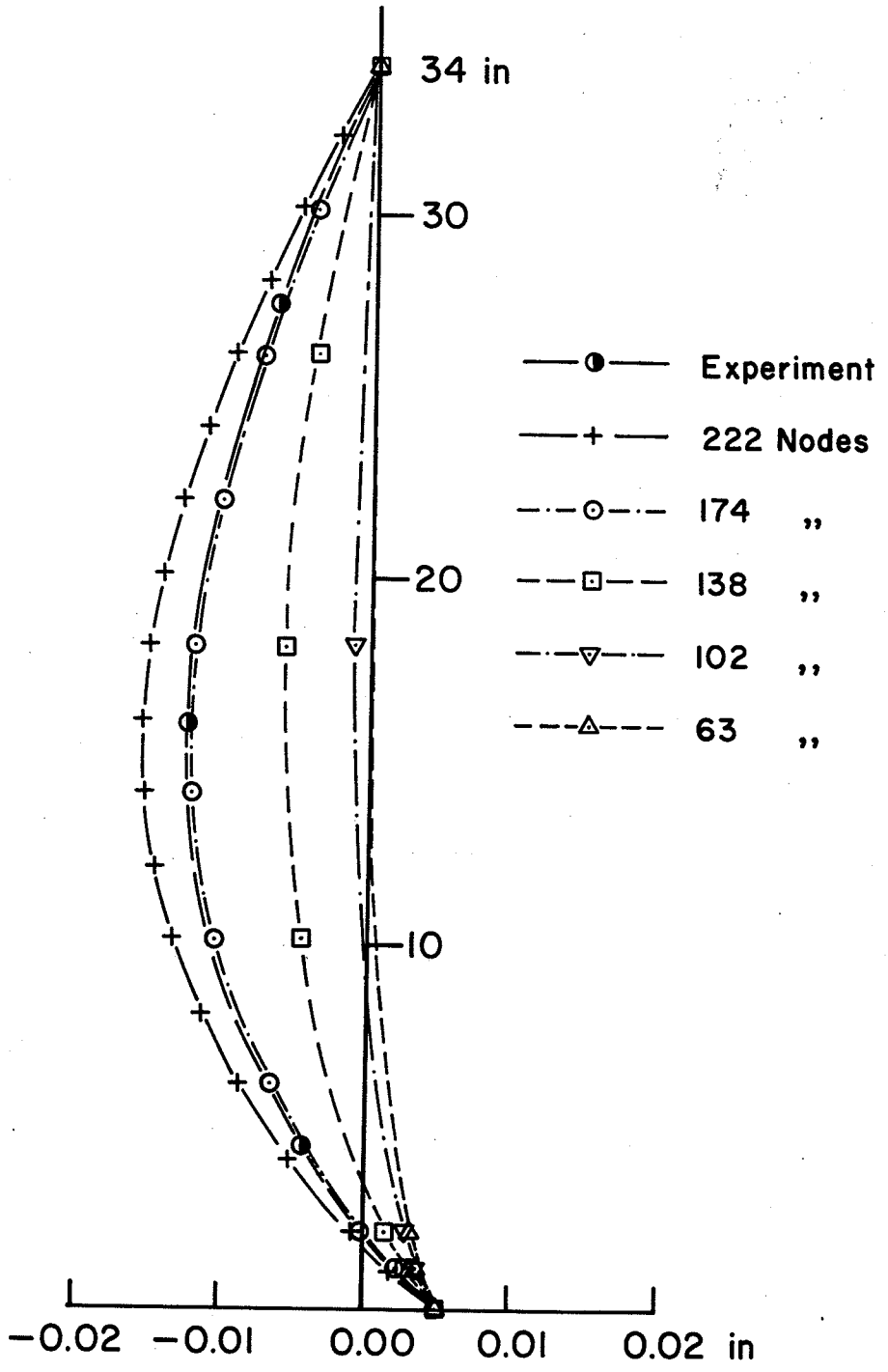

Fig. 5.7 . Deflections of Compression Web of Specimen 5B00 .

5.3. Stresses and Strains on Chord Faces

The stresses and strains on the chord faces of a specimen can be calculated using a finite element analysis for the idealized models. The stresses consist of both bending and membrane components. The bending stresses near the joint are usually larger than the membrane stresses, since the chord face at the joint is transversely loaded. The strains are calculated from the stresses, using theory of elasticity, and compared with measured values.

The surface bending stresses σ_{xb} and σ_{yb} along the x and y axes can be calculated from the bending moments per unit length M_{xx} and M_{yy} given by the finite element analysis. The directions of M_{xx} and M_{yy} are illustrated in Fig. 5.8. The subscripts xx and yy refer to the local coordinates x and y of a plate element.

According to the theory of elasticity (Wang 1953), the surface bending stresses are related to the bending moments per unit length as follows:

$$\sigma_{xb} = 6\, M_{xx}/t_0^2$$
$$\sigma_{yb} = 6\, M_{yy}/t_0^2 \qquad (5.1)$$

where t_0 = plate thickness.

The bending strains are related to the bending stresses as:

$$\varepsilon_{xb} = (\sigma_{xb} - \nu\sigma_{yb})/E$$
$$\varepsilon_{yb} = (\sigma_{yb} - \nu\sigma_{xb})/E \qquad (5.2)$$

where ν = Poisson's ratio (0.3),

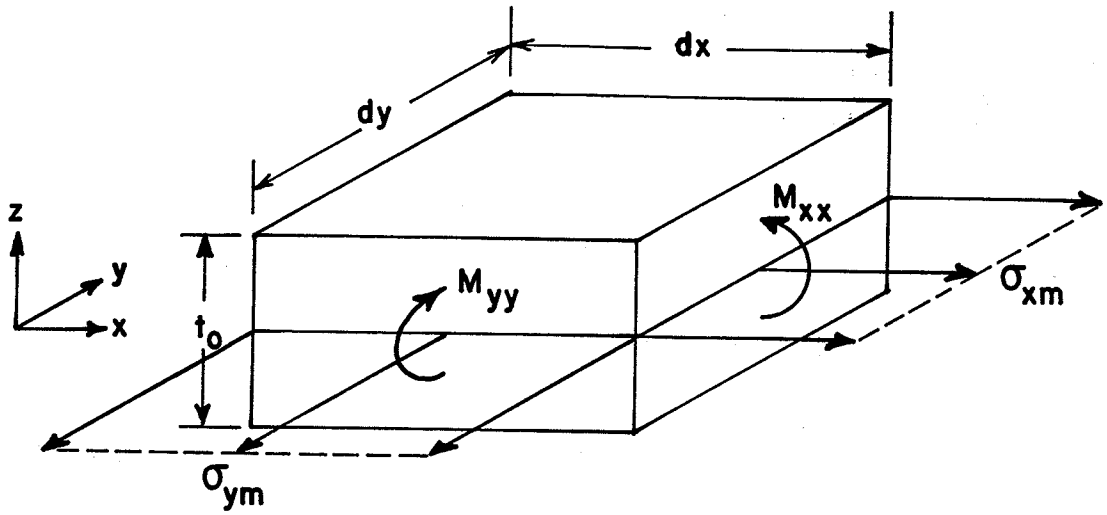

Fig. 5.8. Bending Moments per Unit Length and Membrane Stresses

and E = Young's modulus (29000 ksi or 200000 N/mm^2).

The membrane stresses σ_{xm} and σ_{ym}, shown in Fig. 5.8, are also given by the finite element analysis. The membrane strains in the local x and y directions are:

$$\varepsilon_{xm} = (\sigma_{xm} - \nu\sigma_{xm})/E$$
$$\varepsilon_{ym} = (\sigma_{ym} - \nu\sigma_{xm})/E \qquad (5.3)$$

The total surface strains are equal to the sums of the bending and membrane strains, that is,

$$\varepsilon_{xx} = \varepsilon_{xb} + \varepsilon_{xm}$$
$$\varepsilon_{yy} = \varepsilon_{yb} + \varepsilon_{ym} \qquad (5.4)$$

To illustrate the calculations of stresses and strains on the chord faces, specimen 5B75 is considered. The idealized model of this specimen having 283 nodes and 239 elements as shown in Fig. 5.9 was analyzed by the finite element method. The distributions of bending moments per unit length M_{xx} and M_{yy} along four straight lines passing through the centroids of plate elements of the loaded chord face are shown in Fig. 5.10. It can be seen that these moments are non-uniform, being relatively large near the extremities of the joints. The moments M_{xx} and M_{yy} at section A of specimen 5B75, obtained from two idealized models shown in Fig. 5.9, are given in Fig. 5.11. It can be seen that the moments from the different models agree very well. Moreover, the moments along the centre line of the top chord face are large compared to others.

Since transverse strains at section A of specimen 5B75 were

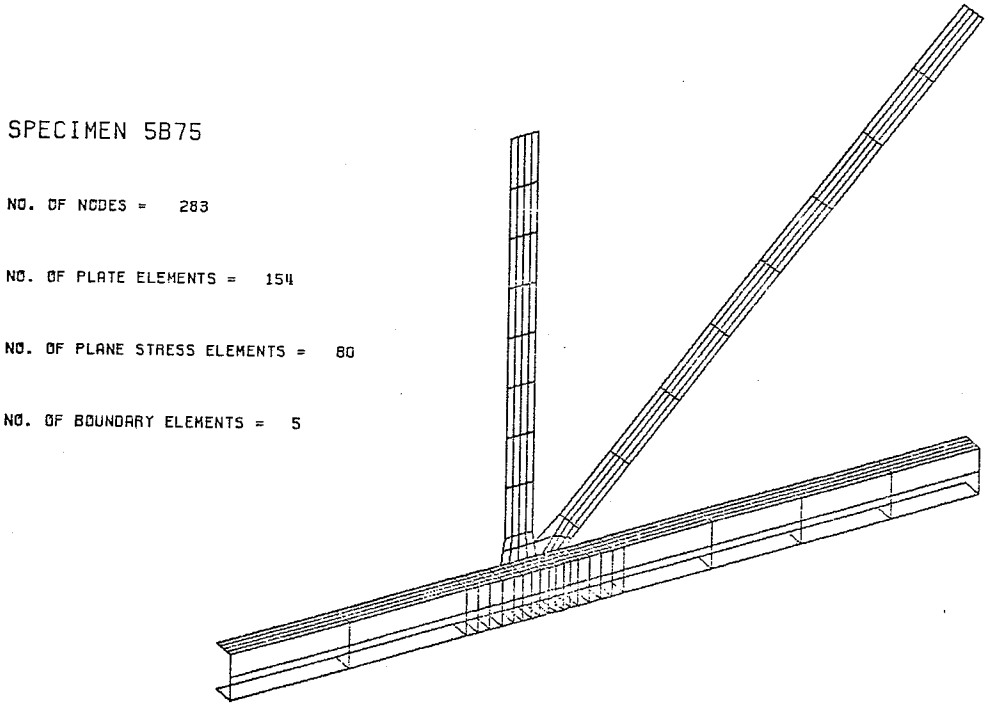

(a)

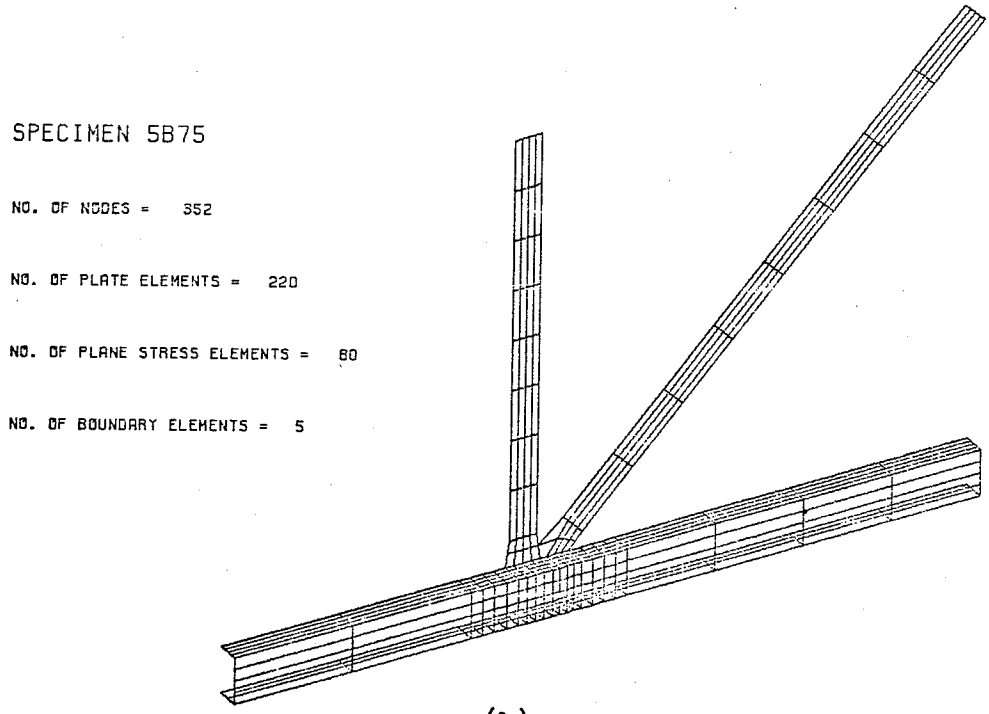

(b)

Fig. 5.9. Finite-Element Models for Specimen 5B75

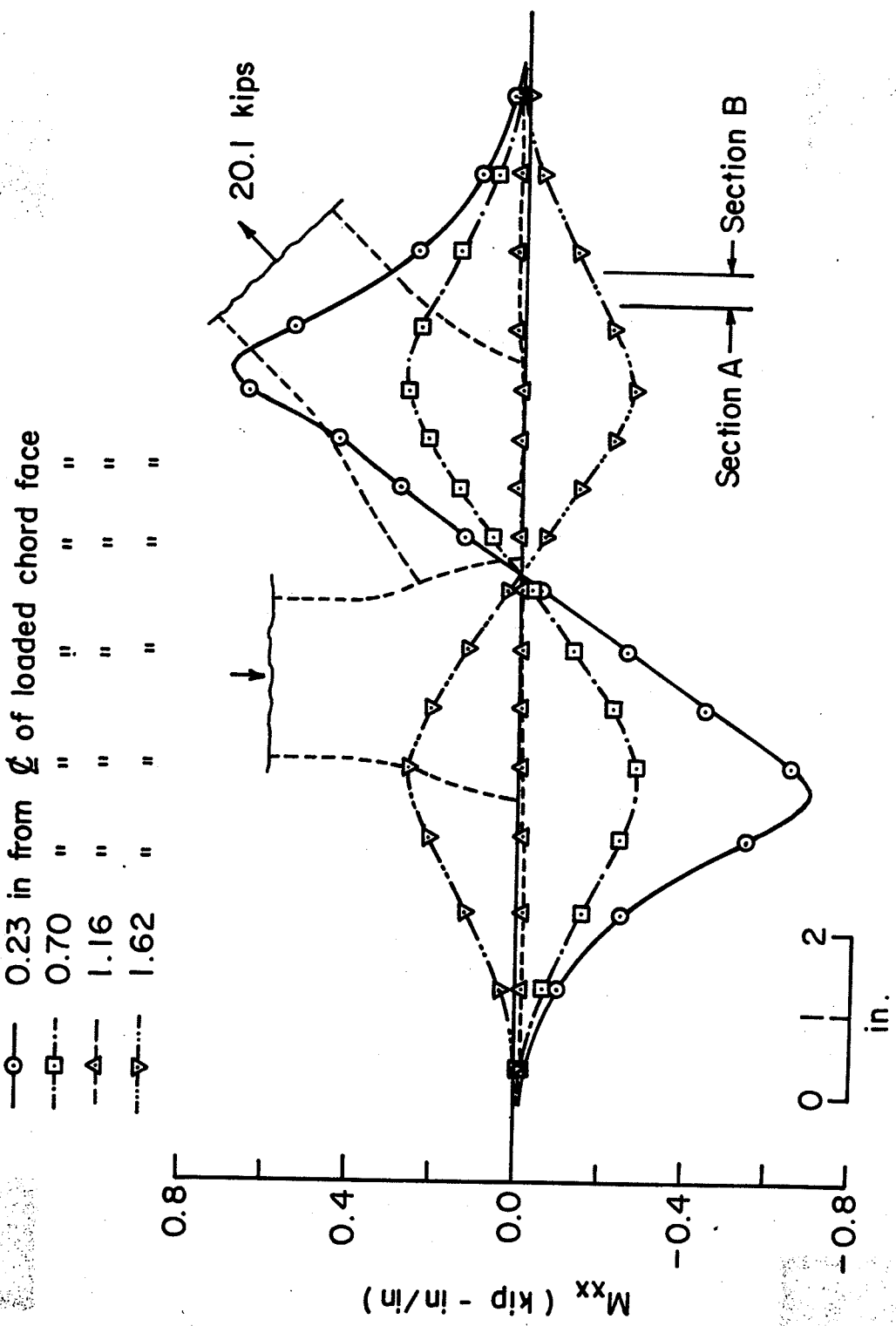

Fig. 5.10a. M_{xx} for Loaded Chord Face of Specimen 5B75 (283 Nodes)

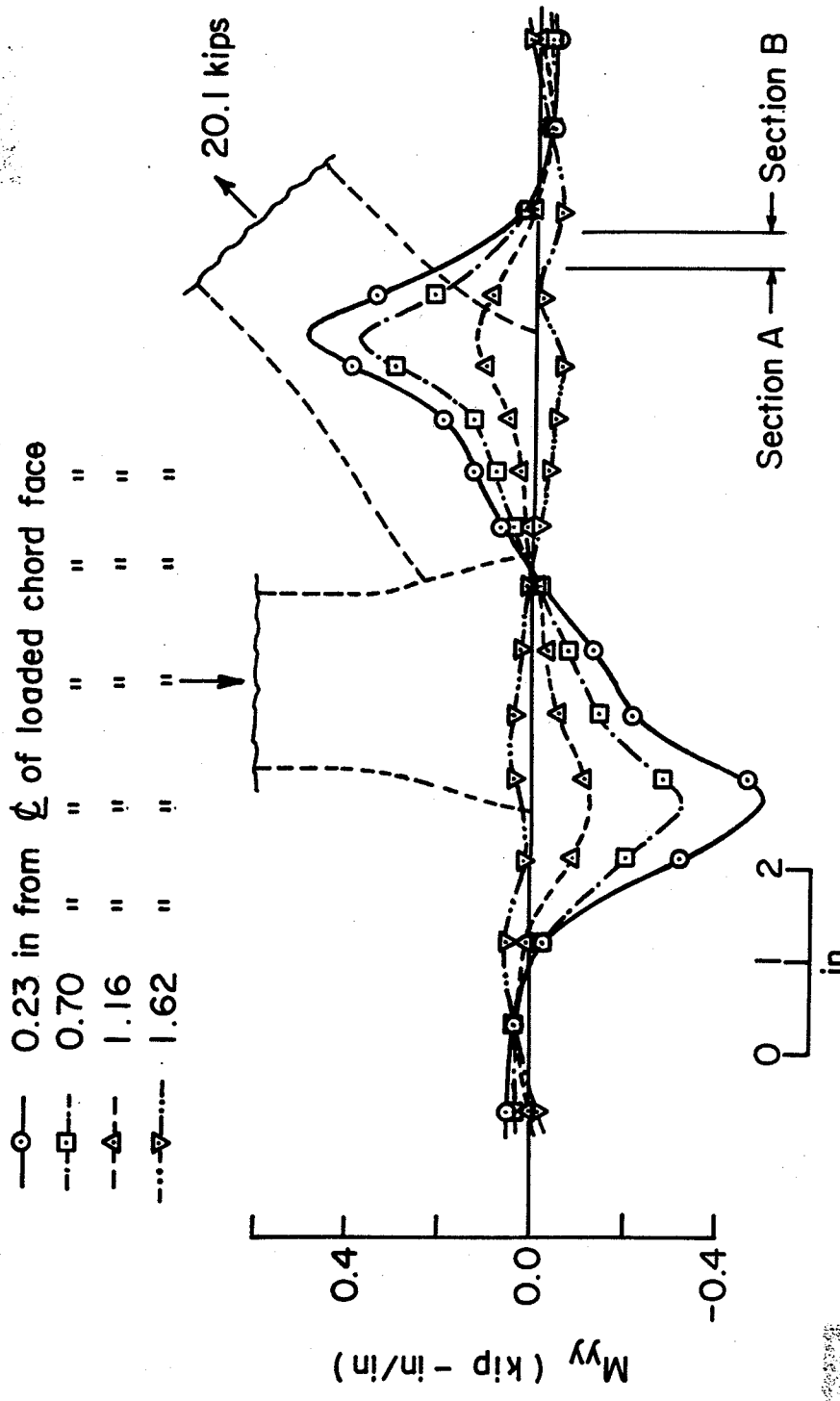

Fig. 5.10b. M_{yy} for Loaded Chord Face of Specimen 5B75 (283 Nodes)

measured, theoretical transverse strains were calculated at the same position and were compared with the experimental values. The transverse strain at point A_1, along the centre of the top chord face at section A, of Fig. 5.11 is calculated as an illustration.

At this point, using Fig. 5.11 and a 283-node model,

M_{xx} = 0.53 kips-in./in., and M_{yy} = 0.25 kips-in./in.

Since t_0 = 0.290 in., using Eq. 5.1,

$\sigma_{xb} = 6(0.53)/0.29^2 = 37.8$ ksi,

$\sigma_{yb} = 6(0.25)/0.29^2 = 17.8$ ksi.

It is noted that σ_{xb} at this point exceeds the average stress of 30 ksi in the tension web member.

The membrane stresses σ_{xm} and σ_{ym} for this point are 2.5 ksi and -10.0 ksi, respectively. They are small compared to the bending stresses σ_{xb} and σ_{yb}.

Using Eq. 5.2, the bending strain is:

$\varepsilon_{xb} = (37.8 - 0.3 \times 17.8)/29000 = 0.00112.$

Using Eq. 5.3, the membrane strain is:

$\varepsilon_{xm} = (2.5 - 0.3(-10.0))/29000 = 0.00019.$

It is noted that the bending strain is about six times as large as the membrane strain. Using Eq. 5.4, the total transverse strain is:

$\varepsilon_{xx} = 0.00112 + 0.00019 = 0.00131.$

In comparison, the experimental strain was 0.00128, a difference of 2%. Thus the experimental and theoretical transverse strains at point A_1 agree very well.

Transverse strains at other points at section A were similarly

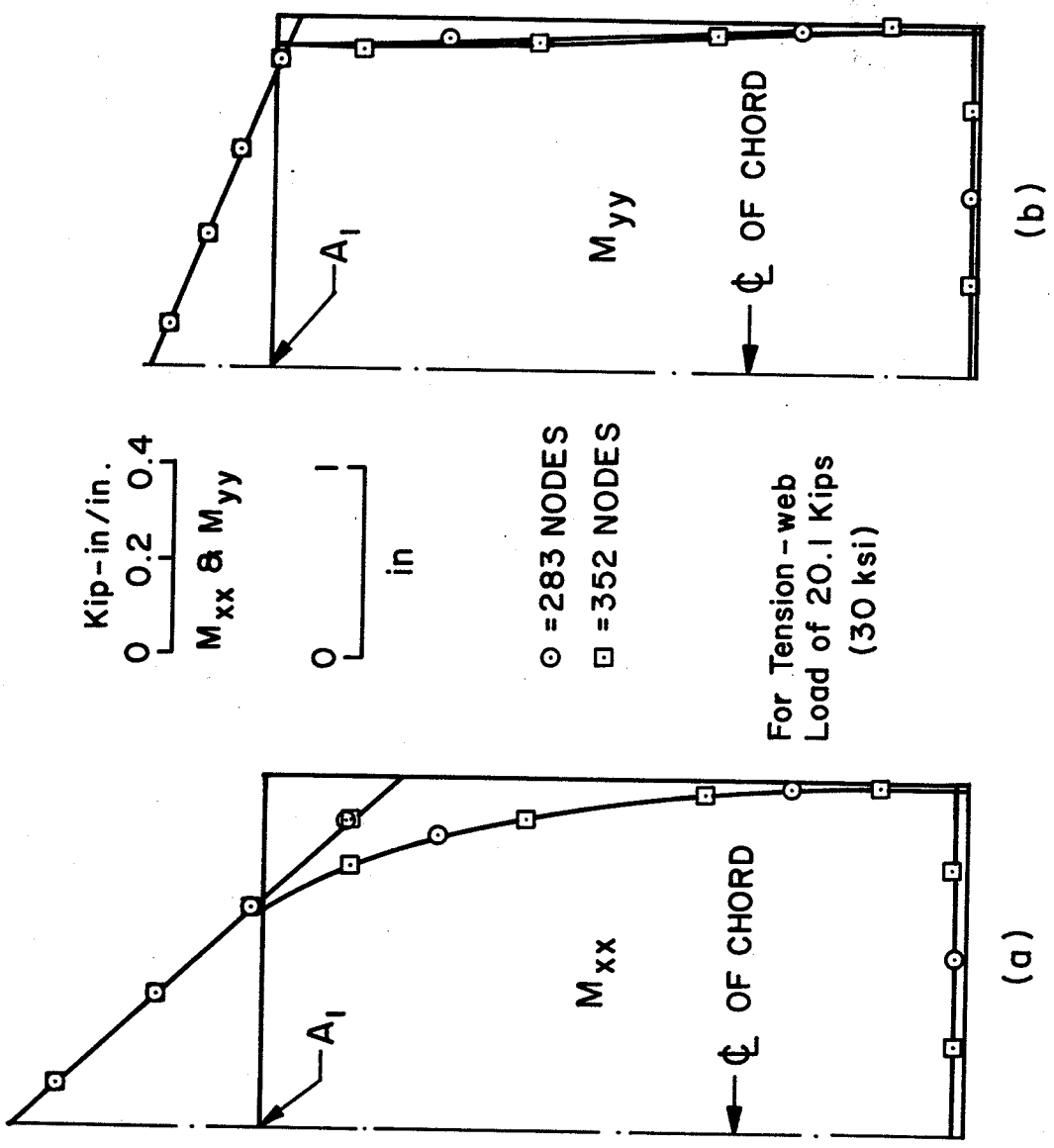

Fig. 5.11. Bending Moments at Section A of Specimen 5B75

calculated and are shown in Fig. 5.12a, while longitudinal strains (along y-axis) for section B of Fig. 5.10 are shown in Fig. 5.12b. It can be seen that the strains on the loaded chord face are much larger than those on other faces. The theoretical strains agree quite well with the experimental ones. This illustrates that the stress and strain distributions of the chord faces can be quite accurately predicted using a finite element analysis and the idealized models presented.

The chord of specimen 5B75 used in this example had a relatively large t_0/b_0. At the load of 20.1 kips (89.4 kN) corresponding to an average axial stress in the tension web of 30 ksi (207 N/mm^2), the stresses and strains were still largely linearly elastic. For specimens with relatively small t_0/b_0, this may not be so. However, the finite element analysis can be extended to cover such cases by including inelastic and large displacement behavior. This has not been done here. The nonlinear analysis would allow the joint strength to be estimated.

5.4. Stresses in Web Members

Maximum and minimum stresses in the web members of specimen 5B75, obtained from a finite element analysis of a 352-node model, as illustrated in Fig. 5.9, are shown in Fig. 5.13. The Figure shows that the stresses in both webs near the overlap are relatively high. For an axial load causing an average stress in the tension web of 30 ksi (207 N/mm^2), a maximum tensile stress of 40.4 ksi (278 N/mm^2) occurs in this web just above the lap. This indicates that failure by tearing of the web will usually start in this area. Experiments have confirmed this.

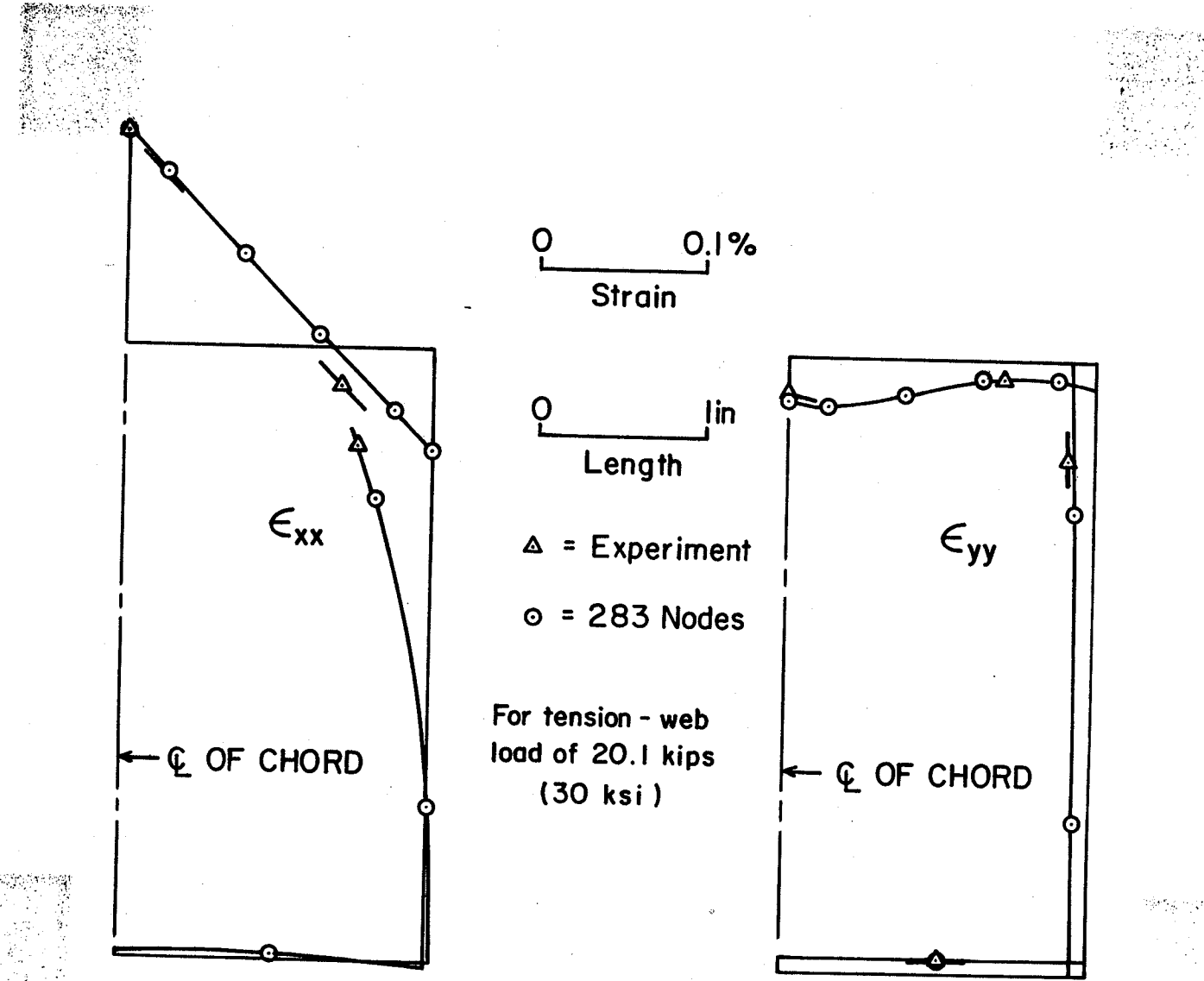

a. Transverse strains at section A

b. Longitudinal strains at section B

Fig. 5.12. Strains on Chord Faces of Specimen 5B75

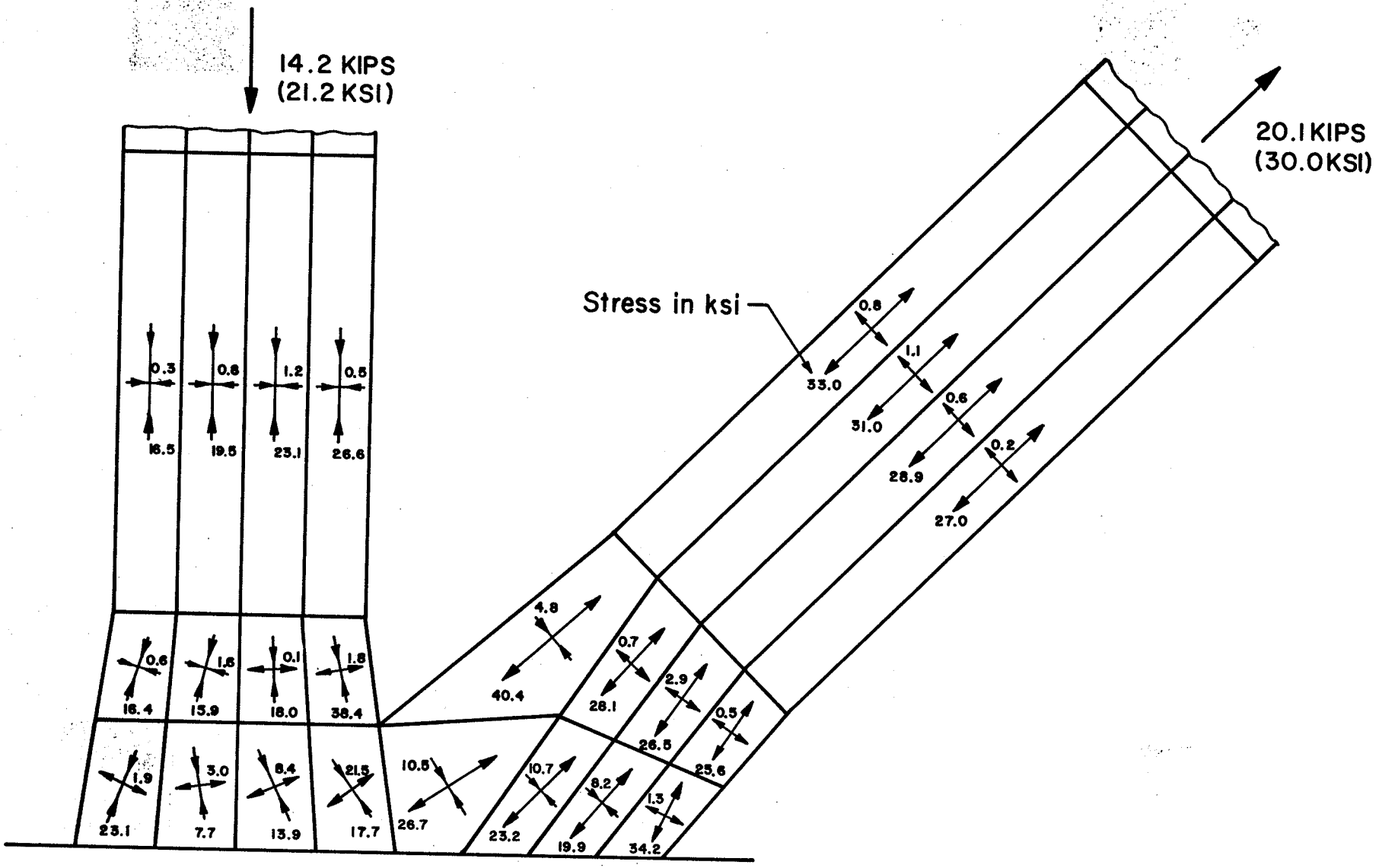

Fig. 5.13. Maximum and Minimum Stresses in Webs of Specimen 5B75 (352 Nodes)

Summary

The finite element method and a simplified model of the joint presented can usually be used to predict the load-deformation behavior and stress distribution of a cropped-web joint up to a load of about half the ultimate load of the joint or about the working loads of the web members. The agreement between the theoretical and experimental results is improved by subdividing the elements, particularly those in the vicinity of the joint. The method can be extended to include inelastic and large displacement behavior so that the joint strength can be estimated.

Chapter 6

CONCLUSIONS AND RECOMMENDATIONS

6.1. Conclusions

Based on test results and theoretical analyses of the cropped-web joints, the following main conclusions have been reached.

(1) The strength of a cropped-web joint with some overlap between the web members is comparable to that of a similar joint with sawn webs and a small gap, provided that the chord thickness/width is smaller than about 0.07. The strength of the cropped-web joint, expressed as the ultimate web-force component normal to the chord, can be accurately estimated using Eq. 3.1:

$$J_u = t_0 b_0 \sigma_e (0.504 + 6.10(d/b_0)^3 - 43.3(d/b_0)^2(t_0/b_0)),$$

where t_0, b_0, and σ_e are, respectively, the thickness, width, and yield stress of the chord, while d is the average diameter of the web members. When t_0/b_0 is larger than about 0.04, the joint strength is usually larger than about 85 to 100% of the yield strength of the tension web or the buckling strength of the compression web member.

(2) The stiffness of a cropped-web joint, with no gap, along the axis of the compression web member can be estimated using Eq. 3.5:

$$k_1 = Ed(0.0012 + 67.4(t_0/b_0)^3 + 6.91(t_0/b_0)^2 o_v),$$

where E is the modulus of elasticity of the chord and o_v is the ratio of overlap to the tension web diameter. The stiffness of the joint along the axis of the tension web can be estimated using Eq. 3.6:

$$k_2 = Ed(0.0127 + 118(t_0/b_0)^3 + 2.31(t_0/b_0)\sigma_v).$$

The stiffnesses k_1 and k_2 can be used to estimate an increase in truss deflection due to local deformations of the loaded chord faces. For most practical trusses, such an increase is usually smaller than about 10 or 15% when t_0/b_0 is larger than about 0.05.

(3) Failure of a cropped-web joint can occur in one or more of the following three main modes:

A. Failure by excessive local deformation of the loaded chord face. It often occurs when the chord wall is relatively flexible compared to the web members, and it usually induces other failure modes to occur.

B. Failure by buckling of the compression web member. It often occurs when the compression web member has a slenderness ratio of about 90 or more. It occurred in most of the specimens tested. It is usually induced by rotational deformation of the chord face at the end of the web member. Thus the buckling is usually in the plane of the truss and in the direction away from the tension web.

C. Failure by tearing of the tension web member. It often occurs when the web members are stiff, and it usually starts near the overlap.

(4) The deformations and stresses in the elastic range of a cropped-web joint can be accurately predicted using the finite element method and the simplified models of the joint presented herein.

6.2. Design Recommendations

Cropped-web joints having no gaps between the web members are recommended as safe and economical substitutes for profiled- or sawn-web joints of tubular trusses. The design loads of the former joints are estimated using the empirical equation 3.1 and applying a performance factor or a safety factor, depending on the design method used, as illustrated in Section 3.7.

For the joints to be efficient, having high strengths compared to the strengths of the web members, the chord thickness should be larger than about 0.04 times the chord width. In addition, the web members should have diameters about 0.4 to 0.6 times the chord width. The compression web member should have a slenderness ratio larger than about 90.

The web members should have no gap between them. They should have an overlap of about 0.5 to 0.75 times the tension web diameter if the chord thickness/width is smaller than about 0.04. If the truss deflection due to changes in member lengths is critical and the chord thickness/width is smaller than about 0.04, the increase in deflection due to joint deformations, which usually is negligible, should be checked.

6.3. Recommendations for Further Studies

In order to further confirm the validity of the strength and stiffness equations obtained in the present tests, a number of cropped-web joints having different parameter values should be tested. These are:

(1) Joints having d/b_0 values of about 0.6, 0.8, and 1.0.

(2) Joints having t_0/b_0 larger than 0.08.

(3) Joints having small gaps or no overlaps between the web members.

(4) Joints having web members the same as those studied herein but with shorter lengths, as joints having compression web members with slenderness ratios smaller than about 90 seemed to give low efficiency.

(5) Joints having rectangular instead of square chords. (Joints having rectangular chords and those having square chords with the same thickness/width ratios probably will have comparable strengths, because the strengths are usually largely governed by the plastic deformations of the loaded chord faces.)

(6) Joints having compression and tension web members with different diameters.

(7) Joints having t/d other than about 5% to 8%.

For the theoretical studies, the joints should be analyzed using a nonlinear finite element program so that the strength and behavior in the plastic range may be predicted. A yield-line approach is also interesting, using the stress pattern obtained from the elastic finite element analyses as a guide.

REFERENCES

Anderson, C. W. 1961. Circumferential Stresses in a Joint between Structural Tubes, Special Report No. 22 of Commonwealth Experimental Building Station, Sydney.

Bathe, K., E. L. Wilson, and F. E. Peterson. 1973. SAPIV: A structural Analysis Program for Static and Dynamic Response of Linear Systems Report No. EERC 73-11, Earthquake Engineering Research Center, College of Engineering, University of California, Berkeley, California.

Beckett, G. A. 1970. "Use of hollow sections in structural engineering", Tube and Pipe Production, Proceedings of the technical meeting of the Iron and Steel Institute, London.

Bouwkamp, J. G. 1964. "Concept of Tubular-joint Design", Journal of the Structural Division, ASCE Proc., Vol. 92, ST2, April.

_____. 1968. Behavior of Tubular Truss Joints under Static Loads, Phase 2, College of Engineering, University of California, Berkeley.

Canadian Institute of Steel Construction (CISC). 1973. Handbook of Steel Construction, 3rd. ed., Universal Offset Ltd., Ontario.

Canadian Institute of Steel Construction (CISC). 1977. Limit States Design Steel Manual, 1st. ed., Universal Offset Ltd., Don Mills, Ontario.

Chebib, F., K. Carpenter, and D. Reimer. 1976. Manitoba Statistical Package, Computer Centre, University of Manitoba.

Cran, J. A., E. B. Gibson, and S. Stadnyckyj. 1971. Hollow Structural Sections--Design Manual for Connections, The Steel Company of Canada, Ltd., 1st. ed.

Dasgupta, A. 1970. The Behaviour of Joints in Tubular Trusses, Ph. D. Thesis, Department of Civil Engineering, University of Nottingham.

Davie, J. and T. W. Giddings. 1971. Research into the Strength of Welded Lattice Girder Joints in Structural Hollow Sections, CE 70/3, CIDECT Programme 5EC. University of Sheffield.

Dasai, S. C. and J. F. Abel. 1972. Introduction to the Finite Element Method for Engineering Analysis. Van Nostrand Reinhold Co.

Eastwood, W., C. Osgerby, A. A. Wood, and D. I. Blockley. 1967a. An Experimental Investigation into the Behaviour of Joints between Structural Hollow Sections, Department of Civil and Structural Engineering, University of Sheffield.

Eastwood, W., C. Osgerby, A. A. Wood, and D. I. Blockley. 1967b. A Theoretical Investigation into the Elastic Behaviour of Joints between Structural Hollow Sections, University of Sheffield.

_____ and A. A. Wood. 1970. Welded Joints in Tubular Structures Involving Rectangular Sections, Conference on Joints in Structures, Session A, Paper 2, Department of Civil and Structural Engineering, University of Sheffield.

_____, C. Osgerby, A. A. Wood, and B. L. Mee. 1970. An Experimental Investigation of Joints in Rectangular Hollow Sections, Department of Civil and Structural Engineering, University of Sheffield.

Frovich, L. E. 1973. A Preliminary Investigation into the Behaviour of Various Flattened-End Truss Connection Configurations, M. Sc. Thesis, Department of Civil Engineering, University of Manitoba.

Gibson, E. B. and R. M. Pastor. 1974. Hollow Structural Sections--Welded Joint Research Summaries, The Steel Company of Canada, Ltd. (Stelco), Hamilton, Ontario.

Hlavacek, V. 1973. Strength of Welded Tubular Joints in Lattice Girders, Building Research Institute, Technical University, Prague.

Jamm, W. 1951. Form Strength of Welded Tubular Connections and Tubular Structures under Static Loading, (Translation from German), Schweissen Und Schneiden, Vol. 3.

_____, G. Zimmerman, and G. Lewenton. 1952. Welded Connections of Pipe Structures--Node Points, Patent Right No. 831 598, Class 37, Group 5, Republic of Germany Patent Office.

Kennedy, J. B. and A. M. Neville. 1976. Basic Statistical Methods for Engineers & Scientists, Thomas Y. Crowell Co., N.Y.

Libson, C. and N. J. Sheth. 1973. Statistical Design and Analysis of Engineering Experiments, McGraw-Hill Book Co.

Mee, B. L. 1969. The Structural Behaviour of Joints in Rectangular Hollow Sections, Ph. D. Thesis, Department of Civil and Structural Engineering, University of Sheffield.

Morris, G. A., L. E. Frovich, and N. Thiensiripipat. 1974. An Experimental Investigation of Flattened-End Tubular Truss Joints, Department of Civil Engineering, University of Manitoba.

Mouty, J. 1977. Theoretical Prediction of Welded Joint Strength, Proceedings of International Symposium on Hollow Structural Sections, CIDECT, Toronto.

Otto Graff Institute of the Stuttgart College of Technology. 1967. Tests on Welded Steel Tube Node Joints, CIDECT Research Note.

Przemieniecki, J. S. 1968. Theory of Matrix Structural Analysis, McGraw-Hill Book Co., New York.

Robinson, H. C. 1969. Literature Survey on Tubular Steel Joints, Part Thesis for Ph. D. Degree, Department of Civil and Structural Engineering, University of Sheffield.

Sammet, H. 1963. The Strength of Tubular Joints without Gusset Plates in Steel Constructions, (translated from "Schveisstechnik", Nov. 1963, Vol. 13, No. 11, pp. 481/486).

Stelco. 1973. Structural Steels--Selection and Uses, The Steel Company of Canada, Ltd.

Thiensiripipat, N. and G. A. Morris. 1975. Statical Behavior of Cropped -End Connections in Tubular Trusses, Department of Civil Engineering, University of Manitoba.

Tubemakers of Australia Limited. 1960. Report on Behaviour of Welded Joints in Tubular Structures, Stewarts and Lloyds Division, Technical Office.

Wang, Chi-Teh. 1953. Applied Elasticity, McGraw-Hill Book Co., Inc.

Wardenier, J. 1977. Testing and Analysis of Truss Joints Made from Rectangular HSS, Proceedings of International Symposium on Hollow Structural Sections, CIDECT, Toronto.

White, R. N., P. Gergely, and R. G. Sexsmith. 1976. Structural Engineering, Combined Edition, Vol. 1 and 2. John Wiley & Sons, Inc.

Zienkiewicz, O. C. 1971. The Finite Element Method in Structural and Continuum Mechanics, McGraw-Hill Book Co.

APPENDIX A

The procedure for obtaining the strength equation for cropped-web joints (Eq. 3.2) using multiple regression analyses is briefly outlined below. Some results of the analyses are given and explained. Similar procedures were used to obtain the stiffness equations for the joints (Eq. 3.6 and 3.7).

For convenience, the joint strength J_u was non-dimensionalized by a term such as $t_0 b_0 \sigma_e$, $t_0^2 \sigma_e$, $t_0 t \sigma_e$, $t_0 d \sigma_e$, before correlating with other non-dimensional parameters, such as d/b_0, t_0/b_0, and o_v. Plots of these parameters showed that $J_u/t_0 b_0 \sigma_e$ is clearly related with d/b_0. Structurally, this is reasonable, as J_u would be expected to vary with $t_0 b_0 \sigma_e$ and d/b_0. This was confirmed by multiple regression analyses, which also gave equations relating the parameters.

Since 32 test results (excluding specimens 1C50 and 1C75) were considered, 29 variables could be used in the analyses in a given run. The variables used included a dependent variable, such as $J_u/t_0 b_0 \sigma_e$, and various independent variables, such as d/b_0, t_0/b_0, o_v, b_0/d, t/d, e/h_0, and their powered products.

For illustration, the result of a stepwise multiple regression analysis of 32 test results (observations), using four variables which gave good results, is given below. The variables are:

(1) $J_u/t_0 b_0 \sigma_e$

(2) $(d/b_0)^2 (t_0/b_0)$

(3) $(d/b_0)^3$

(4) $(d/b_0)(t_0/b_0)^2$.

The means and standard deviations of the variables are given in Table A-1. Table A-2 shows the correlation matrix of the variables. Table A-3 gives the results of the step-wise multiple regression analysis. This Table shows that in the first step, variable 3 was entered, because it had the largest correlation with the dependent variable (variable 1). In this step, the multiple correlation coefficient, normally denoted by r, is 0.850. Therefore the third variable accounts for r^2 = 72.2% of the variation in the first. The level of confidence that this is true is found as follows.

In this step, the degrees of freedom ν, equal to the number of observations minus the number of independent variables used minus one, are 32-1-1 or 30. Using Table A-49 of Libson and Sheth (1973) or Table A-11 of Kennedy and Neville (1976), the value of correlation coefficient r for the 1% level of significance corresponding to 30 degrees of freedom and 2 variables is 0.449. Since this value is smaller than the value of r obtained (0.850), the third variable accounts for a significant amount of the variation of the first variable.

In the first step of Table A-3, the F-value for analysis of variance is 78.0. This is compared to the F-value obtained from Statistical Tables as follows. The degrees of freedom for the numerator ν_1 to be entered in the Tables are equal to the number of independent variables, which is 1. The degrees of freedom for the denominator ν_2 are equal to ν, which are 32-1-1 or 30. Using Table A-9 of Libson and Sheth, the F-value corresponding to ν_1 = 1 and ν_2 = 30 for the 0.1% level of significance is 13.3. Since this is smaller than the F-value obtained

Table A-1. Means and Standard Deviations of Variables

STEP-WISE MULTIPLE REGRESSION ***** UNIVERSITY OF MANITOBA *****

JOINT STRENGTH (32 OBS., 4 VARI.)

NUMBER OF OBSERVATIONS 32
NUMBER OF VARIABLES 4
NUMBER OF SELECTIONS 2

CONSTANT TO LIMIT VARIABLES 0.0

VARIABLE NO.	MEAN	STANDARD DEVIATION
1	0.78236	0.39873
2	0.01512	0.01062
3	0.15273	0.12370
4	0.00165	0.00116

Table A-2. Correlation Matrix of Variables

CORRELATION MATRIX

ROW 1			
1.00000	0.56222	0.84988	0.16131
ROW 2			
0.56222	1.00000	0.90553	0.88312
ROW 3			
0.84988	0.90553	1.00000	0.61243
ROW 4			
0.16131	0.88312	0.61243	1.00000

Table A-3. Results of Step-wise Multiple Regression Analyses

SELECTION..... 1

DEPENDENT VARIABLE..... 1
NUMBER OF VARIABLES FORCED.... 0
NUMBER OF VARIABLES DELETED... 0

STEP 1

VARIABLE ENTERED..... 3

SUM OF SQUARES REDUCED IN THIS STEP....	3.560	
PROPORTION REDUCED IN THIS STEP.....	0.722	
CUMULATIVE SUM OF SQUARES REDUCED.....	3.560	
CUMULATIVE PROPORTION REDUCED.....	0.722	OF 4.929

FOF 1 VARIABLES ENTERED

MULTIPLE CORRELATION COEFFICIENT...	0.850
(ADJUSTED FOR D.F.).....	0.850
F-VALUE FOR ANALYSIS OF VARIANCE...	78.028
STANDARD ERROR OF ESTIMATE.....	0.214
(ADJUSTED FOR D.F.).....	0.214

VARIABLE NUMBER	REGRESSION COEFFICIENT	STD. ERROR OF REG. COEFF.	COMPUTED T-VALUE
3	2.73948	0.31013	8.833
INTERCEPT	0.36395		

Table A-3.(Continued)

STEP 2

VARIABLE ENTERED..... 2

SUM OF SQUARES REDUCED IN THIS STEP.... 1.177
PROPORTION REDUCED IN THIS STEP..... 0.239

CUMULATIVE SUM OF SQUARES REDUCED..... 4.737
CUMULATIVE PROPORTION REDUCED..... 0.961 OF 4.929

FOR 2 VARIABLES ENTERED
MULTIPLE CORRELATION COEFFICIENT... 0.980
(ADJUSTED FOR D.F.)..... 0.980
F-VALUE FOR ANALYSIS OF VARIANCE... 358.849
STANDARD ERROR OF ESTIMATE..... 0.081
(ADJUSTED FOR D.F.)..... 0.083

VARIABLE NUMBER	REGRESSION COEFFICIENT	STD. ERROR OF REG. COEFF.	COMPUTED T-VALUE
3	6.10172	0.27802	21.947
2	-43.26122	3.23927	-13.355
INTERCEPT	0.50439		

STEP 3

VARIABLE ENTERED..... 4

SUM OF SQUARES REDUCED IN THIS STEP.... 0.072
PROPORTION REDUCED IN THIS STEP..... 0.015

CUMULATIVE SUM OF SQUARES REDUCED..... 4.810
CUMULATIVE PROPORTION REDUCED..... 0.976 OF 4.929

FOR 3 VARIABLES ENTERED
MULTIPLE CORRELATION COEFFICIENT... 0.988
(ADJUSTED FOR D.F.)..... 0.987
F-VALUE FOR ANALYSIS OF VARIANCE... 377.240
STANDARD ERROR OF ESTIMATE..... 0.065
(ADJUSTED FOR D.F.)..... 0.067

VARIABLE NUMBER	REGRESSION COEFFICIENT	STD. ERROR OF REG. COEFF.	COMPUTED T-VALUE
3	8.65704	0.65798	13.157
2	-95.49690	12.91801	-7.393
4	261.08423	63.24625	4.128
INTERCEPT	0.47249		

(78.0), the first variable significantly depends on the third variable.

For the first step, the regression equation obtained is:

$$J_u/t_0 b_0 \sigma_e = 0.364 + 2.74(d/b_0)^3 \qquad \text{(A-1)}$$

The computed t-value given is 8.83, equal to the square root of the F-value since there is only one independent variable. Thus the coefficient of the independent variable is also statistically significant at the 0.1% level.

In step 2 of Table A-3, the second variable was entered and Eq. 3.2 or A-2 resulted:

$$J_u/t_0 b_0 \sigma_e = 0.504 + 6.10(d/b_0)^3 - 43.3(d/b_0)^2(t_0/b_0) \qquad \text{(A-2)}$$

The values of r, F, and t were changed and similarly analyzed. The results have been given in Section 3.7. The two independent variables account for 96.0% of the variation in the dependent variable. The regression is significant at the 0.1% level. The partial regression coefficients are also significant at this level. This is because the t-values obtained from the regression are equal to 21.9 and -13.4, and the t-value for the 0.1% level of confidence and 29 degrees of freedom is only 3.66 (using Table A-3 of Libson and Sheth or Table A-8 of Kennedy and Neville).

In step 3, the fourth variable was entered and the following equation was obtained:

$$J_u/t_0 b_0 \sigma_e = 0.472 + 8.66(d/b_0)^3 - 95.5(d/b_0)^2(t_0/b_0) + 261(d/b_0)(t_0/b_0)^2 \qquad \text{(A-3)}$$

At this stage, about 97.6% of the variation in the dependent variable are accounted for. The coefficients are also significant. The values of $J_u/t_0 b_0 \sigma_e$ obtained from the experiments and Eq. A-3 are given for comparison in Table A-4. It can be seen that they agree very well.

Similarly, Table A-5 shows that the experimental values of $J_u/t_0 b_0 \sigma_e$ agree very well with the values estimated using Eq. A-2. Because of this and because of simplicity, this equation was used.

Similar results were obtained using a multi-linear regression analysis program. Unlike the step-wise multiple regression analysis program, it does not automatically select a variable which has a high correlation to give good results and the analysis is not done in a series of steps.

Table A-4. Values of Independent Variables Using Eq. A-3

SELECTION..... 1

TABLE OF RESIDUALS

CASE NO.	Y VALUE	Y ESTIMATE	RESIDUAL
1	0.67670	0.69509	-0.01839
2	0.58451	0.69509	-0.11058
3	1.09639	1.13937	-0.04298
4	0.41832	0.53312	-0.11480
5	0.62123	0.65255	-0.03132
6	0.64410	0.63753	0.00657
7	0.65195	0.63753	0.01442
8	0.54524	0.57485	-0.02961
9	0.57073	0.57485	-0.00412
10	0.63551	0.58246	0.05305
11	0.64139	0.58246	0.05893
12	0.55656	0.48831	0.06825
13	0.53171	0.48831	0.04340
14	0.38873	0.46745	-0.07872
15	0.47050	0.46745	0.00305
16	0.48395	0.46745	0.01650
17	1.02092	0.86912	0.15180
18	0.97849	0.86912	0.10937
19	0.57757	0.68763	-0.11006
20	0.70685	0.68763	0.01922
21	0.55933	0.53821	0.02112
22	0.55518	0.53821	0.01697
23	0.45140	0.47490	-0.02350
24	0.45567	0.48205	-0.02638
25	0.50370	0.48979	0.01391
26	1.85783	1.90087	-0.04304
27	1.92958	1.90087	0.02871
28	1.47596	1.41051	0.06545
29	1.32581	1.41051	-0.08470
30	1.06269	1.11443	-0.05174
31	1.03926	0.98643	0.05283
32	1.01789	0.99146	0.02643

Table A-5. Values of Independent Variables Using Eq. A-2

SELECTION..... 2

TABLE OF RESIDUALS

CASE NO.	Y VALUE	Y ESTIMATE	RESIDUAL
1	0.67670	0.73133	-0.05463
2	0.58451	0.73133	-0.14682
3	1.09639	1.13858	-0.04219
4	0.41832	0.56661	-0.14829
5	0.62123	0.67885	-0.05762
6	0.64410	0.66717	-0.02307
7	0.65195	0.66717	-0.01522
8	0.54524	0.61049	-0.06525
9	0.57073	0.61049	-0.03976
10	0.63551	0.61833	0.01718
11	0.64139	0.61833	0.02306
12	0.55656	0.47730	0.07926
13	0.53171	0.47730	0.05441
14	0.38873	0.38299	0.00574
15	0.47050	0.38299	0.08751
16	0.48395	0.38299	0.10096
17	1.02092	0.87175	0.14917
18	0.97849	0.87175	0.10674
19	0.57757	0.72483	-0.14726
20	0.70685	0.72483	-0.01798
21	0.55933	0.54833	0.01100
22	0.55518	0.54833	0.00685
23	0.45140	0.40168	0.04972
24	0.45567	0.42634	0.02933
25	0.50370	0.45056	0.05314
26	1.85783	1.80632	0.05151
27	1.92958	1.80632	0.12326
28	1.47596	1.43644	0.03952
29	1.32581	1.43644	-0.11063
30	1.06269	1.16822	-0.10553
31	1.03926	1.03281	0.00645
32	1.01789	1.03844	-0.02055